General comments from the authors

First of all we would like to express our great acknowledgments to both referees for their time in revising our paper. In view of their major critics the authors had to modify substantially the paper. As a result the revised manuscript is quite different from the first submission. Because of the many changes, two versions of the paper are sent: one with all the visible changes (as supplement), and one with all changes accepted.

The revised manuscript deals with the comparison of monthly and seasonal averages of AERONET products at two sites in the western Mediterranean Basin: in Ersa and Palma. In this version Alborán is left for the very last section in which only temporally coincident measurements at the three sites are compared to examine possible North-South gradients. The authors would like to address three comments, all made by both referees, in a common way:

Representativeness of the AERONET dataset considered in the paper

In order to strengthen the representativeness of the dataset a series of actions have been led:

1. The dataset, originally from 2011-2014, is now also including 2015, so that it is based on a 5-year period. In that period more AOD level 2.0 data are available in Ersa, but not in Palma. And unfortunately level 2.0 product inversions are still not available for 2015.
2. As mentioned in the short comment posted by the authors in the Interactive Discussion on 11 March, AERONET data were checked against satellite data for the period 2011-2014 (satellite data are not available yet for 2015). MODIS, OMI and MISR AOD extracted daily in Ersa and Palma were compared, as well as OMI and MISR AAOD and SSA. The results are unfortunately not as good as expected and for that reason they are not included in the revised manuscript. However we would like to comment quickly our results. Fig. 1 shows the comparison between AERONET AOD daily mean and the satellite AOD in Ersa. AERONET AOD were calculated at the satellite wavelength (550, 555 and 500 nm for MODIS, MISR and OMI, respectively) from AOD_{440} and $AE_{440\text{-}870}$. One sees large discrepancies between both ground- and satellite-based AODs. Satellite AODs are in general higher than AERONET AODs. The same tendency was shown on SEVIRI data recently over the Balearic Islands by Chazette et al. (2016) who found a systematic overestimation of SEVIRI AOD of 35 % compared to AERONET. Chazette el al. (2016) explain that aerosol mixing causes this difference by making difficult the identification of the proper aerosol model in the satellite retrieval. Fig. 2 shows the monthly AERONET AOD_{440} (like in the paper) and the monthly means of the satellite AODs in Ersa. The shape of OMI AOD is similar but the values are much higher (bias > 0.05). OMI and MISR AODs seem anti-correlated to AERONET. Similar discrepancies are observed in Palma. OMI and MISR AAOD are underestimated compared to AERONET, which results in an overestimation of the satellite SSA. In addition very few points are available for comparison given the AERONET restrictions ($50 < SZA < 80º$ and $AOD_{440} > 0.4$).
   All in all we decided to leave the comparison with the satellite data out of the paper, and maybe address the subject of the validation of satellite products related to the aerosol absorption properties in another paper.

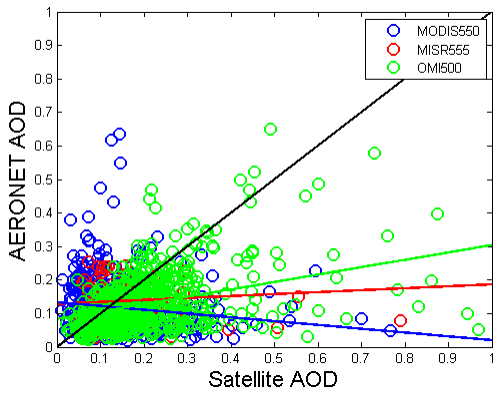

Fig. 1

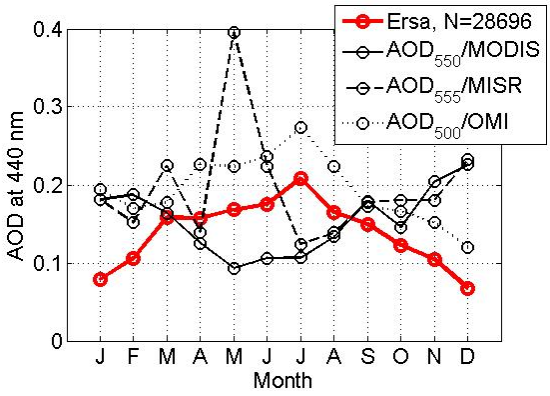

Fig. 2

3. With the new Ersa dataset (2011-2015) each monthly mean is computed with at least 3 to 5 years of data. In Palma each monthly mean is computed with 1 to 3 years of data. To check the representativeness of Palma data we have computed the monthly mean in Ersa for the same days than the Palma dataset included in the period August 2011 – December 2013, and superimposed it on the monthly means calculated over the whole Ersa dataset. Considering only the period of the Palma dataset leads to negligible differences for January and from May to December. The largest differences, up to -0.04, are found during the spring months. We suspect the Palma dataset to lead to an underestimation of the mean values during spring and warn the reader about the limitation of our climatology during that period.

Frequency/intensity of the high AOD events

Another critical point addressed by both referees is the characterization of the aerosol types mentioned all along the paper (initial version). In the revised manuscript a graphical classification method based on Gobbi et al. (2007) has been applied to all AOD retrievals (AERONET *.lev20 files) and to all product inversions (AERONET *.dubovik files) for the data with non-NaN values (see Fig. 2, 3, 6 and 11(a)-(c) in the revised paper). The graphical method is based on (δAE vs. AE) plots superimposed onto a grid of theoretical constant fine mode radii and fraction of the fine mode contribution to the AOD at 675 nm. δAE represent the Ångström exponent difference ($\delta AE = AE_{440\text{-}675} - AE_{675\text{-}870}$). With the dataset corresponding to the AOD retrievals, although the condition $AOD_{675} > 0.15$ is applied to minimize errors in the δAE calculation, the (δAE, AE) plots show the signature of almost all aerosol types with the added difficulty of mixed cases. With the dataset corresponding to the product inversions, much less points are left (49 in Ersa and 82 in Palma) and they fall within two well defined clusters corresponding to mineral dust and pollution. For this dataset we have quantified the frequency of mineral dust and pollution cases with their number (absolute and relative) of occurrences per season and their intensity with the seasonal mean AOD_{440} for each of both aerosol types (see Table 2 in the revised paper). The graphical method is presented in a new dedicated section (Section 3). The analysis of the graphs related to the AOD data and the product inversion dataset have been added at the beginning of Sections 5.1 and 5.3, respectively.

North-South gradients

North-South gradients are explored in a new dedicated section (Section 7) at the end of the paper, where all three stations (Ersa, Palma and Alborán) are considered. In this new section, and as suggested repeatedly by Referee #2, we have looked only at temporal coincident measurements in the period August – December 2011. Outside this period, at least one of the three sites does not have data available. This section is presented as a case study of possible North-South gradients during the period August-December 2011. During this period a similar number of AOD retrievals (~3700 – 3900) is available at each site. In turn, for the product inversions the number of measurements available (3 in Ersa, 7 in Palma and 5 in Alborán) is statistically poor and for that reason the AERONET inversion products based on that statistics (AAOD, AAE, RRI, IRI and SSA) are not analyzed in the paper. It is a pity, but this is what one can expect from case studies: they have their limitations. We believe anyway that the discussion of the differences between Ersa and Palma observed for AAOD, AAE, RRI, IRI and SSA is already representative of the temporal and spatial distributions of these parameters, and their complexity, in the western Mediterranean Basin.

References

Chazette, P., Totems, J., Ancellet, G., Pelon, J., and Sicard, M.: Temporal consistency of lidar observables during aerosol transport events in the framework of the ChArMEx/ADRIMED campaign at Menorca Island in June 2013, Atmos. Chem. Phys., 16, 2863-2875, doi: 10.5194/acp-16-2863-2016, 2016.

Gobbi, G. P., Kaufman, Y. J., Koren, I., and Eck, T. F.: Classification of aerosol properties derived from AERONET direct sun data, Atmos. Chem. Phys. 7, 453–458, 2007.

Answer from the authors to Referee #1

General comments: This paper presents a seasonal analysis of the optical, microphysical, and radiative aerosol properties in two insular sites in the western Mediterranean (Ersa and Palma de Mallorca). A third insular site in Alborán is chosen to examine the possible gradients in the aerosol properties between Northeast and Southwest (NE-SW) areas within the Basin. The analysis is based in AERONET measurements and inversion products. The authors conclude that the (NE-SW) gradient were observed in 3 extensive (AOD, CVc and ARFBOA) and 3 intensive (AE, rVc and Sphericity) parameters.
However I have several reasons regarding to the publication of this paper on ACP: The paper is too long and lacks a clear focus. The authors report the data and the seasonal averages at each site, describing the aerosol properties individually with no interrelation between them. This result in a mostly descriptive paper, that presents a lot of ideas and comments which are not well organized, making the reading difficult. This is reflected in the text and in a many figures which only describe the annual evolution of the aerosol parameters (e.g Fig.2). Some results sections describe how the parameters are obtained (sect. 4.2; 4.4 and 4.5). Please consider a new Methodology section in order to facilitate the paper reading.
Authors' reply: As said in our general comments, the paper has been completely restructured and revised in such a way that most of the text is new compared to the initial submission. Figures 1-10 and Tables 1-3 refer to the seasonal variations of a series of AERONET products in Ersa and Palma. Figure 11, refer to the case study used to explore possible North-South gradients. A new Methodology section has been added which describes the graphical method used to classify the aerosols. Part of introduction has been re-written to make clearer the focus of the paper. Most of the re-writing has been made trying to link as much as possible the findings found along the way.

In some cases the discussion is mainly based in the literature and the data and figures do not support the affirmations done in the text. (e.g.P19-L8. The sentence: "The influence of European pollution decreases along the NE–SW axis and, logically, the coarse mode volume median radius decreases " seems logical. However the authors do not support this affirmation with their data. e.g. P20-L20: The authors conclude: "We conclude that the differences in the IRI440 values and in the behavior of the IRI spectra are due to a higher influence of mineral dust and/or BrC in Palma" without supporting it with the data they are using).
Authors' reply: The analysis of the figures about seasonal variations is made in parallel with the aerosol classification obtained with the new methodology (Fig. 2, 3 and 6 and Table2). In particular with Fig. 6 and Table 2 we quantify the frequency and intensity of the two aerosol types which contribute to large AODs (pollution and mineral dust).
The sentence: "The influence of European pollution decreases along the NE–SW axis and, logically, the coarse mode volume median radius decreases " has been kept in the text. We now demonstrate that relatively more European pollution episodes occur in Ersa than in Palma and that the coarse mode volume median radius decreases from Ersa to Palma. Dubovik et al. (2002) findings about dust and urban aerosol coarse mode radii (recalled in the text) make the logical between our two findings.
The second sentence "We conclude that the differences in the IRI440 values and in the behavior of the IRI spectra are due to a higher influence of mineral dust and/or BrC in Palma" has been removed since we have no information allowing us make this hypothesis.

I see some inconsistences in the analysis of individual aerosol parameters separately. E.g. P24-L23. the authors assert that the asymmetry parameter at Alborán indicates that the scattering direction is driven by marine aerosols. However, when they analyze the SSA (P23-L20-25) the authors affirm that is probably due to the dust mixing with urban/industrial.

Authors' reply: In the revised manuscript the aerosol classification for SSA allows us to distinguish between pollution and mineral dust and therefore to discuss the results having always in mind the type of aerosol (mineral dust or pollution) or mixing (mineral dust + pollution) concerned. The two conclusions cited by the referee have been deleted in the revised manuscript. Let's note anyway that mineral dust and pollution influence very differently the seasonal mean of SSA and *g*. In the new Fig. 8a1 the SSA spectra of the whole dataset is very close to that of mineral dust, while in Fig. 8b1 the spectra of *g* of the whole dataset seems in the middle of the spectra of mineral dust and pollution, and even a little closer to pollution.

I think that the dataset used is too short in order to stablish an aerosol climatology in the western Mediterranean. However, I found that a more in deep analysis of the NW-SE gradient of the aerosol properties would be interesting to investigate the mixing mechanisms in the Mediterranean. Why do not use this data to investigate the NW-SE gradient during the period of simultaneous measurements in the three sites? Why the authors have limited the NW-SE gradient analysis to summer season? I suggest on one hand, synthesize the discussion and statistical analysis the data of the first part of the paper and on the other hand try to answer the question that the authors expose in last paragraph of the seccion 4.3: "In our opinion two major and interesting questions remain opened: why the absorption properties of the long-range transport aerosol in Alborán are observed neither in Palma, nor in Ersa? What are the processes which inhibits the BC and/or soot absorption properties during the transport to the northern part of the WMB?"

Authors' reply: Please see our general comments and in particular the paragraph "Representativeness of the AERONET dataset considered in the paper". The dataset of Ersa has been enlarged and has been used to check the representativeness of the one of Palma. NW-SE gradients are now examined only in the last section of the paper (2 pages) as a case study and many parameters of interest for investigating mixing mechanisms (AAOD, SSA, etc.) are not shown because of a too low statistics (see again our general comments). The authors believe that investigating mixing mechanisms (one of the goals of ChArMEx) is a crucial issue for studying the aerosols in the Mediterranean that can be assessed in dedicated field campaigns with in-situ measurements, among others. Our paper aims at showing the result of this mixing, and we believe that investigating further mixing mechanisms should be left for a new paper, in addition to the one from Denjean et al. (2016), also maybe using ChArMEx summer 2013 field campaign.

On the other hand, the aerosol forcing is a consequence of the impact of the different aerosol types on the radiative field. If the authors want to validate the AERONET forcing at TOA with the CERES database, I suggest a new paper on this topic using longer data series from more AERONET stations. The results obtained in this paper are compared to those obtained in the literature for Mediterranean and no Mediterranean sites. It could be especially relevant in the case of aerosol radiative forcing since many of these sites to be compared with have a very different surface albedo with respect to the observed in the Mediterranean Islands. Then, the results may be substantially different.

Authors' reply: Validating the aerosol forcing at the TOA has appeared to us a necessity to follow on with the discussion on the AERONET forcings at the TOA. We are planning a new paper on the validation of AERONET forcings at the TOA at more sites and with longer data series. The non-Mediterranean sites considered in the paper have been selected based on the aerosol type they are representative of and which are also found in Ersa and/or Palma.

The authors should keep always in mind the dataset they are working with in term of the restrictions imposed to some parameters in the AERONET L2 inversion retrievals. i.e. AOD440nm > 0.4 and 50 º< sza < 80º. Under these restrictions most of the studied cases will be mainly due

to Saharan dust outbreaks or severe pollution episodes as the authors stated several times throughout the paper (e.g. P9 - L19; P17-L15). This will be reflected in the monthly and seasonal averages only if the frequency and intensity of these events represent a notable fraction of the total number of retrievals passing the aforementioned restrictions. However, no analysis of the frequency and intensity of these events has been done and most of the conclusions are based on that.

Authors' reply: Please see our general comments about Frequency/intensity of the high AOD events! The graphical method based on Gobbi et al. (2007) has been used to classify the aerosol. The method applied to the AERONET product inversions (parameters like AAOD, AAE, RRI, IRI and SSA) has shown that the restrictions AOD_{440} > 0.4 and 50 º< SZA < 80º led to 2 well-differentiated types of particles: pollution and mineral dust. Table 2 gives some number to quantify the occurrence of both aerosol types and their intensity (in terms of AOD).

Specific comments:

P3-L13: please change "..the fraction fine mode to total AOD ...." by " ...the fine mode fraction to total AOD.." as this parameter is usually named

Authors' reply: This formulation has actually been replaced by " ...the fine mode fraction of total AOD.." in the entire manuscript. We hope this is what the referee meant.

P4-L26: please change "..the fraction of fine mode to total AOD ...." by "...the fine mode fraction to total AOD.." as this parameter is usually named

Authors' reply: This formulation has actually been replaced by " ...the fine mode fraction of total AOD.." in the entire manuscript. We hope this is what the referee meant.

P12-L6: please change "There is relative few aerosol measurements.." by " There are relative few aerosol measurements.."

Authors' reply: This formulation has been changed in the entire manuscript. Thank you!

P14 – L6: The authors state that the AOD maxima observed in Fig. 3 for Ersa and Palma are related to mineral dust outbreaks. However there is nothing in Fig.3 supporting this affirmation. The monthly mean AE values are higher than 1, which is mainly associated to the presence of small particles (Eck et al., 1999), or mixed cases (Pace et al., 2006; Schuster et al., 2006). What basis have been used to assert this idea? The author should be explained better.

Authors' reply: We have now information available on the frequency and intensity of mineral dust and pollution events for each season of the year (Section 5.3, Figure 6 and Table 2). With these results we now assert that the AOD maxima "are due to a combination of mineral dust outbreaks and pollution events in Ersa and mostly to mineral dust outbreaks in Palma (see the seasonal aerosol frequency and classification in Section ¡Error! No se encuentra el origen de la referencia.**)". The fact that the AE stays above 1 even in summer means that if mineral dust outbreaks increase (in number), then episodes with smaller aerosols (like pollution or biomass burning) also increase. Here again mineral dust does not influence the two parameters AOD and AE the same manner: while AOD is greatly influenced by the increase of mineral dust episodes, AE is not.**

P14-L26: It is really difficult to use AE in a monthly basis to classify the aerosol type, since the monthly statistics tends to smooth the values. Since the Ersa and Palma show AE higher than 1 for almost all months and also slightly different between both sites, I think that is not possible to differentiate the aerosol type asserting: "The slightly higher values in Ersa compared to Palma indicate the presence of finer particles at Ersa throughout the year". Can the author support this asseveration using other arguments? I think that a rough aerosol classification using AOD and AE make sense only using instantaneous measurements.

Authors' reply: In the graphical method used in the revised paper each point is precisely an instantaneous value of (δAE, AE, AOD). The rough aerosol classification mentioned by the referee can be found in the revised manuscript at the beginning of Section 5.1 (and Figures 2 and 3).

P19-L20: Why the authors do not compare the dust refractive index provided by AERONET with those values obtained for the dust layers during the Charmex flights (e.g Denjean et al., 2016)?
Authors' reply: We now compare our results to Denjean et al. (2016) the refractive index (RRI and IRI) and for the single scattering albedo. Thank you!

P22-L5-L20: I think that the description of the SSA spectral behaviour is too detailed and difficult to follow. The authors try to observe differences between the sites and seasons that I think they are within the SSA uncertainties. The SSA differences for 440nm among sites and seasons could be representative of different absorbent aerosol types. However the spectral behaviour for larger wavelengths is nearly flat. I suggest to shorten the discussion reducing it to the essential which is observed in Fig. 8.
Authors' reply: This section has been significantly reduced. SSA is now determined for both mineral dust and pollution and their mixing.

P23-L9: I am not sure if the differences in time and aerosol volume sampled between the Nakajima code and AERONET retrieval can be reflected in a such way using a monthly statistics. I believe that these differences are mostly due to the different algorithms.
Authors' reply: This part of the paper has been deleted.

P24-L10: The authors assert: "....at constant AOD the solar radiation scattered to the surface is greater for mineral dust than for urban/industrial aerosols." And this is not totally true since it is dependent on the solar zenith angle. Larger asymmetry parameter indicates larger forward scattering. Since the AERONET almucantar measurements are done at sza > 60º, most of the scattered radiation is returned back to space, reducing the scattered radiation reaching the ground surface (e.g. di Sarra et al., 2008)
Authors' reply: Placed in a general context, not only in the context of AERONET measurements, this sentence has been replaced by "This result implies that at near-infrared wavelengths (λ > 670 nm), constant AOD and low SZA the solar radiation …".

P.25-L.20. It is not clear for me if the authors have used the AERONET fluxes retrieval or they used their own calculations. Can you explained better? If the flux retrieval have been done by the authors it should be interesting to have a brief description of the used methodology. If not, why the authors start the sentence with: "Similar to the AERONET retrieval approach.." it should be changed by "The AERONET retrieval approach...".
Authors' reply: This was a mistake in the text. The sentence starts now with "In the AERONET retrieval approach, …". Thank you!

P35-L19. (43% of them)...I think that it should be the same value in P35-L19 than in P35-L24
Authors' reply: This Section has been removed.

P37-L2: The AERONET product comparison is not carried out during the 4-year period (2011-2014). As we can see in Fig. 1 there are no more than 2-years of simultaneous measurements at Ersa and Palma.
Authors' reply: The phrasing has been modified in the abstract and in the conclusion.

P38-L13: The authors assert "the gradient of rcV (a decrease along the NE–SW axis) reflects the decreasing influence of European pollution along the NE–SW axis". I think it is an affirmation too

strong for the analysis of a single parameter, and only in summer. I see no clear relationship with the European pollution

Authors' reply: The authors agree with this comment that the affirmation is too strong. It has been deleted in the revised manuscript.

Bibliography

Pace, G., di Sarra, A., Meloni, D., Piacentino, S. and P. Chamard, Aerosol optical properties at Lampedusa (Central Mediterranean). 1. Influence of transport and identification of different aerosol types, Atmos. Chem. Phys., 6, 697–713, 2006.

Schuster, G. L., Dubovik, O., and Holben, B. N., Angstrom exponent and bimodal aerosol size distributions, J. Geophys. Res., 111, D07207, doi:10.1029/2005JD006328, 2006.

Eck, T. F., Holben, B. N., Reid, J. S., Dubovik, O., Smirnov, A., O'Neill, N. T., Slutsker, I. and Kinne, S., The wavelength dependence of the optical depth of biomass burning, urban and desert dust aerosols, J. Geophys. Res., 104, 31,333– 31,350, 1999.

Answer from the authors to Referee #2

Summary: Authors don't understand what to put in figure captions. All caption lack details to allow the figures to be understood.
Authors' reply: In the revised manuscript we have tried to detail as much as possible the figure and table captions, saying where the data are from, the criteria applied, etc. The inconvenient is that some captions are quite long.

I'm am confused about what microphysical properties are analyzed. Typically, microphysical properties is measurement of the aerosol size distribution not just a fit of the size distribution.
Authors' reply: The microphysical parameters analyzed in the paper are the volume concentration and median radius of both fine and coarse mode of the retrieved AERONET particle volume size distribution. The AERONET size distribution is given in 22 radius bins without being fitted (Figure 5). The fit to a lognormal size distribution, made internally in AERONET and not a posteriori by the authors, is the only way to quantify both the volume concentration and median radius of each of the two size modes.

Captions need to define what is given in the figure and text provide interpretation. Paper need to be revised to do this. Caption do not define what is in the figure and text contains some of this information.
Authors' reply: Please see answer from 2 comments above!

Conclusion states that the frequency and intensity increases along the NE-SW axis; however, paper does not present anything that address if it is the frequency or intensity that gives the gradient. Why is it both, why not just one ot the other.
Authors' reply: As said in our general comments, an aerosol classification method has been applied to AERONET measurements and the revised manuscript counts now with information on the frequency and intensity of mineral dust and pollution events for each season of the year at both Ersa and Palma (Section 5.3, Figure 6 and Table 2).

Conclusion states that AOD and ARF annual cycles are well correlated. How could this be otherwise. AOD is major factor in ARF so they have to be correlated. How is this a conclusion of the paper. It just follows from the equation to calculate ARF.
Authors' reply: The conclusions have been totally re-written and this statement was deleted.

Page 37, line 27. "This result" be direct and state what is being talked about. Do not understand this conclusion.
Authors' reply: The conclusions have been totally re-written.

Paper does not define what is needed for gradient in the summer means? Seems to be a decrease along all three sites. Looking at 18 parameters, and getting 6 to show this seems to be just the result of luck. Most parameters are with in the standard deviation. How unlikely is it to get this result be chance assuming the values are randomly distributed?
Authors' reply: This Section of the initial version has been deleted in the revised manuscript.

Paper states repeatably that gradient is related to higher frequency and intensity. It would be nice to know how frequency and intensity contribute. Is the northerly site frequency of dust events that is important and the intensity the same or is the frequency similar and intensity less?
Authors' reply: Please see answer from 2 comments above!

Paper really lack data for a long-term climate average. There is only the last half of 2012 where all three sites have data. This is where the treads need to be computed from. Don't mix data

from different time periods, the data set is not long enough. For example, on Page 38, line 18, states that "we have observed a homogeneous spatial distribution (except during the month of March and April) of the fine particle loads over the three sites". How is this possible, figure 2 indicates the there is no data in March for one of the sites. Hence, the data does not support the conclusions of the paper.

Authors' reply: This sentence in particular has been deleted in the revised manuscript. Please see the paragraph "Representativeness of the AERONET dataset considered in the paper" in our general comments where we explained how we enlarged the database and how we checked the representativeness of Palma database which is shorter than the Ersa one.

Paper lacks focus, tries to confuse the reader with a lot of plots that don't contribute to the paper's conclusions. I see nothing in the paper that is not better supported by other papers; hence nothing new.

Authors' reply: We are sorry for the confusion. The novelty of the revised manuscript lies in the analysis of absorption properties (AAOD, AAE, SSA, RRI and IRI) separately for mineral dust and pollution and for the total (mineral dust + pollution) and in the validation of AERONET radiative fluxes at the top of the atmosphere.

I would suggest just focusing on the time period when there is data from all three sites and determining to what extent frequency and intensity contributes to different in AOD for dust events. Another option is just focus on two sites and the time period of them sites. It is confusing to include both.

Authors' reply: In the revised manuscript we present the two options suggested by the referee: 1) comparison at two sites of monthly and seasonal means of all AERONET products available during the 5-year period 2011-2015 (as said in our general comments Year 2015 was added to the dataset in the revised manuscript); 2) a short case study (2 pages) of temporally coincident measurements at the 3 sites. Alborán data are just in the case study.

The Solar Radaitive forcing comparison should be in it's own paper.

Authors' reply: Validating the aerosol forcing at the TOA has appeared to us a necessity to follow on with the discussion on the AERONET forcings at the TOA. We are planning a new paper on the validation of AERONET forcings at the TOA at more sites and with longer data series.

The pyranometer measurements don't seem to be openly available. Also, none of the software used in the analysis is openly available. The lack of data and software make it impossible to reproduce results. Furthermore, the method used is not fully described.

Authors' reply: The pyranometer measurements were taken from the Solar Radiation Network (SolRad-Net) Data Display at http://solrad-net.gsfc.nasa.gov/cgi-bin/type_one_station_flux?site=Barcelona&nachal=0&year=17&aero_water=0&level=1&if_day=0&shef_code=P&year_or_month=1, and are openly available.

The graphical method used to assess the aerosol classification has been thoroughly described and referenced in the text.

For generating monthly and seasonal figures, we did not use any particular software. We made use of simple Matlab routines, written by ourselves, to read AERONET text format files (*.lev20, *.dubovik, etc.) and to calculate monthly means, seasonal means, standard deviations, number of points, etc.

Figures and Captions: Figure 2: y-axis labels should have same accuracy. Hence 1.0 and not 1. 'Year' text is way too small, likewise 1.82 text.

Authors' reply: We made an effort to enlarge all sub-figures' fonts (titles, axis labels and legends). We have used by default a font size of 22 for the titles, and 20 for the axis labels and

legends. In some sub-figures the legend font size was reduced because of too little space available in the sub-figure. However, once inserted in one of the figure of the revised manuscript, all font sizes do not appear the same because each sub-figure is reduced differently depending on the number of sub-figures contained in the figure.

Figure 3: Month font is too small. Use solid circles. Give y-axis labels to same scale.
Authors' reply: The font size of "Month" has been enlarged. All circles have been replaced by solid circles (except in Fig. 9, in order to be able to distinguish circles that almost overlap). Y-axis scales was set equally in the new figures of AOD and AOD^f.

Figure 4: All fonts too small. Can't read or understand figure.
Authors' reply: Please see answer from 2 comments above!

Figure 5: All fonts too small. Either the label or the units are wrong on the figure. It is either dV/dr [umˆ3/umˆ-2] or dV/dlnr [umˆ3]. How are these volume size distribution determined? What months make up the season? How are the averages determined?
Authors' reply: The authors would like to refer to the document available online at http://aeronet.gsfc.nasa.gov/new_web/Documents/Inversion_products_V2.pdf which describes the AERONET inversion products. In the text it is referenced as AERONET (2016). There, we find the definition of the particle size distribution in terms of volume concentration dV(r)/dln(r) as a function of the number concentration dN(r)/dln(r) (Eq. 2):

$$\frac{dV(r)}{dln(r)} = V(r)\frac{dN(r)}{dln(r)}$$

This quantity is usually expressed in $\mu m^3 \cdot cm^{-3}$.
In the case of a discrete size distribution (which is the case of the one of AERONET), the volume concentration is not given for a single value of *r*, but for an interval Δr, hence the unit of $\mu m^3 \cdot cm^{-2}$ which is later converted to $\mu m^3 \cdot \mu m^{-2}$. Strictly speaking one should define the volume concentration as dV(r)/dln(r) * Δr, however it never appears this way in the literature.
The total volume concentration is the integral (the sum in case of a discrete size distribution) of dV(r)/dln(r) over the full range or radii (Eq. 5).

Figure 6: All fonts too small. Use same accuracy of the y-axis values.
Authors' reply: Please see answer from 4 comments above!

Figure 7: All fonts too small. The values are wrong. Can't be a values up to 10,000, must be 10ˆ-3 not 10ˆ3.
Authors' reply: 10^3 was replaced by 10^{-3} in the revised manuscript.

Figure 8 All fonts too small.
Figure 9 All fonts too small.
Figure 10 All fonts too small.
Figure 11 All fonts too small.
Figure 12 All fonts too small.
Authors' reply: According to the font, please see answer from 6 comments above!

Detailed Comments:
Page 5, Line 22-23: Please don't use acronyms WMB, just spell out.
Authors' reply: The acronym WMB for the western Mediterranean Basin was deleted in the revised manuscript.

Page 6, Line 6-21: Delete, no point in just stating what will be talked about. Section headers handle this and a well organized paper.

Authors' reply: The authors believe that the presentation of the structure of the paper at the end of the introduction helps in understanding the focus and objectives of the paper. Many scientific papers, probably a majority, and including ACP, follow this way of doing. The paper organization was kept in the revised manuscript.

Page 6, Line 26: Sites are not on a North-South axis. Seems that you would want sites close to the North African desert region and one far away.
Authors' reply: The sites are aligned along a Northeast – Southwest axis, and the text says "approximately aligned on a North–South axis". The criterion was to have sites at decreasing latitude along a North–South axis.

Page 8, Kine 9: Official reference to Web sites should be given instead of http references in the text.
Authors' reply: Such references have been added in the revised manuscript following ACP guidelines.

Page 8, Line 11: Author really don't understand the data they are analyzing as evident by saying, "the wavelengths at which the almucantar scans are performed." Scans are not done at a wavelength. Filters are used to get these wavelengths.
Authors' reply: This sentence has been replaced in the revised manuscript by: "All the inversion products spectrally resolved are given at 440, 675, 870 and 1020 nm."

Page 8, Line 16, define SZA.
Authors' reply: SZA= Solar Zenith Angle. It is defined the first time Solar Zenith Angle appears in the text in page 6.

Page 8, Line 16-18. These restriction to AOD above certain values need to be given in the caption of figures.
Authors' reply: The restrictions on the data presented have been added in all figures' captions.

Page 11, Line 1-6. Good to label the Azores, Bay of Biscay and Gulf of Lion in figure 1. There is wet and dry scavenging. Not clear what is being talked about.
Authors' reply: Bay of Biscay and Gulf of Lion have been added in Fig. 1. We refered to "wet scavenging". It has been specified in the text.

Page 11, Line 26: Space between value and km.
Authors' reply: Done!

Page 13, Line 1: "by the same authors, found in the same range that those for other suburban sites in Spain, suggests an important regional contribution of such aerosols" Be direct, state authors name, the range, what "such aerosol"?
Authors' reply: This sentence has been totally re-written and now says: "Carbonaceous aerosols in Mallorca have been found by Pey et al., (2009) in the same range that those in other suburban sites in Spain, which suggests an important regional contribution of carbonaceous aerosols."

Page 13, Line 15: Where does this dust event frequency come from? Paragraph is out of place.
Authors' reply: This sentence has been deleted in the revised manuscript.

Page 13, Line 20: Captions need to define the figure and text provide interpretation. Paper need to be revised to do this. This line is just one example of material that need to be in caption not in the text.

Authors' reply: We have tried as much as possible to be more direct in the text with the interpretation putting the reference to the figures and tables between parentheses. We also believe that presenting briefly (in less than 1 line) the next figure allows to make a smooth transition between two sections or two paragraphs.

Page 13, Line 25: Can't see annual cycle in figure only the maximum values. Not sure why figure 1 is included. Can just state time period of analysis. No point in figure. Remove or provide some reason for time series figure.
Authors' reply: Figure 2 has been removed in the revised manuscript.

Page 14, Line 2-3: it would be nice to have some analysis showing exactly how often and how much less the intensity differences between the slights. Seem this is a major objective of the paper.
Authors' reply: This question is answered in the revised manuscript thanks to the aerosol classification assessed on the AERONET level 2.0 inversion products. We refer here again the referee to our general comments and in particular to the paragraph "Frequency/intensity of the high AOD events".

Page 14, Line 16-18: What years are these summer averages over. One site only had one year of data. Should not the comparison be for the same time periods. Also, with the large standard deviations, I don't see how you can say there is a gradient. Taking into account the standard deviations, the values are the same.
Authors' reply: It is now indicated in the caption of Table 1. These values are the annual mean of all instantaneous measurements available in the period 2011-2015.
Alborán is not included anymore in the discussion of the monthly and seasonal variations.
For the representativeness of Palma data see the paragraph "Representativeness of the AERONET dataset considered in the paper" in our general comments. The standard deviations are of the same order of magnitude at Ersa and Palma. So we do believe that their magnitude is caused more by the natural variability of AOD at both sites, especially during the seasons with high number of strong dust and pollution events, than by a low statistics.

Page 14, Line 22: I don't see how there is a difference in the seasonal cycle. Need to provide standard deviations. Cycle look the same to me.
Authors' reply: There is indeed no annual cycle visible on the monthly AE. We have used the word "pattern" and by "different seasonal patterns" we mean that the monthly variations at both sites have different "shapes". The standard deviations have been added in the figure.

Page 15, Line 1-2: Don't see the clear gradient. Large standard deviations. Again, is this for the same time period or different.
Authors' reply: This statement has been deleted in the revised manuscript. In general we do not talk anymore about NE-SW gradients in the most part of the paper since it is based only on two sites (Ersa and Palma). Instead of gradient we talk about differences and Table 1 reveals a difference between Ersa and Palma (higher AE at Ersa than at Palma) during all season but especially during spring-summer-autumn, which is briefly commented.
The AE data are treated the same way than the AOD: the monthly means are computed from instantaneous values available in the period 2011-2015. It is clearly stated in the caption of Table 1.

Page 35, line 10: If data from all three sites are required for the gradient, why not just look at the summer of 2012 so the data is comparable. Why includes additional summer values for two of the sites?

Authors' reply: As said in a previous answer: the paper has been totally re-structured with 1) the comparison at two sites of monthly and seasonal means of all AERONET products available during the 5-year period 2011-2015; and 2) a short case study (2 pages) of temporally coincident measurements at the 3 sites. Alborán data are just used in the case study.

Page 35, line 15-20: The parameters analyzed are not independent. SSA and RRI/IRI are related for example. The percentage of parameters that are intensive and extensive are not useful because the parameters are not independent. Also, done of the parameters show a gradient above the standard deviation of the measurements. I suggest that a randomly generated data set would give gradients by looking at parameters using this analysis.
Authors' reply: This section has been removed in the revised manuscript.

Figures and Captions:
Figure 1: Figures are independent of text so all acronyms need to be defined. What is WMB? Define SW and NE. Give credit that this image was made using Google Earth.
Authors' reply: We have defined as much as possible the acronyms used in the figure captions. Credit to Google Earth has been added in the figure caption.

Figure 2: N is number of points but for what? Define AOD and give what time period the measurement is over. Is it an instantaneous measurement of an average? Can only tell the maximum values from plot. Box-and-whisker plots for a week or month would give far more information. Easy to make plot that does not show much information.
Authors' reply: Fig. 2 (of the initial submission) has been removed in the revised manuscript according to referee #2's ssuggestions.

Figure 3: Define acronyms. Monthly average of what time period measurements?
Authors' reply: We have defined as much as possible the acronyms used in the figure captions. The time period has been indicated in the figure caption.

Figure 4: Define acronyms. Define better what the box-and-whisker represent. Minimum and maximum values are defined twice. Season in legend should start with capital letter.
Authors' reply: We have defined as much as possible the acronyms used in the figure captions. All box-and-whisker plots were removed in the revised manuscript. The seasons are defined in the text at the end of Section 3, and were replaces by the first letter in capital of the months forming each season (e.g. summer, i.e. June-July-August = JJA). This nomenclature presents 2 advantages: it is shorter and it is a time reference independent of the Earth hemisphere the reader lives in.

Figure 5: Need to provide more caption information.
Authors' reply: All figure captions have been written with more details.

Figure 6: Don't understand what is the "Same as Figure 4:. Finally, a acronym that is defined RRI, why define this one and not all the others. Where do these measurements come from? How are they determined?
Authors' reply: In the revised manuscript Fig. 3 is the same than Fig. 2 but for another site. However we have followed the referee advice and repeat entirely the figure caption. In all figure captions the measurements used are specified.

Figure 7: Don't understand what is the "Same as Figure 4:. Please just provide the information in the caption. Why confuse the reader?
Figure 8: More details to describe what is in the figure.
Figure 9: More details to describe what is in the figure.

Authors' reply: Please see the previous answer!

Figure 10: Define what a data point is on this plot. How large of an area is the CERES data? What time duration of AERONET data.

Authors' reply: The nominal footptint of CERES is 20km. This can be checked in the CERES web page at https://ceres-tool.larc.nasa.gov/ord-tool/products?CERESProducts=SSFlevel2 in the Spatial Resolution submenu that applies for the TOA fluxes that we downloaded. It was indicated in the initial submission paper in page 27, line 12-13: "for a spatial resolution equivalent to its instantaneous footprint (nadir resolution 20 km equivalent diameter)".

All measurements (pyranometer, AERONET and CERES) are instantaneous measurements. At the surface we compared the closest pyranometer and AERONET measurements within ± 1 min. At the TOA we compared the closest CERES and AERONET measurements within ± 15 min. This is already stated in the initial submission at page 27, line 4 and 16.

The caption of Fig. 9 has been further detailed and now it also mentions the time difference allowed between observed and AERONET fluxes.

Figure 11: Monthly data is given, not seasonal as stated in caption. Define acronyms. Again, how is the data determined?

Authors' reply: "Monthly" now replace "Seasonal". Thank you! Acronyms have been defined and the origin of the data has been explicitly indicated.

Figure 12: Define what time period summer is. Define acronyms.

Authors' reply: Figure 12 (in the initial submission) has been removed in the revised manuscript. The seasons are now defined in the text at the end of Section 3.

Aerosol optical, microphysical and radiative properties at ~~three~~ regional background insular sites in the western Mediterranean ~~Basin~~

Michaël Sicard[1,2], Rubén Barragan[1,2], François Dulac[3], Lucas Alados-Arboledas[4,5], Marc Mallet[6]

[1]Remote Sensing Laboratory, Universitat Politècnica de Catalunya, Barcelona, Spain

[2]Ciències i Tecnologies de l'Espai - Centre de Recerca de l'Aeronàutica i de l'Espai / Institut d'Estudis Espacials de Catalunya (CTE-CRAE / IEEC), Universitat Politècnica de Catalunya, Barcelona, Spain

[3]Laboratoire des Sciences du Climat et de l'Environement, (IPSL/LSCE), CEA-CNRS-UVSQ, Université Paris-Saclay, Gif-sur-Yvette, France

[4]Dpt. Applied Physics, Faculty of Sciences, University of Granada, Granada, Spain

[5]Andalusian Institute for Earth System Research (IISTA-CEAMA), Granada, Spain

[6]Laboratoire d'Aérologie, Université de Toulouse / CNRS, Toulouse, France

Correspondence to: msicard@tsc.upc.edu

Abstract

In the framework of the ChArMEx (the Chemistry-Aerosol Mediterranean Experiment, http://charmex.lsce.ipsl.fr/) program, the seasonal variability of the aerosol optical, microphysical and radiative properties derived from AERONET (Aerosol Robotic Network; http://aeronet.gsfc.nasa.gov/) is examined in two regional background insular sites in the western Mediterranean Basin ~~(WMB)~~: Ersa (Corsica Island, France) and Palma de Mallorca (Mallorca Island, Spain). A third site, ~~in~~ Alborán (Alborán Island, Spain), with only a few months of data is considered for ~~exploring~~examining ~~the~~ possible Northeast–Southwest (NE–SW) gradients of the aforementioned aerosol properties. The AERONET dataset is exclusively composed of ~~AERONET (Aerosol Robotic Network;)~~level 2.0 inversion products available

Con formato: Fuente de párrafo predeter., Alemán (Alemania)

during the~~a~~ f~~our~~ive-year period (~~2011-2014~~5). AERONET solar radiative fluxes are validated with ground- and satellite-based flux measurements. To the best of our knowledge this is the first time that AERONET fluxes are validated at the top of the atmosphere. The main drivers of the observed annual cycles and NE–SW gradients are 1) mineral dust outbreaks in spring in the North and in summer in the South, and 2) European pollution episodes in autumn. A NE–SW gradient exists in the western Mediterranean Basin for the aerosol optical depth and especially its coarse mode fraction, which all together produces a similar gradient for the aerosol direct radiative forcing. The aerosol fine mode is rather homogeneously distributed. Absorption properties are quite variable because of the many and different sources of anthropogenic particles in and around the western Mediterranean Basin: North African and European urban areas, the Iberian and Italian Peninsulas, forest fires and ship emissions. As a result the aerosol direct forcing efficiency, more dependent to absorption than the absolute forcing, has no marked gradient.

~~Products such as the aerosol optical depth (AOD), the fraction fine mode to total AOD, the particle size distribution, the sphericity, the radiative forcing and the radiative forcing efficiency show a clear annual cycle. The main drivers of the observed annual cycles are mineral dust outbreaks in summer and the transport of European continental aerosols in spring. A NE–SW gradient is observed on 6 parameters (3 extensive and 3 intensive) out of the 18 discussed in the paper. The NE–SW gradient of the AOD, the Ångström exponent, the coarse mode volume concentration, the sphericity and the radiative forcing at the surface are related to mineral dust outbreaks, while the NE–SW gradient of the coarse mode volume median radius is related to the decreasing influence of European continental aerosols along the NE–SW axis. The fact that two thirds of the parameters discussed in the paper do not present a NE–SW gradient is partly explained by two relevant findings: 1) a homogeneous spatial distribution of the fine particle loads over the three sites in spite of the distances between the sites and the differences in local sources, and 2) low values and the absence of spectral dependency of the absorption found in the southwesternmost site.~~

Short summary

The seasonal variability of the aerosol optical, microphysical and radiative properties at ~~three~~ two insular sites in the western Mediterranean Basin is presented based on AERONET Level 2.0 data. The AERONET-derived surface and top of atmosphere radiative fluxes are validated with ground-based and satellite data, respectively. The main drivers of the observed annual

cycles and NE–SW gradients are 1) mineral dust outbreaks in spring in the North and in summer in the South, and 2) European pollution episodes in autumn ~~mineral dust outbreaks in summer and European continental aerosols in spring~~. The lack of NE–SW gradients of some aerosol properties is attributed to: a homogeneous spatial distribution of the fine particle load and a large variability of the absorption ~~low values in the southwesternmost site~~properties.

1 Introduction

Climate change projections identify the Mediterranean region as a climatologically sensitive area especially vulnerable to global change (Giorgi, 2006; Giorgi and Lionello, 2008). General and regional climate models simulate ~~for the Mediterranean Basin~~ significant changes in the water cycle of the Meditterranean region, a substantial precipitation decrease and a temperature increase before the end of the century (Sanchez-Gomez et al., 2009; Mariotti et al., 2015). Atmospheric aerosols are one of the factors that influence the Mediterranean climate ~~change~~ through their impact on the radiation budget (Markowicz et al., 2002; Nabat et al., 2014; 2015). Specifically, atmospheric aerosols influence the Earth's energy budget both directly, because they absorb and scatter solar and terrestrial radiation, and indirectly, because they act as cloud condensation nuclei modifying the structure and the properties of clouds (Twomey, 1974; Albrecht, 1989; Pincus and Baker, 1994). How those impacts distribute themselves in space and time over the greater Mediterranean Basin remains an open question (Mallet et al., 2016~~5~~, ~~this special issue~~).

The columnar amount of atmospheric aerosol, which can be quantified by the aerosol optical depth (AOD), has a direct effect on the solar and infrared radiation reaching the Earth's surface. An increase or decrease ~~of~~in AOD can result in enhanced or reduced solar radiation at the surface, an effect that Norris and Wild (2007) called solar "brightening" and "dimming", respectively. For that reason the AOD is often used to quantify the aerosol impact on the surface solar radiation. Numerous studies documenting the spatial variability of the AOD over the Mediterranean Basin are based on long time series of satellite-based observations (Barnaba and Gobbi, 2004; Papadimas et al., 2008; Nabat et al., 2012; 2013, among others) and in a lesser extent on ground-based remote sensing observations (Mallet et al., 2013; Lyamani et al., 2015, among others). The temporal variability of the AOD over the whole Mediterranean Basin has been assessed for the first time by Papadimas et al. (2008) ~~with~~ using the AOD retrieved at ~~the wavelength of~~ 550 nm and the ~~fraction of~~ fine mode fraction ~~to~~ of total AOD products (both

over land and ocean) of the Moderate Resolution Imaging Spectroradiometer (MODIS) instrument during the period 2000-2006.

Although the AOD is a key parameter to understand the variability of the aerosol impact on the Earth's energy budget, its analysis is not enough to assess this variability at the scale of the Mediterranean Basin because of the great complexity of the aerosol composition and distribution over the Basin. Bounded to the North by the European continent and to the South by the African continent, the ~~Basin~~ Mediterranean atmosphere is largely affected by maritime ~~aerosols~~particles, urban/industrial aerosols from European and North African urban areas, extreme biomass burning episodes and mineral dust from North African arid areas. Anthropogenic particles emitted from ship traffic are also present all-year round while biomass burning aerosols from forest fires from both European and African continents are limited to the summer season. A detailed list of long term analyses or case studies about one or several types of those aerosols can be found in Mallet et al. (2016~~5, this special issue~~). All those aerosol types have very different optical, microphysical and radiative properties. Consequently, in addition to the AOD, other parameters like the absorption properties, the size of the particles, their shape, etc. are needed to assess the variability of the aerosol impact on the Earth's energy budget at the scale of the Mediterranean Basin.

In this study we perform a seasonal analysis of the aerosol optical, microphysical and radiative columnar properties at two regional background insular sites ~~in Ersa~~at Ersa (Corsica, France) and Palma de Mallorca (Mallorca, Spain) ~~over~~ with data from a recent period ~~a four-year period~~ (2011-2015~~4~~). ~~By complementing this dataset with a few months of measurements in the remote island of Alborán (Spain) we obtain the gradient of the aerosol properties on a northeast – southwest (NE–SW) axis in the middle of the western Mediterranean Basin (WMB).~~ The dataset is exclusively composed of AERONET (Aerosol Robotic Network; http://aeronet.gsfc) level 2.0 inversion products. Insular sites were selected in order to determine the properties of aerosols representative of the whole basin minimizing local influences. ~~Insular sites were selected in order to minimize the influence of local, non-natural aerosols.~~ The choice of the western Mediterranean ~~WMB~~ Basin was motivated by the ChArMEx (the Chemistry-Aerosol Mediterranean Experiment, http://charmex.lsce.ipsl.fr/) program~~. ChArMEx~~ which is a collaborative research program federating international activities to investigate Mediterranean regional chemistry-climate interactions. One of the goals of ChArMEx is precisely to improve our knowledge of the potential impacts of aerosols over the Mediterranean Basin (Dulac et al., 2014; Mallet et al., 2016). In its implementation strategy ChArMEx proposes Enhanced Observation Periods (EOP) to study the daily to seasonal scale variability of several parameters

measured at several sites and to monitor East–West and North–South gradients over a period of 2-3 years. The AERONET sun-photometer from Ersa was deployed in that framework. In order to examine possible North–South gradients over the whole western Mediterranean Basin, and not only in its northern part, we complement the dataset with five months of coincident measurements in 2011 in the remote island of Alborán (Spain) between Spain and Morocco.

The paper is organized as follows: Section 2 of the paper presents the three sites, the dataset and details all the AERONET products used in the paper and their associated accuracy. The methodology used to perform a tentative aerosol classification is presented in Section 3. A atmospheric dynamics of the region is addressed in Section 4 with a general regional description in Section 4.1 and peculiarities of the geographical and atmospheric conditions as well as the aerosol loading specific to each of the three sites in Section 4.2. Differences in aerosol optical properties between Ersa and Palma are discussed in Section 5: in terms of monthly variations of the total AOD, Ångström exponent and fine mode fraction of total AOD (Section 5.1), and particle volume size distribution (Section 5.2) and seasonal variation of the aerosol absorption optical depth, absorption Ångström exponent and the refractive index (Section 5.3), and single scattering albedo and asymmetry factor (Section 5.4). In order to go one step further, we also analyze the AERONET products of aerosol radiative forcing (Section 6). We first validate the fluxes estimated by AERONET with ground- and satellite-based flux measurements (Section 6.1) and then present the monthly variations of the aerosol radiative forcing and of the aerosol radiative forcing efficiency at both sites (Section 6.2). In addition, a discussion is proposed in Section 7 on the possible North–South gradients of the aerosol properties based on five months of coincident measurements in 2011 at Ersa, Palma and Alborán. Finally, conclusions are proposed in Section 8.

2 Sites and instrumentation

2.1 Sites

The sites selected for this analysis had to fulfill the following criteria: to be located in the western Mediterranean Basin, to be insular sites in order to be representative of aerosol regional

background conditions, to be approximately aligned on a North–South axis and to have a recent long-term database (≥ 2 years). At the same time we wanted to take advantage of the ChArMEx EOP (2–3 years) in the framework of which a supersite was installed at the northern tip of Corsica Island (France), at Ersa (Lambert et al., 2011; Dulac et al., 2014, Mallet et al., 2016). In that site, situated at 43.00ºN, 9.36ºE, 80 m asl (above sea level), an AERONET sun-photometer is operated since June 2008. According to the AERONET Data Display Interface and applying the above mentioned criteria the second site that was selected is Palma de Mallorca in the Balearic Islands (Spain) situated at 39.55ºN, 2.62ºE, 10 m asl, and operated since August 2011. Both sites are on the Northeast–Southwest (NE–SW) axis, a major route for dust transport in the western Mediterranean Basin (Moulin et al., 1998). In the last Section of the paper, a third site considered for examining possible NE–SW gradients is Alborán (Spain, 35.94ºN, 3.04ºW, 15 m asl) situated East of Gibraltar midway between the Spanish and the Moroccan coasts. There, an AERONET sun-photometer was operated for a rather short period of time, between June 2011 and January 2012, thanks to collaboration between the Atmospheric Physic Group of the University of Granada and the Royal Institute and Observatory of the Spanish Navy. Indeed all three sites, reported in **Figure 1**, fall onto a quasi-perfect NE–SW straight line and Palma, situated in the middle, is approximately equidistant to both Ersa (~670 km) and Alborán (~640 km).

2.2 AERONET sun-photometers and products

AERONET is a federated network of ground-based sun-photometers (Holben et al., 1998) which retrieves global aerosol columnar properties. Along with aerosol optical depths at several wavelengths λ, (AOD_λ), AERONET products are the Ångström exponent (AE) between pairs of wavelengths, the precipitable water vapor and the total, fine and coarse mode AOD at 500 nm derived from the Spectral Deconvolution Algorithm (SDA), from which the fine/coarse mode fractions can be calculated (O'Neill et al., 2001; 2003).

$$AE_{\lambda_1-\lambda_2} = -\frac{\ln\left[\frac{AOD_{\lambda_1}}{AOD_{\lambda_2}}\right]}{\ln\left[\frac{\lambda_1}{\lambda_2}\right]} \quad (1)$$

Con formato: Sangría: Primera línea: 0 cm, Espacio Antes: 6 pto, Ajustar espacio entre texto latino y asiático, Ajustar espacio entre texto asiático y números

Further AERONET inversion data products include volume size distribution, the spectral complex refractive index (real and imaginary), the spectral aerosol absorption optical depth, the spectral single scattering albedo, the spectral asymmetry factor, the spectral phase function and the sphericity, i.e. the volume fraction of spherical particles (Dubovik et al., 2000a; 2002a; 2006; Sinyuk et al., 2007). A series of assumptions are made to perform the inversion of those parameters. They can be found in the AERONET Version 2 Inversion Product Descriptions (AERONET, 2016) ~~at http://aeronet.gsfc.nasa.gov/new_web/Documents/Inversion_products_V2.pdf~~. All the inversion products spectrally resolved are given at 440, 675, 870 and 1020 nm~~, the wavelengths at which the almucantar scans are performed~~.

The data shown in this work are based on AERONET level 2.0, cloud-screened and quality-assured data (Smirnov et al., 2000) inverted with the AERONET Version 2.0 retrieval algorithm (Holben et al., 2006). In practice the main differences between Version 1.0 and Version 2.0 are the additional criteria applied in Version 2.0 on: the solar zenith angle (SZA; $-50 < SZA < 580^{o}$ for all products) and the AOD at 440 nm ($AOD_{440} > 0.4$ for the aerosol absorption optical depth, the single scattering albedo and the real and the imaginary parts of the refractive index; $AOD_{440} > 0.2$ for the sphericity). The accuracy of AERONET Version 2.0, level 2.0 inversion products is evaluated and discussed in Dubovik et al. (2000b; 2002b) and the additional criteria for Version 2.0 retrieval in Holben et al. (2006). The accuracy of some products has been estimated with numerical sensitivity tests for different aerosol types, namely water-soluble, dust and biomass burning (Dubovik et al., 2000b).

- The estimated accuracy of AOD_{λ} is ±0.02 (Eck et al., 1999).
- The accuracy of the Ångström exponent is estimated to be ±0.25 for $AOD_{440} \geq 0.1$ and of the order of 50 % for $AOD_{440} < 0.1$ (Toledano et al., 2007).
- The accuracy of the volume size distribution is estimated to be: 15 % for water-soluble, 35 % for dust and 25 % for biomass burning in the intermediate particle size range ($0.1 \leq$ radius $r \leq 7$ µm); and 15-100 % for water-soluble, 35-100 % for dust and 25-100 % for biomass burning for the edges ($0.05 \leq r < 0.1$ µm and $7 < r \leq 15$ µm).
- The accuracy of the real (imaginary in %) part of the refractive index is estimated to be ±0.025 (50 %) for $AOD_{440} > 0.2$ for water-soluble and ±0.04 (50 and 30 %, respectively) for $AOD_{440} \geq 0.5$ for dust and biomass burning.

Con formato: Subíndice

Con formato: Subíndice

- The retrieved aerosol absorption optical depth at wavelength λ ($AAOD_\lambda$) has an accuracy of ±0.01 at λ ≥ 440 nm.
- The accuracy of the single scattering albedo at wavelength λ (SSA_λ) is estimated to be ±0.03 for AOD_{440} > 0.2 for water-soluble and for $AOD_{440} \geq 0.5$ for dust and biomass burning.
- The uncertainty of the asymmetry factor at wavelength λ (g_λ) ~~uncertainty~~ ranges between ±0.03 and ±0.08 for pollution and biomass burning aerosols and is ±0.04 for desert dust particles.

It is important to note that some products such as the AAOD, the real and the imaginary parts of the refractive index and the SSA are retrieved only if the criteria~~a~~on AOD_{440} > 0.4 is fulfilled. Such aerosol loads are generally associated to desert dust ~~events~~outbreaks or severe pollution episodes (Gkikas et al., 2012; 2016).

Other parameters of interest for this work delivered by the AERONET inversion algorithm are the instantaneous solar broadband (0.2 – 4 μm) downward and upward fluxes, as well as the aerosol radiative forcing and radiative forcing efficiency at the surface and at the top of the atmosphere. A brief description on how the fluxes are calculated is given ~~at http://aeronet.gsfc.nasa.gov/new_web/Documents/Inversion_products_V2.pdf~~in the AERONET Version 2 Inversion Product Descriptions (AERONET, 2016). The gaseous absorption is calculated by the GAME (Global Atmospheric Model) radiative transfer model (Dubuisson et al., 1996). We consider all instantaneous measurements available.

~~Table 1 indicates the availability of AERONET inversions at the three sites during the period 2011-2014. At Ersa almost all months are represented at least three times (except November and December), while at Palma all months are represented at least twice (except the first four months of the year).~~

3 Methodology

The methodology used to classify the aerosols based on AERONET level 2.0 inversion products is the graphical method from Gobbi et al. (2007). The Ångström exponent, calculated between two wavelengths λ_1 and λ_2, $AE_{\lambda_1-\lambda_2}$, and defined as

Código de campo cambiado

$$AE_{\lambda_1-\lambda_2} = -\frac{\ln\left[\frac{AOD_{\lambda_1}}{AOD_{\lambda_2}}\right]}{\ln\left[\frac{\lambda_1}{\lambda_2}\right]}, \quad (1)$$

is commonly used as a good indicator of the dominant size of the atmospheric particles contributing to the total AOD: values of AE < 1 indicate size distributions dominated by coarse mode aerosols (radii > 0.5 μm) while values of AE > 1.5 indicate size distributions dominated by fine mode aerosols. When different aerosol types are present in the atmospheric column, AE does not provide information on the relative contribution of coarse and fine mode particles. For this reason, the Ångström exponent difference is introduced and the Gobbi et al. (2007) method consists in ~~visually converting~~deriving the Ångström exponent ($AE_{440\text{-}870}$) and the Ångström exponent difference ($\delta AE = AE_{440\text{-}675} - AE_{675\text{-}870}$), defined as a measure of the Ångström exponent curvature, $dAE/d\lambda$, ~~to both~~ the fine mode aerosol radius and the contribution of the fine mode aerosol to the total AOD. Several authors have investigated how the spectral variation of AE can provide further information on the aerosol size distribution (Schuster et al., 2006, and references therein). In particular Kaufman (1993) pointed out that negative values of $AE_{440\text{-}613} - AE_{440\text{-}1003}$ indicated the dominance of fine mode particles, while positive differences indicated the effect of two separate modes with a significant coarse mode contribution. The graphical method developed by Gobbi et al. (2007) uses these complementarities between AE and δAE. The method has been applied, among others, by (i) Gobbi et al. (2007) at sites characterized by high pollution, biomass burning and/or mineral dust concentrations; (ii) Basart et al. (2009) to quantify the contribution of mineral dust on a yearly basis at sites in and around the Sahara – Sahel region; and (iii) Perrone et al. (2014) to distinguish between mostly pollution and mineral dust in Lecce, Italy.

Instantaneous values of the Ångström exponent difference vs. the Ångström exponent (δAE, AE) are plotted on a classification framework with reference points determined for a variety of fine mode (r_f^f) and coarse mode (r^c) radii and of fine mode fractions of total AOD (η). To this end, Mie calculations were performed to calculate the aerosol spectral extinction coefficients for r_f^f values of 0.05, 0.1, 0.15, 0.2, 0.3 and 0.5 μm, for r_f^c values of 0.75, 1, 2, and 4 μm, and η fractions of 1, 10, 30, 50, 70, 90 and 99 %, assuming a bimodal, lognormal size distribution. Each (δAE, AE) grid point is obtained as the average of the four pairs obtained for the four r_f^c values. The grid used in this paper was taken from Gobbi et al. (2007) with a refractive index of 1.4-0.001*i*, typical of urban/industrial aerosols, in order to both provide a common reference and address the relative changes (fine mode growth/hydration or coarse particle growth/cloud

Código de campo cambiado

Con formato: Superíndice

Con formato: Superíndice

Con formato: Superíndice

Con formato: Superíndice

Con formato: Fuente: Sin Negrita

contamination, see Gobbi et al. (2007) for definition) at each location. As suggested by Gobbi et al. (2007), the condition $AOD_{675} > 0.15$ has been applied on all the (δAE, AE) plots in order to guarantee errors less than 30 % on δAE. The values of δAE in Table 1 are also given with this criterion: $AOD_{675} > 0.15$. Note, however, that the AOD plotted in the (δAE, AE) plots of the paper is AOD_{440} (and not AOD_{675}) in order to be directly comparable with the AERONET criteria based on AOD_{440}.

The seasonal variations shown in the paper are made for the following four seasons: summer (JJA, June-July-August), autumn (SON, September-October-November), winter (DJF, December-January-February) and spring (MAM, March-April-May).

4 Atmospheric dynamics

4.1 Atmospheric dynamics of the ~~WMB~~western Mediterranean Basin

The Mediterranean region features an almost enclosed sea surrounded by very urbanized littorals and important mountain barriers. The gaps between the major mountainous regions act as channels for the air mass transport toward the Mediterranean Basin which constitutes a crossroads of air masses carrying aerosols from different natural and anthropogenic sources (Lelieveld et al., 2002). In particular in the ~~WMB~~western Mediterranean Basin those channels are the Strait of Gibraltar and the Ebro Valley in Spain, the Rhône Valley in France and the Po valley in Italy. The atmospheric dynamics of the ~~WMB~~western Mediterranean Basin is mainly governed by the extended subtropical anticyclone of the Atlantic (Azores anticyclone) and can be roughly divided into cold and warm periods (Maheras et al. 1999; Kallos et al., 2007), respectively associated with low and high aerosol loads. A significant amount of literature exists about the relationship between the synoptic conditions in the Mediterranean Basin and the occurrence of aerosol episodes (e.g. Moulin et al., 1998; Gangoiti et al., 2001; Lelieveld et al., 2002; Kallos et al., 2007, and papers cited therein; Papadimas et al., 2008; Gkikas et al., 2012).

In winter and part of spring, the Azores anticyclone presents its lowest intensity and usually stays west of the ~~WMB~~western Mediterranean Basin (Millán et al., 1997). Weak gradient anticyclonic conditions ~~in~~ are recurrent over the ~~WMB~~western Mediterranean Basin and favor the stagnation of pollutants near populated and industrialized areas around the Basin (Lyamani et al., 2012). The thermal inversions associated to such anticyclonic conditions and the local breezes that may be activated by solar radiation help the pollutants to disperse over the Basin. Winter is also the time when the Azores anticyclone leaves room to an anticyclone that may

Con formato: Subíndice
Con formato: Fuente: Sin Negrita
Con formato: Fuente: Sin Negrita
Con formato: Subíndice
Con formato: Fuente: Sin Negrita
Con formato: Fuente: Sin Negrita
Con formato: Sin Resaltar

form over the Bay of Biscay. It is a favorable situation for the entry of Atlantic air masses through the Gulf of Lion to the ~~WMB~~western Mediterranean Basin allowing to the renewal of air masses and the removal of aerosols that may have accumulated over the Basin (Escudero et al., 2007). Moreover the aerosols are also removed by wet scavenging, which is the strongest removal mechanism (Pruppacher and Klett, 1997), due to the large precipitation amounts.

In summer, the Azores anticyclone is strengthened and its eastern edge enters the ~~WMB~~western Mediterranean Basin between the Iberian and the Italian peninsulas, whereas thermal lows develop over the Iberian Peninsula and the Sahara region (Millán et al., 1997). The summer months in the region are characterized by the absence of large-scale forcing and the predominance of mesoscale circulations. In particular, as far as the Iberian Peninsula is concerned, the interaction of the sea-land and mountain-induced breezes, the strong orography, the convergence of surface winds from the coastal areas towards the central plateau and the strong levels of subsidence over the ~~WMB~~western Mediterranean Basin results in the re-circulation of air masses and the consequent ageing and accumulation of pollutants (Millán et al., 1997; Pérez et al., 2004; Sicard et al., 2006). Furthermore, additional factors come into play such as low precipitation, high photochemistry that boosts the formation of secondary organic aerosols, and the increased convective dynamics that favors resuspension. Summer is also a period favorable to the transport towards the Basin of aerosols such as desert dust from Morocco and western Algeria to the northwestern Mediterranean basin following the SW-NE axis of our stations when Atlantic low pressure systems arrive over Spain (Bergametti et al., 1989; Moulin et al., 1998; Valenzuela et al., 2012a), and forest fire~~s~~ smoke ~~towards the Basin~~ (Bergametti et al., 1992; Guieu et al., 2005; Pace et al., 2005)~~)~~. The summer and annual amount of desert dust exported to the Basin is controlled by the large-scale North Atlantic Oscillation (NAO; Moulin et al., 1997; Papadimas et al., 2008; Pey et al., 2013) which also partly controls the number of fires around the Basin: during period of high NAO index (defined by Hurrel, ~~(~~1995~~)~~), drier conditions prevail over southern Europe, the Mediterranean Sea, and northern Africa (Papadimas et al., 2008).

4.2 Peculiarity of each of the three sites

Corsica, where the Ersa site is located, is a North–South ~~a 80 × 180 km²~~ elongated French island (~80 × 180 km^2) situated in the northern part of the ~~WMB~~western Mediterranean Basin. It has the highest mountains (behind Mount Etna) and the largest number of rivers than any Mediterranean island. The highest peak reaches 2710 m and there are about twenty other summits higher than 2000 m. The ~~northern~~northern tip of the island is at about 160 km from the

coast of southern continental France and at about 80 km from the coast of Italy. The dominant wind directions are W and E-SE (Lambert et al., 2011). The site is perfectly suited for regional background studies since it is not impacted by any type of local anthropogenic aerosol. There ~~is~~ are relatively few aerosol measurements over Corsica in the scientific literature at present despite the recurrent high summer pollution peaks and intense rainfalls observed in the island in the last few years (Lambert and Argence, 200~~7~~8). However, the French scientific community has started the installation of a multi-site instrumented platform, called CORSiCA (Corsican Observatory for Research and Studies on Climate and Atmosphere-ocean environment), dedicated to oceanographic and atmospheric studies in the framework of the HyMeX (Hydrological cycle in the Mediterranean Experiment) and ChArMEx projects (Lambert et al., 2011). ~~In the framework of ChArMEx Léon et al. (2015, this special issue) presented the aerosol vertical distribution at Ersa obtained from lidar measurements during more than one year. In that study less than 10 % of the observation days were affected by desert dust events. AOD_{355} was estimated to be 0.61 for dust and 0.71 for pollution building up in the Gulf of Genova. Carbonaceous aerosols were highlighted as the main driver of the aerosol optical properties in summer (Sciare et al., 2014).~~ Carbonaceous aerosols and dust in a lesser extent were highlighted as the main driver of the aerosol optical properties of surface aerosols at Ersa in summer (Nicolas et al., 2013; Sciare et al., 2014). Carbonaceous aerosols also control the averaged aerosol column properties on a yearly basis in the northwestern basin (Mallet et al., 2013). From MODIS satellite products, Gkikas et al. (2016) report less than 4 episodes per year of strong desert dust episodes (AOD > 0.44, defined as the annual mean + 2 standard deviations) at Ersa in the period 2000-2013.

The island of Mallorca is approximately 2.5 times smaller than Corsica in surface. The mountainous chain of the island, the Sierra de Tramuntana, is situated in the northwestern part and its highest peak reaches 1445 m. The AERONET sun-photometer is situated at the airport of the capital, Palma de Mallorca (~420,000 inhabitants), approximately 8 km east of the city center and ~~the~~ harbor area. The winds are driven by the topographic effects of the Sierra de Tramuntana chain. The dominant wind directions observed close to the city center are SW and NE to which a NW component adds in winter (Pey et al., 2009). There are also relatively few aerosol measurements over Mallorca in the scientific literature. In average 20 % of the days/year are affected by desert dust events (Pey et al., 2009). ~~The amount of e~~Carbonaceous aerosols in Mallorca have been found ~~observed~~ by ~~the~~ Pey et al., (2009)~~same authors, found~~ in the same range that those ~~for~~ in other suburban sites in Spain, which suggests an important

Con formato: Sin Resaltar
Con formato: Sin Resaltar
Con formato: Sin Resaltar

regional contribution of ~~such~~ carbonaceous aerosols. Gkikas et al. (2016) report an average of almost 6 intense (AOD > 0.50) desert dust episodes per year in the period 2000-2013.

The Alborán island is a tiny (7 ha), totally flat island situated in the Alboran Sea, about 200 km East of the Gibraltar Straight, 50 km north of the Moroccan coast and 90 km south of the Spanish coast. There is no local anthropogenic emission source on and near the island, except for an important shipping route at the north of it (www.marinetraffic.com). The only aerosol measurements ever performed ~~in Alborán~~at Alborán are those ~~presented~~ used in this work. They are extensively discussed in Lyamani et al. (2015) and Valenzuela et al. (2015). During the AERONET measurement period of June 2011 – January 2012, 3540 % of the air masses originated on the Atlantic/Iberian Peninsula, ~~days were dominated by pure maritime aerosols and~~ 31 % on North Africa~~of the days were dominated by desert dust~~, 21 % on the European/Mediterranean region and 13 % were pure maritime aerosols (Lyamani et al., 2015; Valenzuela et al., 2015). During the dust events, Valenzuela et al. (2015) stress~~es~~ that the aerosol properties are clearly different from pure mineral dust and that most of the desert dust intrusions over Alborán can be described as a mixture of dust and anthropogenic fine absorbing particles independently of the dust source area. Gkikas et al. (2016) report an average of almost 10 episodes per year of strong desert dust episodes (AOD > ~0.59) in the period 2000-2013.

~~The frequency of desert dust events referenced here (<10, 20 and 31 % at Ersa, Palma and Alborán, respectively) are in agreement with the long-term study over the whole Mediterranean Basin made by Pey et al. (2013).~~

5 Seasonal and annual variability of aerosol properties at Ersa and Palma

5.1 AOD, AE and fine mode contribution

~~Figure 2 shows the hourly variation of the AOD at 440 nm at the three sites. This figure aims at showing the representativeness of the dataset at Ersa and Palma. The number of points, N, at each site is reported in the figure. One sees that Ersa and Palma have at least 2 years of data within the 4-year period and that Alborán has a single sample of data between June 2011 and January 2012. Both at Ersa and Palma the AOD shows a marked annual cycle with maxima in spring and summer in Ersa and in summer in Palma, and minima in December and January at both stations. The AOD reaches peak values as high as 1.82 at Ersa and 1.12 at Palma.~~The seasonal aerosol classification performed ~~The episodes with high aerosol loads (AOD > 0.5) at Alborán are also detected in Palma with less intensity and less frequency. There is no clear correlation with Ersa.~~with the methodology described in Section 3 is presented in Figure 2 for

Con formato: Sin Resaltar
Con formato: Sin Resaltar
Código de campo cambiado
Con formato: Fuente: Sin Negrita
Código de campo cambiado

Ersa and in Figure 3 for Palma. Seasonal mean values of AE and δAE are given in Table 1. The graphs were made with the whole AOD dataset. We first observe that in winter at both sites the criteria $AOD_{675} > 0.15$ removes a lot of points and results in a poor statistics (N=24 at Ersa and N=4 at Palma). As discussed further in this Section, we believe that the statistics in spring at Palma is not totally representative of the site: N=68 is rather low and no point with $AOD_{440} > 0.4$ is found (Figure 3d), whereas at Ersa many points do have $AOD_{440} > 0.4$ (**Figure 2**d). For the rest of the seasons, moderate to large AODs ($AOD_{440} > 0.4$) gather in two well differentiated cluster. In summer Ersa and Palma present an important fine mode cluster (AE > 1.4; δAE < 0 and AE > 1.2; δAE < 0.2, respectively) associated to ($70 < \eta < 90$ %; $0.10 < r^f < 0.15$ μm) and ($\eta > 60$ %; $0.10 < r^f < 0.18$ μm), respectively, and corresponding to polluted and continental air masses. At both sites the AOD_{440} increase observed is associated to an increase of the fine mode radius and of the fine mode fraction. The same behavior has been observed in the western Mediterranean Basin by Basart et al. (2009) and was attributed to an increase of r^f following coagulation-aging and hydration of fine particles (Titos et al., 2014; Granados-Muñoz et al., 2015). In this fine mode cluster the largest AODs are logically found at Ersa which is closer to the European continent than Palma. At the same time coarse particles, likely maritime aerosols, superimpose their signal onto this fine mode. A concurrent increase in AOD_{440} and coarse mode fraction along the r^f curves (between 0.10 and 0.12 μm) and for $\eta < 70$ % is observed. During the same summer season both sites also present an important coarse mode cluster (AE < 0.7; -0.1 < δAE < 0.2 and AE < 0.7; 0 < δAE < 0.4, respectively) associated to $\eta < 40$ % at both sites and corresponding to mineral dust. In this coarse mode cluster the largest AODs are logically found at Palma which is closer to the African continent than Ersa. The AOD increase is linked to a decrease of δAE towards 0 which is related to almost pure mineral dust as observed in Sub-Sahelian sites (Basart et al., 2009). The points of this coarse mode cluster for which δAE exhibits positive values indicate the presence of small particles mixed with this coarse mode. The difference between the summer mean values of AE (larger at Ersa than at Palma; 1.46 vs. 1.14) and δAE (lower at Ersa than at Palma; 0.05 vs. 0.29) given in Table 1 reflect the general trends found from **Figure 2**a and Figure 3a. In autumn the frequency of moderate to large AOD events decreases at both sites compared to summer. Both fine and coarse mode clusters are also present but with less variability. The fine mode cluster at Ersa and Palma is marked by (AE > 1.4; δAE < -0.2) and (AE > 1.5; δAE < 0.0), respectively, and is associated to ($70 < \eta < 95$ %; $0.11 < r^f < 0.15$ μm) and ($70 < \eta < 90$ %; $0.10 < r^f < 0.14$ μm), while the coarse mode cluster is marked by (AE < 0.7; δAE < 0.3) and (AE < 0.5; δAE < 0.3) and is associated to $\eta < 30$ and $\eta < 20$ %. The spring plot for Ersa (**Figure 2**d) is similar

Código de campo cambiado
Con formato: Fuente: Sin Negrita, Inglés (Estados Unidos)
Con formato: Fuente: 12 pto
Con formato: Subíndice
Con formato: Subíndice
Código de campo cambiado
Con formato: Fuente: Sin Negrita, Inglés (Estados Unidos)
Con formato: Fuente: 12 pto
Con formato: Subíndice
Con formato: Subíndice
Con formato: Superíndice
Con formato: Subíndice
Con formato: Superíndice
Con formato: Fuente: Sin Negrita, Inglés (Estados Unidos)
Con formato: Fuente: 12 pto
Código de campo cambiado
Código de campo cambiado

to that of summer but with less occurrences. The most interesting differences are a greater number of high-AOD (AOD_{440} > 0.6) dust events (coarse mode cluster) in spring compared to summer and conversely a greater number of high-AOD (AOD_{440} > 0.6) pollution events (fine mode cluster) in summer compared to spring. In the five-year period 2011-2015 Ersa has at least three full years of data, while Palma has more sparse data. Before starting with the monthly analysis, the representativeness of Palma data is checked with Ersa data by taking the subset of Ersa data coincident in time with those of Palma (which are comprised in the period August 2011 – December 2013). In **Figure 4**a the monthly means of this restricted dataset (black bullets) are superimposed on the monthly means of the whole dataset (red bullets). In all cases the monthly means of the 08/11–12/13 dataset are within the monthly variability of the whole dataset. In summer and autumn, the representativeness of the 08/11 – 12/13 dataset is good: the difference between both datasets is lower than 0.01. The highest differences, 0.02 – 0.04, are reached during the period February–May. In the Palma restricted dataset only spring 2013 contributes to the spring mean. Curiously during that spring no moderate to large AODs (AOD_{440} > 0.4) were observed (see Figure 3d). This result may produce the underestimation of the 08/11 – 12/13 dataset compared to the whole dataset observed at Ersa in March and April and suggests that Palma monthly means during those months may also be underestimated. Given the restriction of the Palma dataset, the discussion of the Palma spring means has to be taken cautiously in the following.

The monthly mean

~~The monthly mean values of AOD_{440}, $AE_{440-870}$, the fine mode AOD_{440} and of the sphericity are shown in Figure 3. The seasonal mean values of AOD_{440} and $AE_{440-870}$ are given in Table 2.~~

AOD_{440} shows a clear annual cycle at Ersa and Palma (**Figure 4**a). Maxima of 0.22~~1~~ ~~in Ersa~~at Ersa and 0.25 ~~in Palma~~at Palma are observed in July. Those maxima are due to a combination of mineral dust outbreaks and pollution events at Ersa and mostly to mineral dust outbreaks at Palma (see the seasonal aerosol frequency and classification in Section 5.3)~~, being these events more frequent in summer~~. The decreasing trend in AOD during the autumn months (from September to November~~SON~~) is identical at ~~all~~ both ~~three~~ sites. The ~~spring~~ AOD in spring is lower ~~in Palma~~at Palma than ~~in Ersa~~at Ersa, while it is the opposite in summer/autumn. The background AOD in spring ~~in Ersa~~at Ersa is dominated by small particles located in the marine boundary layer, present throughout the year (Sciare et al., 2014), while at Palma the predominance of the Atlantic advection meteorological scenario in spring leads to the renovation of air masses at regional scale through the Gulf of Lion and to the cleaning of the atmosphere (Escudero et al., 2007). The summer mean AOD_{440} (± standard deviation) is

Con formato: Subíndice

Código de campo cambiado

Con formato: Fuente: Sin Negrita, Inglés (Estados Unidos)

Con formato: Fuente: 12 pto

0.19±0.10 and 0.23±0.12 at Ersa and Palma, respectively, while the winter averages vary between 0.07 and 0.08.

In order to see the contribution of the fine mode particles we have plotted the fine mode AOD_{440}, AOD^{f}_{440}, in **Figure 4**b. Except for two months (March and April) the annual cycles at both Ersa and Palma are similar in shape and magnitude. Similar maxima are found in summer (0.13±0.09 at Ersa and 0.12±0.07 at Palma). In March and April AOD^{f}_{440} is more than double at Ersa than at Palma. In addition to the possible underestimation of the Palma dataset in spring (see two paragraphs above), the maps of AOD per aerosol type from Barnaba and Gobbi (2004) suggest a contribution of aerosols of continental origin already in spring over Corsica and not before summer over the Balearic Islands. We cannot confirm this result with the (δAE, AE) plots because of the limited representativeness of Palma data during the spring months.

~~AOD_{440} shows also a NE–SW gradient during the summer months. The summer mean AOD_{440} is (± standard deviation) 0.18±0.10, 0.23±0.12 and 0.27±0.14 in Ersa, Palma and Alborán, respectively, while the winter averages vary between 0.07 and 0.09. The NE–SW gradient observed in summer is reproduced on the annual mean (0.16±0.10, 0.18±0.12 and 0.20±0.13 in Ersa, Palma and Alborán, respectively, and listed in that order from NE to SW in the rest of the paper) which indicates that the summer values contribute significantly to the annual means.~~

The monthly $AE_{440–870}$ plot (**Figure 4**~~Figure 3cb~~) shows different seasonal patterns at ~~the~~ both ~~three~~ sites. ~~In Ersa~~At Ersa it slightly increases in ~~winter/~~spring/summer ~~(from 0.98 in January) to~~ and reaches a maximum value of 1.5~~06~~ in September. ~~In Palma~~At Palma, it oscillates between 0.84 (March) and 1.34 (September) without any significant seasonal trend. The ~~slightly~~ higher values ~~in Ersa~~at Ersa compared to Palma indicate the presence of finer particles at Ersa throughout the year. The $AE_{440–870}$ annual means at Ersa and Palma are 1.37±0.47 and 1.14±0.46, respectively, with maxima in summer (1.46±0.45 and 1.14±0.47, respectively). The coarse mode fraction (not shown, see Sicard et al., 2014) looks reversely correlated to the AE: it decreases at Ersa in spring/summer and reaches a minimum in July, while no marked trend is observed at Palma. The fact that $AE_{440–870}$ is lower in spring than in summer at Ersa reflects the higher frequency of dust events in spring compared to summer as found earlier from our aerosol classification.

Código de campo cambiado

Código de campo cambiado

Con formato: Resaltar

5.2 Volume size distribution

Figure 5 shows the seasonal variability of the aerosol particle size distribution at both sites. Seasonal mean values are given in Table 1 for (r_V^f , C_V^f) and (r_V^c , C_V^c), the volume median radius and the volume concentration of the fine and coarse modes, respectively. The annual volume concentration values (varying between 0.017 and 0.021 $\mu m^3 \cdot \mu m^{-2}$ for the fine mode and between 0.027 and 0.046 $\mu m^3 \cdot \mu m^{-2}$ for the coarse mode) at both sites are typical of maritime (Smirnov et al., 2002) and/or background/rural (Omar et al., 2005) environments. The annual values at Palma are very similar to the mean size distribution averaged over several sites in the western Mediterranean Basin by Mallet et al. (2013). The winter fine mode volume concentrations are similar at both sites (~ 0.010 $\mu m^3 \cdot \mu m^{-2}$). In spring the fine mode volume concentration more than doubles (w.r.t. winter) at Ersa while it is stable at Palma. This behavior is reflected on AOD_{440}^f (**Figure 4**b) which doubles from winter to spring at Ersa because of the contribution of aerosols of continental origin already in spring over Corsica and not before summer over the Balearic Islands. The domination of large particles (mostly mineral dust) is particularly remarkable during the summer period at both sites. Relatively large coarse mode concentrations are also visible in spring at Ersa and in autumn at Palma. A clear summer inter-site difference is observed on the coarse mode volume concentration (0.032±0.036 at Ersa vs. 0.063±0.063 at Palma) and also on the C_V^c / C_V^f ratio (1.7 vs. 2.5, respectively). The summer coarse mode volume median radii (2.49±0.41 and 2.43±0.41) fall in the range of values for dusty sites (1.90 – 2.54 µm; Dubovik et al., 2002b) and are in agreement with the average value of 2.34 µm found for the western Mediterranean Basin by Mallet et al. (2013). As commented by Dubovik et al. (2002b) the absence of dynamics between the particle radius and the aerosol loading explains that dust median radii are smaller than those of urban/industrial aerosols. The influence of European pollution decreases from Ersa to Palma and, logically, the coarse mode volume median radius decreases. In the same line, we also observe that inter-season r_V^c decreases with increasing mineral dust frequency (see the seasonal aerosol frequency and classification in Section 5.3).

~~At Alborán the AE is lower, especially in June and August (0.43 – 0.45) owing to the high African dust load of the Alborán Sea region in summer (Moulin et al., 1998). There is also a clear NE–SW gradient between the 3 stations on the annual means (1.38±0.48, 1.14±0.46, 0.81±0.40), especially strong in summer (1.44±0.47, 1.14±0.47, 0.61±0.33). The coarse mode fraction (not shown, see Sicard et al., 2014) looks reversely correlated to the AE: it decreases~~

Código de campo cambiado
Con formato: Fuente: 12 pto
Código de campo cambiado
Código de campo cambiado
Código de campo cambiado
Código de campo cambiado
Código de campo cambiado
Código de campo cambiado
Código de campo cambiado

~~in Ersa in winter/spring and reaches a minimum in July, while no marked trend is observed at Palma. The coarse mode fraction also shows a NE–SW gradient more evident in summer (0.26, 0.42, 0.61) than on the annual means. Here again this result clearly evidences the predominant contribution of large particles in Alborán during the summer months which decreases quasi-linearly as we move to Palma and then Ersa.~~

~~In order to see the contribution of the fine mode particles we have plotted the fine mode AOD_{440}, AOD^{f}_{440}, in Figure 3c. Except for two months (March and April) the annual cycles at both Ersa and Palma are similar in shape and magnitude. In Alborán, the monthly AOD^{f}_{440} presents larger fluctuations but is similar to the results at the other two stations. Maxima are found in summer (0.13±0.09 in Ersa, 0.12±0.07 in Palma and 0.09±0.04 in Alborán). Because of those similarities no NE–SW gradient is observed on AOD^{f}_{440}. Our findings, in agreement with Lyamani et al. (2015), suggest a homogeneous spatial distribution of the fine particle loads over the three sites in spite of the distances between the sites and the differences in local sources. In March and April AOD^{f}_{440} is more than double in Ersa than in Palma. The maps of AOD per aerosol type from Barnaba and Gobbi (2004) suggest a contribution of aerosols of continental origin already in spring over Corsica and not before summer over the Balearic Islands. An interesting conclusion so far is that the seasonal variations of the fine particle load are quite homogeneous over the WMB in spite of heterogeneous origins (of the fine particles): mostly European/continental at the north of the Basin and from North African urban/industrial areas (Rodríguez et al., 2011) and/or from ship emissions (Valenzuela et al., 2015) at the south.~~

~~Finally the sphericity (Figure 3d) could be retrieved for a few months of the year only because it requires that the sun-photometer measurements cover the scattering angle range from aureole to > 120º which is not possible for large solar zenith angles during winter months. The sphericity presents huge variations resulting in large monthly standard deviations (see Table 2). As expected it is strongly correlated to desert dust intrusions and therefore presents a clear summer NE–SW gradient. It reaches minima in summer of 57±45, 41±41 and 25±32 % in Ersa, Palma and Alborán, respectively.~~

Con formato: Resaltar

~~5.5~~5.3 AAOD, ~~and~~ absorption Ångström exponent ~~AAE~~and refractive index

Besides aerosol amount and size, other important aerosol properties are those related to their absorpting ability. It must be kept in mind that AERONET level 2.0 inversion products linked to the aerosol absorption properties like the aerosol absorption optical depth, the absorption Ångström exponent (AAE) and the refractive index are performed with the following

restrictions: 50 < SZA < 80º and AOD_{440} > 0.4. To gain an insight into the seasonal frequency, intensity and aerosol type under such restrictions, we show in Figure 6 the (δAE, AE) plots only for those AERONET level 2.0 inversion products in our dataset that meet those criteria. There is in general twice more data available in summer than in the other seasons. The plots for both sites show without ambiguity that such restrictions lead to only two types of aerosols: mineral dust corresponding to the coarse mode cluster (δAE < 0.3; $AE_{440-870}$ < 0.75; η < 40%) and pollution corresponding to the fine mode cluster ($AE_{440-870}$ > 1.0; η > 70%). The seasonal number and ratio of each of these two aerosol types and their respective seasonal mean AOD_{440} are given in Table 2. In summer 58 % (84 %) of the measurements correspond to mineral dust at Ersa (Palma) and 42 % (16 %) to pollution. In autumn the predominance is opposite: 33 % (40 %) of the measurements correspond to mineral dust at Ersa (Palma) and 67 % (40 %) to pollution. In spring at Ersa 64 % of the measurements correspond to mineral dust and 36 % to pollution. The seasonal mean AOD_{440} for pollution is quite constant (~0.46 – 0.47) and has negligible inter-site and inter-season variations, which suggests that the intensity of pollution events is quite uniform over the western Mediterranean Basin. The seasonal mean AOD_{440} for mineral dust (MD) is more variable (higher standard deviations). The higher annual AOD_{440} values found at Ersa (0.55) vs. Palma (0.51) suggest that a significant number of MD events with 0.40 < AOD_{440} < 0.50 detected at Palma do not reach Ersa. The limitation of the graphical method used here is that no information related to the aerosol absorption properties is retrieved. In the following we will try to link the dominant aerosol size, type and frequency found with the absorption properties.

~~The seasonal variations of the spectral dependency of the aerosol absorption optical depth are shown in the top part of Figure 4, while the annual means of the AAOD spectra are shown in the bottom part of Figure 4. Seasonal mean values are given in Table 2.~~ Bergstrom et al. (2007) report~~ed~~ that the spectral AAOD for aerosols representing the major absorbing aerosol types (pollution, biomass burning, desert dust and mixtures) decreases with wavelength and can be approximated with a power-law wavelength dependence, the absorption Ångström exponent ~~(AAE)~~ which can be calculated between two wavelengths λ_1 and λ_2, $AAE_{\lambda_1-\lambda_2}$, as:

$$AAE_{\lambda_1-\lambda_2} = -\frac{\ln\left[\frac{AAOD_{\lambda_1}}{AAOD_{\lambda_2}}\right]}{\ln\left[\frac{\lambda_1}{\lambda_2}\right]} \quad (2)$$

The range of values of AAE provides useful information on shortwave absorption produced by different types of aerosols, namely black carbon (BC), organic carbonaceous matter, and

Con formato: Fuente: 12 pto, Sin Negrita
Código de campo cambiado
Con formato: Fuente: 12 pto
Con formato: Subíndice
Con formato: Subíndice
Con formato: Subíndice
Con formato: Subíndice
Con formato: Subíndice
Con formato: Subíndice
Código de campo cambiado
Código de campo cambiado
Código de campo cambiado

mineral dust (Russell et al., 2010). However, recently, Mallet et al. (2013) highlighted the difficulties in attributing AAE values larger than 1, the value for pure BC, to organic species (and/or mineral dust) or to coated BC since they all produce AAE > 1 (Lack and Cappa, 2010).

The seasonal variations of the spectral dependency of the aerosol absorption optical depth are shown in **Figure 7**a. Seasonal mean values are given in Table 1. At each site the spectra are shown for the whole dataset (All) and for mineral dust (MD) and pollution (Pol) cases determined with the classification obtained from Figure 6 (see first paragraph of this Section). In both Ersa and Palma the AAOD decreases with increasing wavelength. The annual $AAOD_{440}$ is 0.023±0.018 ~~in Ersa~~at Ersa and 0.040±0.020 ~~in Palma~~at Palma. The associated $AAE_{440\text{-}870}$ is 1.66±0.66 and 1.88±0.53, respectively. The spectra of AAOD for pollution are quite similar in shape and magnitude at both sites and present weak inter-season variations. It is rather low (< 0.02) with low spectral dependency (AAE oscillates between 1.10 and 1.24) and is slightly higher at Palma than at Ersa. The mineral dust AAOD ($0.023 < AAOD_{440} < 0.057$) and AAE ($1.43 < AAE < 2.69$) are much higher than those for pollution and present larger inter-season and inter-site variations. ~~The box-and-whisker plots of the AAOD indicate a higher spread of the values at 440 nm than at the other wavelengths, as well as a general good symmetry of the point distribution around the mean (mean ≈ median). Palma is logically characterized by a larger AAOD than Ersa because of the nearby city and harbor of Palma de Mallorca and because of the higher frequency of dust events.~~ At Ersa in spring $AAOD_{440}$ (AAE) reaches its highest value, 0.035 (2.11), when the mineral dust outbreaks represent 64 % (the highest percentage) of the cases. At Palma the highest values of $AAOD_{440}$ (AAE), 0.043 (1.98), occur in summer also when the mineral dust outbreaks are the most frequent (84 %). The summetime average of $AAOD_{440}$ ~~in Ersa~~at Ersa (0.018) measured over the whole dataset is within the error bar of the value found by Mishra et al. (2014~~, this special issue~~; 0.020) at the same site from a larger dataset of AERONET observations. It is however lower than the average value given in Mallet et al. (2013) for the ~~WMB~~western Mediterranean Basin calculated at sites characterized mostly as urban and dusty, which could indicate that they considered more dusty sites than urban ones in the computing of their basin average.~~.~~ The mineral dust AAOD spectra at both sites are similar in magnitude and shape to the measurements made during PRIDE (Puerto Rico Dust Experiment, 2000; aerosols: Saharan dust) and ACE-Asia (Aerosol Characterization Experiment-Asia, 2001; aerosols: Asian dust, urban and industrialized) (Bergstrom et al., 2007; Russell et al., 2010). The pollution and MD AAE found here are in agreement with the ~~The AAE in both sites are higher than the~~ mean values observed at several Mediterranean AERONET sites for ~~for the WMB (1.32) and for~~ urban sites (1.31) ~~but are smaller than the~~

Código de campo cambiado

Con formato: Fuente: 12 pto, Sin Negrita

Con formato: Fuente: 12 pto

Con formato: Subíndice

~~mean value of 1.96 for~~ and dusty sites (1.96), respectively (Mallet et al., 2013) ~~(Mallet et al., 2013)~~. ~~It is worth remembering that the AERONET level 2.0 products retain only cases with AOD_{440} > 0.4 for estimating AAOD. This condition, applied in clean sites such as Ersa and Palma, yields AAOD strongly influenced by mineral dust and also, but very seldomly, by pollution. It results that the AAE values found are mostly representative of mineral dust and not so much of organic particles. Indeed t~~The annual mean values of AAE (1.66 and 1.88 at Ersa and Palma, respectively) fall within the range 1.5 – 2, in which the AAE at different wavelength pairs vary ~~in~~at the dusty site of Solar Village, Saudi Arabia (Russell et al., 2010). It results that on a yearly basis AAE is strongly influenced by mineral dust outbreaks, even at Ersa. ~~The few points available in Alborán (N=15) give a summer mean $AAOD_{440}$ of 0.016±0.010 and an AOD spectra almost without any wavelength dependency (AAE = 1.05±0.26). A further inspection of the 15 cases indicates that they all correpond to dust events. In 12 cases (80 %) the airmasses arriving in Alborán are from the southwest quadrant. The AAOD value is the lowest of the whole Mediterranean Basin if we compare with the results from Mallet et al. (2013) given for AERONET sites all around the Mediterranean Basin and in which the minimum (0.023) is found precisely in Ersa. The AAE, nearly equal to 1, is totally surprising since the predominant aerosol is expected to be mineral dust. Curiously the summer value of 1.05 in Alborán is close to 1.12 observed during TARFOX (Tropospheric Aerosol Radiative Forcing Observational Experiment, 1996; location: US Atlantic coast) and 1.05 observed during ICARTT (International Consortium for Atmospheric Research on Transport and Transformation, 2004; location: New England Atlantic coast) (Bergstrom et al., 2007; Russell et al., 2010). Both field campaigns have the peculiarity of being shipborne campaings. All in all, those AERONET retrievals allow to make the hypothesis that, although detected in small amount (low AAOD), BC and/or soot originated from North African urban/industrial areas (Rodríguez et al., 2011) and/or from both the harbor of Algeciras and vessel traffic near the Strait of Gibraltar drive the absorbing spectral behavior in Alborán. The emissions of the two latter have been quantified in the Bay of Algeciras by Pandolfi et al. (2011). Further research (and probably measurements) is (would be) needed to understand the low spectral dependency of AAOD in Alborán.~~

~~5.6 Volume size distribution and refractive index~~

~~Figure 5 shows the seasonal variability of the aerosol particle size distribution at the three sites. Seasonal mean values are given in Table 3. The annual volume concentration values (varying between 0.017 and 0.021 $\mu m^3 \cdot \mu m^{-2}$ for the fine mode and between 0.027 and 0.062 $\mu m^3 \cdot \mu m^{-2}$~~

~~for the coarse mode) at all three sites are typical of maritime (Smirnov et al., 2002) and/or background/rural (Omar et al., 2005) environments. The annual values at Palma are very similar to the mean size distribution averaged over several sites in the WMB by Mallet et al. (2013). The winter fine mode volume concentrations are similar at all three sites and vary between 0.009 and 0.012 $\mu m^3 \cdot \mu m^{-2}$. In spring the fine mode volume concentration more than doubles (w.r.t. winter) in Ersa while it is stable in Palma. This behavior is reflected on AOD^f_{440} (Figure 3c) which doubles from winter to spring in Ersa because of the contribution of aerosols of continental origin already in spring over Corsica and not before summer over the Balearic Islands. The domination of large particles (mostly mineral dust) is particularly remarkable during the summer period at all three sites, and is still clearly visible in autumn in Palma and Alborán. The NE–SW gradient observed on the summer coarse mode fraction commented earlier (0.26, 0.42, 0.61) is also observed on the coarse mode volume concentration (0.032±0.036, 0.063±0.063, 0.083±0.063 $\mu m^3 \cdot \mu m^{-2}$) and also on the C^c_V / C^f_V ratio (1.7, 2.5, 3.6). The summer coarse mode volume median radii (2.49±0.41, 2.43±0.41, 2.33±0.45 µm) falls in the range of values for dusty sites (1.90 – 2.54 µm; Dubovik et al. (2002b)) and are in agreement with the average value of 2.34 µm for the WMB found by Mallet et al. (2013). As commented by Dubovik et al. (2002b) the absence of dynamics between the particle radius and the aerosol loading explains that dust median radii are smaller than those of urban/industrial aerosols. The influence of European pollution decreases along the NE–SW axis and, logically, the coarse mode volume median radius decreases. This result also suggests that the influence of European pollution in the northern WMB (Ersa) is stronger than the influence of North African pollution in the southern WMB (Alborán) in term of particle size.~~

The seasonal ~~and annual~~ spectral variations of the real and the imaginary part of the refractive index (RRI and IRI, respectively) are shown in **Figure 7**~~Figure 6~~b and **Figure 7**c. S~~Figure 7. Sec~~easonal mean values at 440 nm ~~of (~~RRI_{440} and IRI_{440}~~,)~~ ~~the RRI and IRI at 440 nm, respectively,~~ are given in Table 1. ~~Table 3.~~ **Figure 7**b shows a large inter-season and inter-site variability in the shape and amplitude of the RRI spectra. RRI_{440} has an annual mean value of 1.45±0.04 ~~in Ersa~~at Ersa and 1.43±0.06 ~~in Palma~~at Palma. ~~Those~~ These values are on the order of magnitude of those ~~values~~ found by Mallet et al. (2013) from AERONET observations at various sites around the Mediterranean Basin and they are in the upper limit of urban/industrial aerosols (1.33 – 1.45) and lower than "pure" dust (1.48 – 1.56; Dubovik et al., ~~(~~2002b~~)~~). However the values significantly differ by aerosol type: $1.38 < RRI_{440} < 1.45$ and $1.45 < RRI_{440} < 1.55$ for pollution and mineral dust, respectively, agreeing well with the results from Dubovik et al. (2002b). The high variability of RRI_{440} for mineral dust is probably linked to variations

Código de campo cambiado

Código de campo cambiado

Con formato: Subíndice

Con formato: Subíndice

in the dust mineralogy. RRI spectra are nearly constant for pollution. For mineral dust RRI shows in all cases a decrease of ~ 0.02 – 0.04 towards ultraviolet wavelengths, whereas Petzold et al. (2009) determined wavelength-independent RRI from airborne measurements of dust during the SAMUM (Saharan Mineral Dust Experiment) campaign. This difference may be due to differences in the measurement techniques, but also in a wrong mixture of spherical and non-spherical in the AERONET product. Indeed Dubovik et al. (2000b; 2002a) showed that treating non-spherical particles (like mineral dust) like spheres result in an erroneous decrease of RRI with decreasing wavelength. The values of RRI_{440} for MD are in agreement with previous works such as Petzold et al. (2009) who found 1.55 – 1.56 at 450 nm for dust during SAMUM and Denjean et al. (2016) who found 1.50 – 1.55 at 530 nm in dust layers from ~~Airborne measurements of particle size distributions and aerosol absorption coefficients during the SAMUM (Saharan Mineral Dust Experiment) campaign allowed to determine the RRI of desert dust with values between 1.55 and 1.56 (Petzold et al., 2009).~~ airborne measurements over the western Mediterranean Basin during the ChArMEx 2013 field campaign.

~~Figure 6 does not reveal neither a clear NE–SW gradient, nor a significant dependency with the season. The wavelength dependency is slightly stronger in Palma and Alborán than in Ersa. This can be explained by a higher influence of non-spherical particles (mineral dust) over Palma and Alborán, and thus a stronger spectral dependence of the real part of the refractive index (Dubovik et al., 2000b). The box-and-whisker plots show a high spread of RRI at all wavelengths in both Ersa and Palma. Minima and maxima are found below 1.35 and above 1.55, respectively, spanning a large range of values corresponding to different aerosol types.~~

IRI_{440} (Figure 7~~Figure 7, Table 3~~) c) has an annual mean value of (3.1±1.3) × 10^{-3} at Ersa and (4.7±1.8) × 10^{-3} at Palma. ~~While IRI_{440} is different at both sites, the rest of the spectral IRI is similar at both sites.~~ The annual IRI_{440} are in the lower limit of the values found from AERONET observations by Mallet et al. (2013) at various sites around the Mediterranean Basin (3.5-11.9 × 10^{-3}) where the minimum (3.5 × 10^{-3}) was observed at the Italian Island of Lampedusa. Although we previously found that $AAOD_{440}$ was higher for MD than for pollution, the reverse occurs for IRI_{440} which is in general higher for pollution than for MD. This result indicates that these larger MD AAOD values are the result of larger amounts of MD (compared to pollution) in terms of optical depth and not of MD intrinsic absorption properties. IRI_{440} varies in the range (2.3 – 4.9) and (3.0 – 5.1) × 10^{-3} for MD and pollution, respectively, and in general larger values are found at Palma. While the pollution spectrum of IRI is nearly wavelength-independent, that of MD shows a strong increase towards ultraviolet wavelengths. As the imaginary part of the refractive index is driven by iron oxide content (especially

Con formato: Subíndice

Código de campo cambiado

Con formato: Fuente: Sin Negrita

Con formato: Subíndice

Con formato: Subíndice

Con formato: Subíndice

hematite), it results in a higher IRI at shorter wavelengths during episodes with high dust concentrations (Moosmüller et al., 2009). The ranges of IRI_{440} found for pollution and MD are in agreement with previous works: ~~D~~during the TARFOX (Tropospheric Aerosol Radiative Forcing Observational Experiment) campaign in 1996 values of (1 -– ~~8~~8) × 10^{-3} were found off the US Atlantic coast in horizontal layers of distinct aerosol refractive indices using a retrieval based on aerosol in-situ size distribution and remote sensing measurements (Redemann et al., 2000); -~~D~~during SAMUM Petzold et al. (2009) retrieved values of desert dust ~~R~~IRI at 450 nm of (3.1 -– 5.2) × 10^{-3}-; –Denjean et al. (2016) found values of IRI at 530 nm between 0 and 5 × 10^{-3} at different heights in dust layers during the ChArMEx 2013 field campaign.

~~At both Ersa and Palma the seasonal IRI decreases with increasing wavelengths. From 440 to 675 nm the decrease in IRI is stronger at Palma (especially in summer where IRI decreases by a factor larger than 2) than at Ersa. As the imaginary part of the refractive index is driven by iron oxide content (especially hematite), it results in a higher IRI at shorter wavelengths during episodes with high dust concentrations (Moosmüller et al., 2009). However mineral dust is not the only aerosol type which could explain the IRI spectral behavior: brown carbon (BrC), a class of light-absorbing carbonaceous material, has also an IRI that increases towards shorter visible and ultraviolet wavelengths (Moosmüller et al., 2009). We conclude that the differences in the IRI_{440} values and in the behavior of the IRI spectra are due to a higher influence of mineral dust and/or BrC in Palma. Pey et al. (2009) estimated from in-situ measurements in the city of Palma de Mallorca the annual contribution of mineral dust and organic matter on the total aerosol mass concentration to be 29 and 17 %, respectively. This result points out that mineral dust might be the main driver of the IRI_{440} values and the IRI spectra behavior found in Palma. Here again the box-and-whisker plots (bottom plots of Figure 7) show a high spread of IRI at all wavelengths in both Ersa and Palma with minima and maxima below 1 × 10^{-3} and above 8 × 10^{-3}, respectively.~~

~~The summer IRI at Alborán is totally different from the other two sites: it is rather low, 1.14 × 10^{-3} in average, and wavelength-independent. The absence of wavelength dependency points out towards the presence of BC and/or soot and supports the hypothesis of an anthropogenic influenced mineral dust (we recall that all the 15 cases in Alborán correspond to dust events, see Section 4.2). This hypothesis, already formulated by Müller et al. (2009) who determined separately mineral dust and soot absorption coefficients near the source during SAMUM, is confirmed by the results from Valenzuela et al. (2015) that state that most of the desert dust intrusions over Alborán can be described as a mixture of dust and anthropogenic fine absorbing particles (BC and/or soot) independently of the dust source area. In our opinion two major and~~

Con formato: Subíndice

Con formato: Sin Superíndice / Subíndice

~~interesting questions remain opened: Why the absorption properties of the long-range transport aerosol in Alborán are observed neither in Palma, nor in Ersa? What are the processes which inhibits the BC and/or soot absorption properties during the transport to the northern part of the WMB?~~

~~5.9~~5.4 Single scattering albedo and asymmetry factor

The single scattering albedo (SSA) is the ratio of aerosol scattering to total extinction (i.e. scattering + absorption) that provides some information on the aerosol absorption properties. It is useful to relate the AAOD to the AOD:

$$AAOD_{\lambda} = (1 - SSA_{\lambda})\, AOD_{\lambda} \quad (3)$$

The asymmetry factor (g) represents a measure of the preferred scattering direction and varies between -1 (only backward-scattering, i.e. at 180 º relative to the incident direction) and +1 (only forward-scattering at 0º). The SSA and asymmetry factor are of special interest for radiative transfer studies. The seasonal ~~and annual~~ spectral variations of SSA and g are shown in Figure 8. ~~Figure 8 and Figure 9. Seasonal~~ Seasonal mean values at 440 nm (~~of~~ SSA_{440} and g_{440}~~;)~~ ~~the SSA and asymmetry factor at 440 nm, respectively,~~ are given in Table 3~~Table 4.~~. In average ~~the three~~ both sites appear as "moderately" absorbing with annual SSA_{440} varying between 0.92±0.03 and 0.96±0.02~~7~~, even though minima are observed around 0.89 and 0.86 at Ersa and Palma, respectively. In agreement with our previous results (higher $AAOD_{440}$ at Palma than at Ersa) we find lower SSA at Palma compared to Ersa at all wavelengths but especially at 440 nm. MD and pollution SSA spectra have very distinct behaviors: while the first ones increase with increasing wavelength, the second decrease. This result is in agreement with the climatological SSA spectra obtained worldwide by Dubovik et al. (2002b) and plotted by Russell et al. (2010) which shows that SSA_{λ} decreases with increasing wavelengths for urban/industrial aerosols and biomass burning, and conversely increases with increasing wavelengths for desert dust. During summer, autumn and spring at Ersa and autumn at Palma, the seasonal mean of SSA_{λ} calculated with the whole dataset (MD + pollution) increases from 440 to 675 nm and decreases afterwards. This behavior is representative of a mixture of both MD and pollution. During summer at Palma the SSA spectra (calculated with the whole dataset) are very similar to that of MD (84 % of the dataset corresponds to mineral dust, see Table 2). MD and pollution SSA_{440} vary in the range 0.89 – 0.95 and 0.97 – 0.98, respectively. ~~The annual SSA_{440} is 0.92±0.03 at Palma while it is 0.96±0.02 at Ersa. If we compare the SSA spectra with other stations around the Mediterranean Basin (Mallet et al., 2013) we find that the SSA spectra at Ersa has a shape identical to the average of AERONET sites in the WMB but~~

Código de campo cambiado

Código de campo cambiado

Con formato: Subíndice

~~higher values (an difference of approximately +0.04) and that the SSA spectra at Palma has a shape identical to the dusty AERONET sites. The climatological SSA spectra obtained worldwide by Dubovik et al. (2002b) for urban/industrial aerosols, biomass burning and desert dust has been plotted by Russell et al. (2010). The spectral behavior of those three aerosol types is: SSA_λ decreases with increasing wavelengths for urban/industrial aerosols and biomass burning, and increases with increasing wavelengths for desert dust. Maritime aerosols have large (> 0.97), wavelength independent SSA (Dubovik et al., 2002b). A monotonous (here increasing) SSA spectra is only observed at Palma during the summer season and corresponds to the signature of mineral dust. During the rest of the seasons available in our statistics (summer, autumn and spring in Ersa and autumn in Palma), SSA_λ increases from 440 to 675 nm and decreases afterwards. This behavior does not fit with any of those of the climatology just mentioned and are therefore representative of a mixture of aerosols, namely urban/industrial aerosols and mineral dust.~~ For comparison Denjean et al. (2016) found SSA at 530 nm ranging from 0.90 to 1.00 in layers of different aerosol types in the western Mediterranean Basin during the ChArMEx 2013 field campaign. Inter-season variations are more pronounced for MD than for pollution. As a consequence of higher MD $AAOD_{440}$ in autumn, MD SSA_{440} is smaller in autumn than in summer.

The annual mean values of the asymmetry factor at 440 nm (g_{440}) are 0.69±0.03 and 0.70±0.03 at Ersa and Palma, respectively. The mean values of both pollution and MD g_{440} show very little ~~In Alborán, as expected from our previous results (low AAOD and IRI), SSA is high (summer mean: 0.97±0.02) and shows a poor wavelength dependency. Here again the values of SSA and the shape of its spectra are representative of a mixture of aerosols. In view of the results from Dubovik et al. (2002b) and Russell et al. (2010), such a mixture could be quantitatively produced by a mixture of urban/industrial aerosols (e.g. from Goddard Space Flight Center; SSA_{440} = 0.98, SSA_λ decreases with increasing wavelengths) and mineral dust (e.g. from Bahrain, Persian Gulf; SSA_{440} = 0.92, SSA_λ increases with increasing wavelengths). For comparison Denjean et al. (2015, this special issue) found SSA_{530} ranging from 0.90 to 1.00 ± 0.04 in mineral dust layers in the WMB during summer 2013. Last, it is worth noting that the SSA spectra found in our studies at Alborán are quite different from the results of Valenzuela et al. (2015) for North Atlantic air masses. Several reasons explain those differences:~~

~~• Valenzuela et al. (2015) make use of the Nakajima et al. (1996) retrieval scheme adapted for non-spherical particles (Olmo et al., 2008) while in this study the AERONET retrieval scheme is used (see Section 2.2 for references about the AERONET inversion algorithm).~~

Con formato: Subíndice

Con formato: Subíndice

Con formato: Fuente: Cursiva

Con formato: Fuente: Cursiva, Subíndice

Con formato: Fuente: Cursiva

Con formato: Fuente: Cursiva, Subíndice

Con formato: Normal, Sin viñetas ni numeración

- Nakajima code uses sky radiance measurements in the solar principal plane while AERONET uses almucantar sky radiance measurements.

- By not using the same configuration for the sky radiance measurements, the inversions from Valenzuela are not coincident in time with those of our study and the positions of the aerosol volume sampled are also different.

- AERONET retrieval applies the criteria $AOD_{440} > 0.4$ for retrieving the SSA while Nakajima code does not apply any criteria.

- Despite small standard deviations (<0.02, see Figure 8) which indicate good stability of our results, our statistics is based on a small amount of numbers (N=15).

- Previous works (e.g. Alados-Arboledas et al., 2008; Olmo et al., 2008; Valenzuela et al., 2012a) have studied the differences between both the Nakajima and the AERONET retrieval scheme and have found SSA retrieved with the Nakajima code in general lower than with the AERONET code, with a difference of up to 7%.

Figure 9 shows that the asymmetry factor has a general tendency to decrease with increasing wavelengths. inter-season and inter-site variations: they range between 0.68 and 0.70, and between 0.71 and 0.73, respectively. Figure 8b shows that the spectra of g have a general tendency to decrease with increasing wavelengths for pollution, while it is nearly constant for MD. These results are in agreement with the climatology from The annual mean values at 440 nm are 0.69±0.03 and 0.70±0.03 at Ersa and Palma, respectively, and minor inter-season variations are observed (Table 4). The decrease for $\lambda > 440$ nm occurs at all wavelengths in Ersa ($g_{1020} = 0.62$) while a slight increase is observed in Palma from 870 to 1020 nm ($g_{1020} = 0.66$). According to Dubovik et al. (2002b) who found similar g_{440} for urban/industrial aerosols and desert dust have a similar g_{440} (0.68 – 0.73) and a decreasing tendency , biomass burning has a g_{440} between 0.64 and 0.69 and strongly decreasing with increasing wavelength for urban/industrial aerosols and maritime aerosol have a slightly higher g_{440} (~0.75). The similarities between urban/industrial aerosols and desert dust make difficult the identification of a predominant aerosol type from the annual means and spectral variations at Ersa and Palma. According to Lyamani et al. (2006) who compared the asymmetry factor spectra at Granada for dust events and urban/industrial aerosols (European contamination) also found that the decrease of the g spectra with increasing wavelengths is much stronger for urban/industrial aerosols than for mineral dust. This result is also observed by Dubovik et al. (2002b) at urban/industrial sites vs. desert dust sites and indicates implies that at near-infrared wavelengths ($\lambda > 670$ nm), and at constant AOD and low SZA the solar radiation scattered to the surface is greater for mineral

Con formato: Fuente: Cursiva

Con formato: Fuente: Cursiva

dust than for urban/industrial aerosols. ~~The stronger spectral variations of g at Ersa are therefore in agreement with the higher influence of aerosols of continental origin at that site. In all cases the spread around the median, which is always close to the mean, is small and indicates a good stability of our results, while outliers are relatively far from the first and third quartile boxes. The summer asymmetry factor at Alborán is higher than at the other two sites (g_{440} = 0.74±0.02) and its spectral variations are similar in shape to that of Palma but slightly stronger (g_{1020} = 0.68±0.02). The g spectra at Alborán is indeed quite similar to that of maritime aerosols (g_{440} = 0.75 and g_{1020} = 0.68±0.02) determined in Lanai, Hawaii, by Dubovik et al. (2002b). Valenzuela et al. (2012b) showed that the asymmetry factor at 440 nm measured in Granada (140 km N–NW of Alborán) over a 6-year period during dust events was ~ 0.70. This result indicates that the preferred scattering direction in Alborán may be driven by marine aerosols.~~

Here again the seasonal means calculated with the whole dataset (MD + pollution) have the signature of neither MD, nor pollution, but are representative of a mixture of both MD and pollution.

6 Solar direct radiative forcing and forcing efficiency at Ersa and Palma

~~**Solar radiative forcing and forcing efficiency**~~

Con formato: Sangría: Izquierda: 0,63 cm

Con formato: Fuente: Sin Negrita

The AERONET Version 2.0 retrieval provides a set of radiative quantities in the solar (so called shortwave) spectrum range including spectral downward and upward total fluxes at the surface, diffuse fluxes at the surface, and broadband upward and downward fluxes as well as aerosol radiative forcing (ARF) and aerosol radiative forcing efficiency (ARFE) both at the bottom of atmosphere (BOA) and at the top of the atmosphere (TOA). The radiative forcing accounts for changes in the solar radiation levels due to changes in the atmospheric constituents. The direct radiative forcing of atmospheric aerosols is defined as the difference in the energy levels between two situations with and without aerosols:

$$ARF_{BOA} = \Delta F^{w}_{BOA} - \Delta F^{o}_{BOA} \quad (4)$$

$$ARF_{TOA} = \Delta F^{w}_{TOA} - \Delta F^{o}_{TOA} \quad (5)$$

where ΔF^{w} and ΔF^{o} are the downward net (downwelling minus upwelling) fluxes with and without aerosols, respectively. With this convention, a negative sign of the ARF implies an aerosol cooling effect and a positive sign an aerosol warming effect, regardless of whether it happens at the BOA or at the TOA. The ARFE is defined as the ratio of ARF per unit of AOD. The ARF analytical definitions used by AERONET (AERONET, 2016~~see~~

~~http://aeronet.gsfc.nasa.gov/new_web/Documents/Inversion_products_V2.pdf~~) are slightly different than Eqs. (4)~~(4)~~ and (5)~~(5)~~:

$$ARF_{BOA}^{AER} = F_{BOA}^{w\downarrow} - F_{BOA}^{o\downarrow} \quad (6)$$

$$ARF_{TOA}^{AER} = F_{TOA}^{0\uparrow} - F_{TOA}^{w\uparrow} \quad (7)$$

While Eq. (7)~~(7)~~ is equivalent to Eq. (5)~~(5)~~ because the downwelling flux at the TOA is independent of the presence or not of aerosols in the atmosphere ($F_{TOA}^{w\downarrow} = F_{TOA}^{o\downarrow}$), the use of Eq. (6)~~(6)~~ yields an overestimation w.r.t. the real value since the upward fluxes with and without aerosols are not taken into account.

~~Similar~~ In ~~to~~ the AERONET retrieval approach, the flux calculations account for the thermal emission, absorption and single and multiple scattering effects using the Discrete Ordinates Radiative Transfer (DISORT) method (Stamnes et al., 1988). The solar broadband fluxes are calculated for SZA between 50 and 80°, by spectral integration in the range from 0.2 to 4.0 µm. The integration of atmospheric gaseous absorption and molecular scattering effects are conducted using the Global Atmospheric Model (GAME) code (Dubuisson et al., 1996; 2004; 2006). It is worth noting that flux calculations are performed for a multi-layered atmosphere with a gaseous vertical distribution calculated with the US standard atmosphere model and a single fixed aerosol vertical distribution (exponential decrease with aerosols up to a height of 1 km). García et al. (2008) tested different vertical profiles and their sensitivity tests led to differences of less than 1 $W \cdot m^{-2}$ on the downward solar flux at the BOA and estimated t~~.~~ ~~T~~hose differences (~ 0.2 – 3 % w.r.t. the instantaneous ARF) ~~were estimated~~ negligible ~~by the same authors~~. Detailed information on the radiative transfer module used by the operational AERONET inversion algorithm can be found in García et al. (2011; 2012a; 2012b).

García et al. (2008) made an intensive validation of AERONET estimations of fluxes and radiative forcings using ground-based measurements from solar databases at 9 stations worldwide but AERONET estimations of the aerosol direct radiative forcing are little used in the literature. Cachorro et al. (2008) used the AERONET ARF estimations to study the impact of an extremely strong desert dust intrusion over the Iberian Peninsula. ~~García et al. (2008) made an intensive validation of AERONET estimations of fluxes and radiative forcings using ground-based measurements from solar databases at 9 stations worldwide.~~ Derimian et al. (2008) used the AERONET estimates of the ARF for mineral dust mixed with biomass burning and for pure mineral dust at M'Bour, Senegal, and tested the impact of neglecting aerosol non-sphericity on radiative effect calculations. García et al. (2011) did a similar work but at regional level for mixtures of mineral dust and biomass burning and mineral dust and urban/industrial

Con formato: Inglés (Estados Unidos)

Con formato: Inglés (Estados Unidos)

aerosols. Valenzuela et al. (2012b) checked AERONET estimates of the radiative fluxes against SBDART (Santa Barbara DISORT Atmospheric Radiative Transfer; Ricchiazzi et al., 1998) computations for desert dust events affecting the Southeastern Iberian Peninsula. García et al. (2012a; 2012b) have used AERONET estimates of the ARF at 40 stations grouped in 14 regions worldwide for six aerosol types: mineral dust, biomass burning, urban/industrial, continental background, oceanic and the free troposphere.

Con formato: Fuente: 12 pto, Inglés (Estados Unidos)

Con formato: Fuente: 12 pto, Inglés (Estados Unidos)

6.1 Validation of AERONET radiative fluxes with ground-based and satellite data

In order to validate AERONET estimations of the solar fluxes at our western Mediterranean stations, we have performed a comparison of the fluxes the most critical for aerosol forcing calculations, namely:

- The solar downward flux at the surface, $F_{BOA}^{\downarrow}$. We have performed a comparison between AERONET estimations and pyranometer measurements. ~~To perform such a comparison, we have~~ us~~ed~~ing the Barcelona AERONET / SolRad-Net (Solar Radiation Network, http://solrad-net.gsfc.nasa.gov/) site which is the closest site to our study area in the ~~WMB~~western Mediterranean Basin where collocated AERONET and solar flux measurements are available. The period with coincident measurements is May 2009 – October 2014. The pyranometer is a Kipp and Zonen CMP21 sensor that provides every two minutes a measurement of the total solar flux in the range 0.3—2.8 µm. Coincident AERONET and pyranometer measurement times were restricted to ± 1 min. We used SolRad-Net level 1.5 data which have been cleared ~~as free~~ of any operational problem~~s~~ The manufacturer accuracy (2 %) and the sensor drift (< 1 %) yield an overall accuracy on the order of 3%.
- The solar upward flux at the TOA, $F_{TOA}^{\uparrow}$. We have performed a comparison between AERONET estimations and CERES (Clouds and the Earth's Radiant Energy System) satellite measurements at Ersa, Palma and Alborán. We used CERES Single Scanner Footprint (SSF) Level 2 products, namely the shortwave (0—5 µm) upward flux at the TOA given for a spatial resolution equivalent to its instantaneous footprint (nadir resolution 20-km equivalent diameter). Measurements from CERES/Aqua and CERES/Terra were used indistinctively. We screened CERES data spatially by accounting only for the pixels in which one of the ground sites falls, and temporally allowing a time difference of ± 15 min. The time of overpass of both CERES/Aqua and CERES/Terra over the three sites varies in the range 10—14 UT. The CERES/Terra instantaneous shortwave TOA flux uncertainties ~~is~~are estimated to be 13.5 $W \cdot m^{-2}$ for

all-sky conditions (CERES, 2016https://eosweb.larc.nasa.gov/sites/default/files/project/ceres/quality_summaries/ssf_toa_terra_ed2B.pdf). According to Loeb et al. (2007) CERES/Aqua TOA flux errors are similar to those of CERES/Terra. Because of the CERES overpass time range (10 –14 UT) the SZA restriction for AERONET level 2.0 data (50 < SZA < 80º) rejects many measurements that coincide in time but are for SZA < 50º. Consequently the use of AERONET level 2.0 data provides very few points for comparison. We have therefore selected AERONET level 1.5 data and checked that now with 40 < SZA < 80º and checked that the cases with 40 < SZA < 50º represent ~ 33 % of the total. We had to deal with two more issues tTo further filter CERES data points, we had to deal with two more issues: 1) sometimes CERES pixels are affected by clouds (when at the coincident time AERONET is not), and 2) because the three sites are in coastline regions CERES pixels contain information from both land and water. The first issue is due to the different techniques used by both AERONET sun-photometers and CERES which make the air mass volumes sampled by both instruments quite different. The second one is in general not problematic, except at given periods of the year and at given hours of the day when the sun glint produces a significant increment of the upward fluxes in the direction of the spaceborne sensor. Both cases result in an increase of CERES upward fluxes at the TOA. To discard those cases, we eliminated from the comparison all pairs of points (CERES, AERONET) that have a difference larger than CERES uncertainty, i.e. 13.5 $W \cdot m^{-2}$. The AERONET level 1.5 data are from 2008–2014 in Ersaat Ersa, 2011–2014 in Palmaat Palma and 2011–2012 in at Alborán.

Figure 9Figure 10a a shows the comparison of downward solar fluxes at the BOA measured by pyranometers vs. that estimated by AERONET. A very good agreement is found between both quantities (correlation coefficient, R, greater than 0.99). To quantify the level of accuracy we calculated the average difference between the AERONET modeled and observed flux. We found +12 $W \cdot m^{-2}$ which, in relative terms, corresponds to an overestimation of AERONET fluxes of +3.0 %, increment found by dividing the average AERONET modeled flux by the observed one. This value is in the range of mean relative errors [-0.6, +8.5 %] found by García et al. (2008) under different aerosol environments at 9 stations worldwide. Derimian et al. (2008) found an overestimation of approximately +4 % in M'Bour, Senegal. According to García et al. (2008) that overestimation is due mostly to the cosine effect (the pyranometer angular response which can deviate up to ± 3 % from the truth at SZA of 70-80º) and to the surface albedo and bidirectional reflectance distribution function (BRDF) assumed by

Con formato: Fuente: 12 pto, Color de fuente: Automático

AERONET. The least-square fit linealr equation relating the AERONET (AER) fluxes to the observation (OBS) is $OBS = 0.98 \cdot AER - 4.50$. Our results are in total agreement with García et al. (2008) who found $OBS = 0.98 \cdot AER - 5.32$. ~~The next step would be to validate the AERONET estimations of ARF against observations. Unfortunately no systematic surface radiative forcing measurements are available in or in the vicinity of Barcelona. However,~~ ~~s~~Since the validation of $F_{BOA}^{\downarrow}$ has been performed regardless of the aerosol load, we can easily assume that the fluxes with turbid (high aerosol load) or clean (low aerosol load) atmospheres follow the same regression line ($OBS = 0.98 \cdot AER - 4.50$). Finally, to correct for the missing upward fluxes in the definition of ARF_{BOA}^{AER}, the latter can be multiplied by the term (1 – SA) where SA stands for the surface albedo. Indeed:

$$\begin{aligned} ARF_{BOA} &= \Delta F_{BOA}^{w} - \Delta F_{BOA}^{o} \\ &= \left(F_{BOA}^{w\downarrow} - F_{BOA}^{w\uparrow}\right) - \left(F_{BOA}^{o\downarrow} - F_{BOA}^{o\uparrow}\right) \\ &= \left(F_{BOA}^{w\downarrow} - SA \cdot F_{BOA}^{w\downarrow}\right) - \left(F_{BOA}^{o\downarrow} - SA \cdot F_{BOA}^{o\downarrow}\right) \\ &= \left(F_{BOA}^{w\downarrow} - F_{BOA}^{o\downarrow}\right)(1 - SA) \end{aligned} \quad (8)$$

Consequently the corrected estimated solar ARF at the BOA, ARF_{BOA}^{c} in W·m^{-2}, has been calculated from the original AERONET radiative forcing, ARF_{BOA}^{AER}, as:

$$ARF_{BOA}^{c} = 0.98 \cdot ARF_{BOA}^{AER} \cdot (1 - SA) \quad (9)$$

The term 0.98 comes from the correction of the fluxes after comparison to pyranometer measurements. We have considered a ~~unique~~ broadband value of SA calculated as the average of the surface albedo at the four AERONET wavelengths (440, 675, 870 and 1020 nm). García et al. (2012b) document that considering the surface albedo at the four AERONET wavelengths yields differences less than 10 % w.r.t. considering spectral surface albedo in the whole solar spectral range (0.2 – 4.0 μm). The corrected solar ARFE at the BOA, $ARFE_{BOA}^{c}$ in W·m^{-2}·AOD$_{550}^{-1}$, defined here as the ratio of forcing per unit of AOD at 550 nm, can be simply calculated from the original AERONET ARFE, $ARFE_{BOA}^{AER}$, as:

$$ARFE_{BOA}^{c} = 0.98 \cdot ARFE_{BOA}^{AER} \cdot (1 - SA) \quad (10)$$

~~Figure 9~~~~Figure 10b~~ b shows the comparison of upward solar fluxes at the TOA measured by CERES vs. estimated by AERONET. The pairs of point (open bullets) outside the shaded area representing CERES uncertainty, 13.5 W·m^{-2}, were not taken into account in the fit and are reported only for completeness. One sees that almost all of these points are on the upper side

Con formato: Fuente: 12 pto, Color de fuente: Automático

of the diagonal indicating an underestimation by AERONET estimates probably due to an increment of the upward fluxes in the direction of the spaceborne sensor caused by clouds or sun glint. Here again, but in a lesser extent compared to the validation of $F_{BOA}^{\downarrow}$, the pairs of points taken into account in the fit calculation (solid color bullets) show a good agreement ~~is found~~ between both ~~quantities~~ AERONET modeled and observed fluxes ($R > 0.92$). The average difference between the AERONET modeled and observed flux is -1.5 $W \cdot m^{-2}$ which, in relative terms, corresponds to an underestimation of AERONET fluxes of -1.6 %. To our knowledge it is the first time that AERONET fluxes at the TOA are validated with satellite measurements. The least-square fit ~~lineal~~ linear equation relating the AERONET (AER) fluxes to the observation (OBS) is $OBS = 0.99 \cdot AER + 2.51$. Like at the BOA, since the validation of $F_{TOA}^{\uparrow}$ has been performed regardless of the aerosol load, the correction of the fluxes can be assumed the same for atmospheres with and without aerosols. Then the corrected ARF at the TOA, ARF_{TOA}^{c}, and the corrected ARFE at the TOA, $ARFE_{TOA}^{c}$, write:

$$ARF_{TOA}^{c} = 0.99 \cdot ARF_{TOA}^{AER} \quad (11)$$

$$ARFE_{TOA}^{c} = 0.99 \cdot ARFE_{TOA}^{AER} \quad (12)$$

6.2 Solar direct radiative forcing and forcing efficiency: monthly variations at Ersa and Palma

The monthly means of the corrected AERONET level 2.0 instantaneous solar ARF and ARFE are shown in Figure 10~~Figure 11 at~~ at both the BOA and ~~the~~ TOA. By plotting the whole dataset of ARF and ARFE as a function of SZA we have observed that both quantities remained approximately constant independently of SZA. However as SZA increases, the slant path increases and it is logical to expect a decrease of the ARF / ARFE related to the decrease of the solar radiation reaching the Earth. This effect has been observed on instantaneous ARFE observations by Di Sarra et al. (2008) and Di Biagio et al (2009), among others. We therefore decided to filter Figure 10~~Figure 11~~ for SZA $\leq 60^{o}$.

The solar ARF is strictly negative and shows a marked annual cycle (at both the BOA and the TOA) at both Ersa and Palma. The solar ARF is lower (in absolute value) during the winter months and reaches maxima (in absolute value) in spring or summer. At the BOA, a maximum (in absolute value) of -20.6 $W \cdot m^{-2}$ is reached at Ersa in March (with a seasonal maximum of -18.0 $W \cdot m^{-2}$ in spring) while the strongest forcing ~~in Palma~~at Palma, -26.4 $W \cdot m^{-2}$, is reached in June (with a seasonal maximum of -22.8 $W \cdot m^{-2}$ in summer). These maxima correspond to the

Con formato: Fuente: 12 pto, Color de fuente: Automático

Con formato: Fuente: 12 pto, Color de fuente: Automático

season with the maximum occurrences of mineral dust outbreaks at each site (64 % at Ersa in spring and 84 % at Palma in summer, see Table 2). During the first months of the year (until April) ARF is more than double ~~in Ersa~~at Ersa than ~~in Palma~~at Palma. It reflects a similar result found earlier on AOD_{440}^{f} (see Section 5.1~~4.1~~ and Figure 4~~Figure 3)~~) and may be attributed to 1) the contribution of aerosols of continental European origin already in spring over Corsica and not before summer over the Balearic Islands, hence ~~. This result is expected since~~ a higher amount of small particles that causes more cooling (Tegen and Lacis, 1996), and 2) the lack of representative measurements during the spring season at Palma (see Section 5.1). The marked peak in July ~~in Palma~~at Palma (correlated with a peak in AOD_{440}, see Figure 4~~Figure 3a)~~ a) is clearly due to mineral dust outbreaks which are more frequent in summer (see Section 5.3). Another effect sums up: in summer $AAOD_{440}$ (Figure 7~~Figure 4) is~~) is more than double ~~in Palma~~at Palma (0.043; SSA_{440} ~ 0.92) than ~~in Ersa~~at Ersa (0.018; SSA_{440} ~ 0.96) in summer. According to Boucher and Tanré (2000), the surface forcing is enhanced when the aerosol absorption is larger. At the TOA, the seasonal cycles are similar at both sites. Maxima (in absolute value) are reached during the same ~~month, July, and the same~~ season, summer, and the same month, July. The July and summer means are, respectively, -14.5 and -12.8 $W \cdot m^{-2}$ ~~in Ersa~~at Ersa and -13.9 and -13.0 $W \cdot m^{-2}$ ~~in Palma~~at Palma. The same difference observed on ARF_{BOA} during the first months of the year is also visible on ARF_{TOA}: ARF_{TOA} ~~in Ersa~~at Ersa is almost double (in absolute value) that ~~in Palma~~at Palma; whereas the stronger influence of the dust outbreaks ~~in Palma~~at Palma (vs. Ersa) on ARF_{BOA} during the summer months is not visible at the TOA. This seems to indicate that ARF_{TOA} is not as much affected by dust long-range transport as it is by long-range transport of small particles of continental origin. As far as aerosol absorption is concerned, Boucher and Tanré (2000) showed that increasing the aerosol absorption decreases the aerosol effect at the TOA. ~~The results in Alborán at both the BOA / TOA in summer (-27.8 / -18.8 $W \cdot m^{-2}$) and autumn (-18.3 / -13.4 $W \cdot m^{-2}$) show higher ARF than in the other two sites.~~

The comparison with the literature is not trivial because of the location of ~~the three~~ Ersa and Palma~~sites we chose~~: clean, insular sites at the crossroads of European and North African air masses; and the limited sun position ($50 < SZA < 60^{o}$). Concerning the background aerosols, García et al. (2012a) showed that for oceanic ~~(region R13)~~ and clean ~~(free troposphere, region R14)~~ sites the annual ARF given for $SZA = 60 \pm 5^{o}$ was low (< 10 $W \cdot m^{-2}$) and rather similar at the BOA and TOA ($ARF_{TOA} / ARF_{BOA} > 0.7$). The situation $ARF_{TOA} / ARF_{BOA} > 0.7$ is found ~~in Ersa~~at Ersa in autumn and ~~in Palma~~at Palma in winter and spring and may indicate the seasons

Con formato: Fuente: Sin Negrita, Color de fuente: Automático

Con formato: Fuente: Sin Negrita, Color de fuente: Automático

Con formato: Fuente: Sin Negrita

Código de campo cambiado

Código de campo cambiado

at each site when background aerosols dominate. It is worth further comparing our results to those of García et al. (2012a; 2012b), in particular from the regions R1 (the northern part of the Sahara-Sahel desert area; mineral dust) and R8 (Europe; urban and industrial pollution) which surround our study area. Interestingly in R8 the largest ARF_{BOA} is reached during winter/spring (-65 < ARF_{BOA} < -45 W·m^{-2}). The same phenomenon occurs ~~in Ersa~~at Ersa but with lower values (ARF_{BOA} ~ -18 W·m^{-2}). ~~A similar ARF summer/autumn cycle (in terms of shape) is also observed between Alborán and R1. The strongest values of ARF_{BOA} (ARF_{TOA}) are reached in summer: around -60 (-20) W·m^{-2} in R1 and around -28 (-19) W·m^{-2} in Alborán. We believe that the ratio ARF_{TOA}/ARF_{BOA} is higher in Alborán than in R1 because 1) the dust transport in Alborán occurs at higher altitude and the aerosol vertical distribution produces a significant effect on the fluxes at the TOA (Meloni et al., 2005), and 2) the days dominated by desert dust do not represent more than 31% of the Alborán data (see Section 3.2). Alborán measurements can also be compared to ARF of dust in Granada (140 km N–NW of Alborán) from Valenzuela et al. (2012a) who found annual means of ARF_{BOA} (ARF_{TOA}) at SZA = 55 ± 5º of approximately -50 (-20) W·m^{-2}. Here again ARF_{TOA}/ARF_{BOA} is higher in Alborán than in Granada. We believe it is due to low aerosol absorption properties (see Section 4.2 and 4.3) in Alborán resulting in relatively large SSA, and therefore in larger ARF_{TOA} (Boucher and Tanré, 2000).~~ Our findings are usually lower than results from case studies: Derimian et al. (2008) found dust ARF_{BOA} (ARF_{TOA}) at SZA = 50º and AOD_{440} = 0.54 on the order of -80 (-25) W·m^{-2} ~~in~~ at M'Bour, Senegal; Cachorro et al. (2008) found dust ARF_{BOA} (ARF_{TOA}) at 53 < SZA < 75º and AOD_{440} ~ 0.5 on the order of -60 (-30) W·m^{-2} ~~in~~ at El Arenosillo, Spain; Lyamani et al. (2006) found ARF_{BOA} (ARF_{TOA}) at SZA = 50º of -43 (-8) W·m^{-2} for dust and -33 (-8) W·m^{-2} for European–Mediterranean air masses ~~in~~ at Granada, Spain; Formenti et al. (2002) found for aged biomass burning with AOD_{500} = 0.39 an ARF_{BOA} (ARF_{TOA}) relatively constant with SZA on the order of -78 (-26) W·m^{-2} ~~in~~ over northeastern Greece. Conversely, ~~I~~at~~n~~ Lampedusa, Italy, under a weak dust intrusion (AOD_{500} = 0.23 and SSA = 0.96) Meloni et al. (2005) found an ARF_{BOA} (ARF_{TOA}) at SZA = 50º on the order of -13 (-7) W·m^{-2}, lower than the summer means at Ersa and Palma~~at any of the three stations presented in our work~~. A few years later at the same site but under a stronger dust intrusion (AOD_{500} = 0.59) Meloni et al. (2015) found an ARF_{BOA} (

ARF_{TOA}) at SZA = 55º on the order of -63 (-45) W·m^{-2}, much larger than the summer means found in our work.

The aerosol radiative forcing efficiency ~~in Ersa~~at Ersa shows an ~~clear~~ annual cycle (Figure 10b), the one at the TOA being reverse of the one at the BOA. Relatively constant minimum absolute values at the BOA [-150; -134 W·m^{-2}] are reached during the period April – October while maximum absolute values at the TOA [-107; -100 W·m^{-2}] are reached during the same period. The ARFE ~~in Palma~~at Palma also shows a clear annual cycle but with some irregularities compared to Ersa. $ARFE_{BOA}$ reaches minimum absolute values from February to October [-133; -117 W·m^{-2}], excepting the month of June, while $ARFE_{TOA}$ has a triangular shape with a maximum in January (-110 W·m^{-2}) and a minimum in June (-71 W·m^{-2}). The reverse behaviour of $ARFE_{BOA}$ (maximum) and $ARFE_{TOA}$ (minimum) in June is due to the combination of 1) the strong increase (in absolute value) of ARF_{BOA} between May and June while ARF_{TOA} increases very little and 2) the strong increase of AOD from May to June (Figure 4~~Figure 3a)~~ a). The annual mean of $ARFE_{TOA}$ is lower ~~in Palma~~at Palma (-85.1 W·m^{-2}, SSA_{440} ~ 0.92) than ~~in Ersa~~at Ersa (-99.2 W·m^{-2}, SSA_{440} ~ 0.96) which reflects that more absorbing aerosols produce a lower absolute $ARFE_{TOA}$ (García et al., 2012b). ~~In Alborán between June and October $ARFE_{BOA}$ varies between -161 and -117 W·m^{-2} and $ARFE_{TOA}$ between -105 and -86 W·m^{-2}.~~

García et al. (2012b) produced summer mean values of $ARFE_{BOA}$ ($ARFE_{TOA}$) for SZA = 60 ± 5º in regions R1 (dust) and R8 (urban/industrial) of approximately -150 (-50) and -165 (-70) W·m^{-2}, respectively, and winter mean values in R13 (oceanic) of approximately -145 (-100) W·m^{-2}. The annual $ARFE_{BOA}$ ~~in Ersa~~at Ersa (-144.4 W·m^{-2}) and ~~in Palma~~at Palma (-132.2 W·m^{-2}) are slightly lower than the values given by García et al. (2012b) but are within the error bars. The explanation is probably that neither Ersa nor Palma are dominated by any of the aforementioned aerosol types but are rather representative of a mixture of them. García et al. (2012b) also showed that the mean $ARFE_{BOA}$ in other dust regions (R2, western Africa) could be lower (-100 W·m^{-2}). The relatively large (in absolute value) annual $ARFE_{TOA}$ ~~in Ersa~~at Ersa (-99.2 W·m^{-2}) and ~~in Palma~~at Palma (-85.1 W·m^{-2}) compared to the results of García et al. (2012b) indicate that $ARFE_{TOA}$, like ARF_{TOA}, is not strongly affected by long-range transport aerosols. Other works like Derimian et al. (2008) found dust $ARFE_{BOA}$ ($ARFE_{TOA}$, both w.r.t. AOD_{440}) at SZA = 50º on the order of -150 (-45) W·m^{-2} ~~in~~ at M'Bour, Senegal. Di Sarra et al.

Código de campo cambiado

Con formato: Fuente: 12 pto

Con formato: Fuente: Sin Negrita, Color de fuente: Automático

(2008) made a multi-year statistical study ~~in~~ at Lampedusa, Italy, and found $ARFE_{BOA}$ (w.r.t. AOD_{496}) at 50 < SZA < 60º on the order of -155 $W \cdot m^{-2}$ for dust and -135 $W \cdot m^{-2}$ for biomass burning/industrial aerosols. ~~They a~~All studies show~~ed~~ that while $ARFE_{BOA}$ for dust is hardly dependent on AOD_{λ}, it is highly dependent on AOD_{λ} for biomass burning/industrial aerosols. Likewise, Di Biagio et al. (2009) found also ~~in~~ at Lampedusa $ARFE_{BOA}$ (w.r.t. AOD_{496}) at 50 < SZA < 60º on the order of -180 $W \cdot m^{-2}$ for dust and -140 $W \cdot m^{-2}$ for urban/industrial aerosols ~~in Lampedusa, Italy~~. During a strong dust intrusion ~~in~~ at Lampedusa (AOD_{500} = 0.59) Meloni et al. (2015) found an $ARFE_{BOA}$ ($ARFE_{TOA}$, both w.r.t. AOD_{500}) at SZA = 55º on the order of -107 (-77) $W \cdot m^{-2}$, much lower than both previous works at the same site (Di Sarra et al., 2008; Di Biagio et al., 2009) and than the summer means found in our work. The reason given by Meloni et al. (2015) is that they used higher SSA values than the ones associated to mineral dust ~~in~~ at Lampedusa.

In summary the aerosol radiative forcing at 50 < SZA < 60º in the ~~WMB~~western Mediterranean Basin is usually lower than case studies at sites dominated by only one aerosol type (dust or urban/industrial aerosols). During the spring (at Ersa) and summer (at Palma) months when dust episodes are more frequent an increase of ARF_{BOA} is observed~~ at all stations along a NE-SW gradient~~. At the TOA ~~the same~~ a maximum is reached in summer at ~~increase is observed but without any~~ both sites ~~NE-SW gradient~~ (Ersa and Palma have roughly the same ARF_{TOA}). The annual cycle of the aerosol radiative forcing efficiency, which unlike the ARF does not depend on the column aerosol amount, ~~does show neither annual cycles with a regular pattern~~is not as marked as that of the ARF~~, nor a NE-SW gradient~~. The explanation comes from the higher dependency of the ARFE to absorption properties which are quite variable over the ~~WMB~~western Mediterranean Basin, especially for mineral dust~~ and do not present a NE-SW gradient (see Section 4.2, 4.3 and 4.4)~~.

~~6 Discussion on NE-SW gradients~~

~~Before concluding it is worth discussing the NE-SW gradient found (or not) as a function of the type of the aerosol parameters or effects (extensive or intensive). By aerosol effects we mean here the aerosol radiative forcing and radiative forcing efficiency. Intensive parameters are frequently used to perform aerosol classification (Burton et al., 2012) because, unlike extensive parameters, they do not vary with aerosol amount. In order to establish a potential NE-SW gradient, all three stations are needed. For that reason, the discussion that follows is based on the summer means at the three stations, summer being the season with the largest~~

amount of observations available. The last column of Table 2, 3 and 4 indicates if the parameter/effect is an extensive or an intensive parameter/effect and if its summer mean presents a NE–SW gradient, i.e. if it is monotonously increasing or decreasing along a NE–SW axis. Among the parameters/effects discussed in the paper, 7 are extensive (AOD, AOD_f, AAOD, C_V^f, C_V^c, ARF_{BOA} and ARF_{TOA}) and 11 are intensive (AE, AAE, Sphericity, r_V^f, r_V^c, RRI, IRI, SSA, g, $ARFE_{BOA}$ and $ARFE_{TOA}$). This list is far from being exhaustive but it may be sufficient to perform a coarse statistics. We find that 3 extensive (AOD, C_V^c and ARF_{BOA}, 43 % of them) and 3 intensive (AE, r_V^c and Sphericity, 27 % of them) parameters/effects do present a NE–SW gradient. We discarded the aerosol radiative forcing at the TOA because the values at Ersa (−12.8 W·m^{-2}) and Palma (−13.0 W·m^{-2}) are nearly the same. Figure 12 shows the correlated variations of the extensive and intensive parameters/effects which show a NE–SW gradient. The higher ratio of extensive (42 %) vs. intensive (27 %) properties presenting a NE–SW gradient indicates that the column aerosol amount has a stronger signature over the WMB than intrinsic (intensive) aerosol properties. All three extensive parameters/effects AOD, C_V^c and ARF_{BOA} increase along the NE–SW axis and are clearly related to the higher frequency and intensity of mineral dust episodes during the summer months. The fact that the increase of AOD and ARF_{BOA} with C_V^c occurs approximately in the same proportions (the plots almost overlap, see Figure 12) indicates that AOD and ARF_{BOA} are closely related over the WMB. The fact that the plots are nearly straight lines indicates a linear geographical gradient which is in agreement with the long-term study of the regional African dust contribution to PM_{10} over the whole Mediterranean Basin made by Pey et al. (2013) and also with the summer means of the dust contribution to satellite-based AOD retrieved by sector over the whole Mediterranean Basin (Barnaba et al., 2004). Similar results are observed for the intensive parameters: r_V^c and Sphericity decrease quasi-linearly with decreasing AE and in the same proportions along the NE–SW axis. The NE–SW gradient of the two intensive parameters AE and Sphericity is here again driven by mineral dust. In turn, and as explained in Section 4.3, the decrease of r_V^c along the NE–SW axis reflects the decreasing influence of European pollution (urban/industrial aerosols median radii are larger than those of dust). This result put together with the increasing C_V^c along the NE–SW axis suggests that the concentration of large particles is higher but their size smaller in relative terms in the southern WMB.

Finally it is worth coming back to the conclusions drawn so far in Sections 4.1–4.4 about the fine mode of the particle size distribution and the absorption properties. As can be seen in the

~~last column of Table 2-4, none of the extensive or intensive parameters related to those two aspects present a NE–SW gradient. The absence of NE–SW gradient of r_V^f and C_V^f is due to a homogeneous spatial distribution of the fine particle loads over the three sites in spite of the distances between the sites and the differences in local sources (see Section 4.1). The absence of NE–SW gradient of the absorption properties (AAOD, AAE, IRI, SSA) is essentially due to the low values and the absence of spectral dependency of the absorption found in Albóran. These findings raise the questions of the composition and its origin of the aerosol type that seems to drive the absorbing spectral behaviour in Albóran, which apparently is not that of mineral dust only.~~

7 On the possible NE–SW gradients of the aerosol properties during August-December 2011

In this last Section we are also additionally considering the third site at Alborán Island (see map in Figure 1) to examine possible NE–SW gradients of the aerosol properties. Although data at Alborán are available from June 2011 to January 2012, the coincident period with simultaneous measurements at all three sites is limited to August to December 2011. The following analysis is based on data from this 5-month period. In that particular period, very few AERONET level 2.0 inversion products (with the following restrictions: $50 < SZA < 80º$ and $AOD_{440} > 0.4$) are available: 3 measurements at Ersa, 7 at Palma and 5 at Alborán. For that reason the AERONET products for which these restrictions apply (AAOD, AAE, RRI, IRI and SSA) are not analyzed in the following. Two products, ARF and ARFE, have too fee measurements available in December and are shown only in the period August to November 2011.

We first plot in Figure 11 the (δAE, AE) plots at the three sites to get an insight into the aerosol types found during the period 08 – 12/2011. The fraction of points with $AOD_{675} > 0.15$ with respect to the total number of measurements increases from North to South: 7, 11 and 38 % at Ersa, Palma and Alborán, respectively. In all three sites only a small number of cases correspond to a fine mode cluster ($\eta > 70$ %; $0.10 < r^f < 0.15$ µm). At Ersa most of the points have a fine mode radius between 0.10 and 0.15 µm. One can distinguish easily a cluster formed most probably by maritime + continental aerosols ($0.75 < AE < 1.3$; $30 < \eta < 70$ %) and another one formed by mineral dust ($\delta AE < 0.3$; $AE < 0.75$). These two aerosol types also appear in the Palma plot. Compared to Ersa, the cluster formed by maritime +continental aerosols at Palma is moved towards ($0.5 < AE < 1.2$; $10 < \eta < 50$ % and $r^f < 0.10$ µm). At Alborán a single large cluster is visible at ($0 < \delta AE < 0.4$; $AE < 1.3$) which indicates that maritime + continental aerosols and mineral dust have a similar signature in the (δAE, AE) representation. This first

Código de campo cambiado

Con formato: Fuente: Sin Negrita

Con formato: Subíndice

analysis reveals that the considered period from August to December 2011 seems to have been dominated by rather large particles and an increasing number from North to South of cases with large AODs. It is important to recall that at Alborán 35 % of the days were dominated by maritime +continental aerosols and 31 % by mineral dust during the period June 2011 – January 2012 (Lyamani et al., 2015; Valenzuela et al., 2015; see also Section 4.2).

The same general decreasing tendency of AOD_{440} (Figure 11d) is observed at all three sites from August to December 2011. During the first three months an increasing NE–SW gradient is observed. The NE–SW gradient of the amount of the fine mode particles, shown by AOD^{f}_{440} (Figure 11e), is not that clear. In August and September AOD^{f}_{440} seems to follow a slightly decreasing NE–SW gradient, although all monthly means are within one another standard deviations. Our findings, in agreement with Lyamani et al. (2015), suggest a rather homogeneous spatial distribution of the fine particle loads over the three sites in spite of the distances between the sites and the differences in local sources. $AE_{440\text{-}870}$ (Figure 11f) present a clear decreasing NE–SW gradient during the whole period 08 – 12/2011 which is the signature of an increasing contribution of large particles from North to South. This result is also reflected by the average size distribution shown in Figure 11i where the coarse mode volume concentration has a clear increasing NE–SW gradient. Let's note, en passant, that the fine mode volume concentration is not significantly different at all three sites, which supports the previous hypothesis of a rather homogeneous spatial distribution of the fine particles. The asymmetry factor at 440 nm (Figure 11j) shows an increasing NE–SW gradient with g_{440} values in the range 0.69 – 0.70 at Ersa and Palma and ~0.75 at Alborán. According to Dubovik et al. (2002b) urban/industrial aerosols and desert dust have a similar g_{440} (0.68-0.73) and maritime aerosols have a slightly higher g_{440} (~0.75). Both g spectra at Ersa and Palma are indeed similar to the autumn average (Figure 8b2). We can thus deduce that g is associated to pollution at Ersa (low g and strong spectral dependency), to pollution and mineral dust at Palma (low g and low spectral dependency) and could be attributed to maritime aerosols and mineral dust at Alborán (high g and low spectral dependency). Without further information on the aerosol properties at Alborán, these results cannot be further evaluated. Indeed at least two other types of aerosol are often found in the southern part of the western Mediterranean Basin: from North African urban/industrial origin (Rodríguez et al., 2011) and/or from ship emissions (Valenzuela et al., 2015). The emissions of both types of aerosols have been quantified in the Bay of Algeciras by Pandolfi et al. (2011).

Con formato: Subíndice

Código de campo cambiado

Código de campo cambiado

Con formato: Sin Resaltar

Con formato: Sin Resaltar

Con formato: Subíndice

Con formato: Fuente: Cursiva

Con formato: Fuente: Cursiva, Subíndice

Con formato: Fuente: Cursiva

The aerosol direct radiative forcing (Figure 11g) at the BOA shows an increasing (in absolute value) NE–SW gradient. At the TOA ARF is higher (in absolute value) at Alborán but it is similar at Ersa and Palma. Alborán measurements can be compared to ARF of dust in Granada (140 km N–NW of Alborán) from Valenzuela et al. (2012b) who found annual means of ARF_{BOA} (ARF_{TOA}) at SZA = 55 ± 5º for African desert dust events of approximately -50 (-20) W·m^{-2}. The difference at the TOA between Alborán and the other two sites may come from low aerosol absorption properties at Alborán ($AAOD_{440}$ <~0.02, see Sicard et al., 2014) producing an increase of ARF_{TOA} (Boucher and Tanré, 2000). The aerosol radiative forcing efficiency at the BOA has a decreasing (in absolute value) NE–SW gradient which denote that particles with higher absorption properties (like Ersa and Palma) will be more efficient in producing forcing at the surface. At the TOA the ARFE has no marked gradient.

98 Conclusion

Four years (2011-2014) of AERONET products from the period 2011-2015 are compared in two regional background insular sites in the northern (Corsica) and center (Balearic Islands) part of the western Mediterranean Basin, in Corsica and in the Balearic Islands. A few months of AERONET measurements available in a third site in Alborán Island are considered for completing the dataset. All three sites are situated along a NE–SW axis in the WMB. The Gobbi et al. (2007) graphical method, based on (δAE, AE) plots, has been used to classify the aerosols in clusters with the AERONET AOD inversions (no restrictions) and with the AERONET product inversions (50 < SZA < 80º and AOD_{440} > 0.4). The AOD data put forward three large clusters: a fine mode cluster corresponding to aerosols of polluted and continental origin, a coarse mode cluster corresponding to mineral dust and, in between, a cluster corresponding to maritime aerosols mixed with either one. The restrictions which apply to the level 2.0 inversion products filter drastically the (δAE, AE) plots and leave out only two aerosol types: pollution and mineral dust. Out of the product inversions, the highest percentages of mineral dust outbreaks occur in spring at Ersa (64 %) and in summer at Palma (84 %), while for pollution they occur in summer at both sites (67 and 60 %).

The differences between both sites (Ersa vs. Palma) in the annual mean of aerosol properties like AOD_{440} (0.16 vs. 0.18), $AE_{440–870}$ (1.37 vs. 1.14) and coarse mode volume concentration (0.027 vs. 0.046 µm^3·µm^{-2}) indicate that in average larger particles are found at Palma (vs. Ersa) which suggests that mineral dust is the main driver of these properties on a yearly basis. AOD_{440} reaches maxima in summer and minima in winter. Higher AOD_{440} values are observed at Ersa

Código de campo cambiado
Código de campo cambiado
Con formato: Subíndice
Código de campo cambiado
Con formato: Subíndice
Con formato: Subíndice
Con formato: Subíndice

in spring and at Palma in summer and reflect, respectively, a contribution of aerosols of continental origin already in spring over Ersa and not before summer over Palma, and a higher frequency of mineral dust outbreaks at Palma in summer. The fine mode AOD_{440} is similar at both sites all year round except in spring when the presence of aerosols of continental origin already in spring over Ersa contributes to increase AOD^{f}_{440}. This result, reinforced by a yearly fine mode size distribution quasi-identical at both sites, suggests a rather homogeneous spatial distribution of the fine particle loads over both sites in spite of the distances between the sites and the differences in local sources.

The absorption properties were retrieved from AERONET level 2.0 inversion products with the following restrictions 50 < SZA < 80º and AOD_{440} > 0.4 (AAOD, AAE, complex refractive index and SSA) for the two types of aerosols able to produce large AOD values: pollution and mineral dust. The seasonal variability was assessed for both pollution and mineral dust cases separately, and for the total cases (pollution + mineral dust). The two latter aerosols have very different signature in terms of amplitude and spectra of the absorption properties. Their separate analysis (and previous classification) is thus the only way to identify their signature in the total means. Except in summer at Palma where the total and the mineral dust seasonal means are nearly equal (because mineral dust represents 84 % of the total), the absorption properties (magnitude and spectral dependency) of the total present the signature of neither pollution, nor mineral dust, but a mixture of both. The mineral dust cases are associated with higher AAOD and AAE ($0.023 < AAOD_{440} < 0.057$ and $1.43 < AAE < 2.69$) and lower SSA ($0.89 < SSA_{440} < 0.95$) than pollution ($AAOD_{440} < 0.02$, $1.10 < AAE < 1.24$ and $0.97 < SSA_{440} < 0.98$) and present larger inter-season and inter-site variations.

The asymmetry factor, which represents a measure of the preferred scattering direction of special importance for direct radiative forcing estimations, showed very little inter-season and inter-site variations: g_{440} ranged within 0.71 – 0.73 for mineral dust with no spectral dependency and within 0.68 – 0.70 for pollution with a general tendency to decrease with increasing wavelengths. The radiative forcing at the surface filtered for 50 ≤ SZA ≤ 60º reaches its maximum (in absolute value) during spring at Ersa (-18.0 $W \cdot m^{-2}$) and summer at Palma (-22.8 $W \cdot m^{-2}$). In spring ARF_{BOA} is almost double at Ersa w.r.t. Palma, spring being the season at Ersa of the beginning of pollution episodes and of the peak of mineral dust events. ARF_{TOA} reaches summer maxima (in absolute value) of ~ -13.0 $W \cdot m^{-2}$ at both sites. The radiative forcing efficiency annual cycles show some irregularities and have quite different shapes at

Con formato: Subíndice

Código de campo cambiado

Con formato: Subíndice

Con formato: Normal, Sin viñetas ni numeración

Con formato: Fuente: Cursiva

Con formato: Fuente: Cursiva, Subíndice

Código de campo cambiado

Código de campo cambiado

both sites. Annual means of $ARFE_{BOA}$ and $ARFE_{TOA}$ are, respectively, -144.4 and -99.2 W·m^{-2} at Ersa and -132.2 and -85.1 W·m^{-2} at Palma which points out that on average the aerosol mixing at Ersa is more efficient in producing forcing than the one at Palma.

A few months, from August to December 2011, of AERONET measurements available in a third site in the southern part of the western Mediterranean Basin (Alborán Island) are considered to examine possible North – South gradients over the whole western Mediterranean Basin. The comparison between the three sites has shown an increasing number of events with large AOD and with larger particles from North to South. As a consequence AOD_{440} and C_V^c increases while $AE_{440\text{-}870}$ decreases from North to South. The fine mode AOD and particle volume size distribution have no marked gradient which again supports one of the findings of this work that confirms a rather homogeneous spatial distribution of the fine particle loads in the western Mediterranean Basin. At the surface the aerosol forcing increases from North to South, while its efficiency decreases. At the TOA no clear gradient is observed for both quantities. It is in partly due to the large variability of the absorption properties, especially for mineral dust, which was previously demonstrated.

In summary, a North-South gradient exist in the western Mediterranean Basin for the aerosol amount (AOD) and especially its coarse mode, which all together produces a similar gradient of the aerosol radiative forcing. The aerosol fine mode is rather homogeneously distributed. Absorption properties are quite variable because of the many and different sources of anthropogenic particles in and around the western Mediterranean Basin: North African and European urban areas, the Iberian and Italian Peninsulas, forest fures and ship emissions. As a result the aerosol forcing efficiency, more dependent to absorption than the forcing, has no marked gradient. The high variations observed on the absorption of mineral dust

~~In Ersa and Palma, products such as AOD, AOD^f, the particle size distribution, the sphericity, the radiative forcing and the radiative forcing efficiency show a clear annual cycle:~~

- ~~AOD, AOD^f, the fine and coarse mode volume concentrations reach maxima during summertime and minima during wintertime. The shape of the annual cycles is different between both sites because of the inter-season changes. The higher values of AOD and C_V^c in Palma in summer are due to the mineral dust outbreaks which are more frequent in summer and whose frequency and intensity increases along the NE–SW axis. The higher values of AOD, AOD^f and C_V^f in Ersa in spring are due to the contribution of aerosols of continental origin already in spring over Corsica and not before summer over the Balearic Islands.~~

Código de campo cambiado
Código de campo cambiado
Con formato: Subíndice
Código de campo cambiado
Con formato: Subíndice
Con formato: Normal, Sin viñetas ni numeración

- The sphericity exhibits minima in summer which are clearly due to the higher frequency of mineral dust outbreaks during this season.

- The radiative forcing at the surface filtered for $50 \leq SZA \leq 60^{o}$ reaches its maximum (in absolute value) during spring ($-18.0\ W \cdot m^{-2}$) and summer ($-22.8\ W \cdot m^{-2}$) in Ersa and Palma, respectively. In spring ARF_{BOA} is almost double in Ersa than in Palma. Interestingly, AOD and ARF_{BOA} annual cycles are very well correlated and thus the same reasons explain the differences between the shapes of the ARF_{BOA} annual cycles at both sites. ARF_{TOA} reaches summer maxima (in absolute value) similar at both sites ($\sim -13.0\ W \cdot m^{-2}$) and values in spring 1.6 times larger in Ersa than in Palma. This result indicates that ARF_{TOA} is not as much affected by dust long-range transport as it is by long-range transport of small particles of continental origin.

- The radiative forcing efficiency annual cycles show some irregularities and have quite different shapes at both sites. $ARFE_{BOA}$ reaches minimum absolute values during the period April – October in the range [-150; $-117\ W \cdot m^{-2}$], while $ARFE_{TOA}$ varies in the range [-107; $-71\ W \cdot m^{-2}$] during the same period.

Among the 18 aerosol parameters/effects discussed in the paper, 3 extensive (AOD, C_V^c and ARF_{BOA}) and 3 intensive (AE, r_V^c and Sphericity) parameters present a NE–SW gradient of their summer means. The relationships between (AOD, ARF_{BOA}) vs. C_V^c and (r_V^c, Sphericity) vs. AE are quasi-linear relationships. While the NE–SW gradient of AOD, C_V^c, ARF_{BOA}, AE and Sphericity are clearly related to the higher frequency and intensity of mineral dust episodes during the summer months, the gradient of r_V^c (a decrease along the NE–SW axis) reflects the decreasing influence of European pollution along the NE–SW axis.

Two main conclusions of our work explain why two thirds of the parameters/effects discussed in the paper do not present a NE–SW gradient. First, we have observed a homogeneous spatial distribution (except during the month of March and April) of the fine particle loads over the three sites in spite of the distances between the sites and the differences in local sources. Second, surprisingly low values and the absence of spectral dependency of the absorption were found in Albóran. This finding points out towards the presence of BC and/or soot (possibly originated from North African urban/industrial areas and/or from both the harbor of Algeciras and vessel traffic near the Strait of Gibraltar) and supports the hypothesis of an anthropogenic

influenced mineral dust as already (all 15 summer cases in Alborán correspond to dust events). This hypothesis, already formulated by in previous works (Müller et al., 2009; Valenzuela et al., (2015), together with the fact that the absorption is higher and wavelength dependent at the other two sites, rises an important question for future works: what are the processes which inhibits the BC and/or soot absorption properties during the transport to the northern part of the WMB?. In the framework of ChArMEx, ongoing investigations might bring some light to this subject in the near future to the anthropogenic particle issue and their mixing with the natural particles transported over the western Mediterranean Basin.

Acknowledgements

This study is performed in the framework of work package 4 on aerosol-radiation-climate interactions of the coordinated program ChArMEx (the Chemistry-Aerosol Mediterranean Experiment; http://charmex.lsce.ipsl.fr). It is also supported by the ACTRIS (Aerosols, Clouds, and Trace Gases Research Infrastructure Network) Research Infrastructure Project funded by the European Union's Horizon 2020 research and innovation programme under grant agreement n. 654169 and previously under grant agreement n. 262254 in the 7th Framework Programme (FP7/2007-2013); by the Spanish Ministry of Economy and Competitivity (project TEC2012-34575) and of Science and Innovation (project UNPC10-4E-442) and EFRD (European Fund for Regional Development); by the Department of Economy and Knowledge of the Catalan autonomous government (grant 2014 SGR 583); and by the Andalusia Regional Government through projects P12-RNM-2409 and P10-RNM-6299. ChArMEx-France is supported through the MISTRALS program by INSU, ADEME, Météo-France, and CEA. The The Spanish Agencia Estatal de Meteorología (AEMET) is acknowledged for the use of the Palma de Mallorca AERONET sun-photometer data, and the Royal Institute and Observatory of the Spanish Navy (ROA) for the support provided at AlboránCEA. The The Spanish Agencia Estatal de Meteorología (AEMET) is acknowledged for the use of the Palma de Mallorca AERONET sun-photometer data, and the Royal Institute and Observatory of the Spanish Navy (ROA) for the support provided in Alborán. The authors want also to thank A. Gkikas for information on intense dust episodes at the 3 AERONET sites.

Con formato: Inglés (Estados Unidos)

References

AERONET: AERONET Version 2 Inversion Product Descriptions: http://aeronet.gsfc.nasa.gov/new_web/Documents/Inversion_products_V2.pdf, last access: 11 April 2016.

~~Alados-Arboledas, L., Alcántara, A., Olmo, F.J., Martínez-Lozano, J.A., Estellés, V., Cachorro, V., Silva, A.M., Horvath, H., Gangl, M., Díaz, A., Pujadas, M., Lorente, J., Labajo, A., Sorribas, M., and Paves, G.: Aerosol columnar properties retrieved from CIMEL radiometers during VELETA 2002, Atmos. Environ., 42, 2654–2667, 2008.~~

Albrecht, B. A.: Aerosols, cloud microphysics and fractional cloudiness, Science, 245, 1227–1230, doi:10.1126/science.245.4923.1227, 1989.

Barnaba, F., and Gobbi, G. P.: Aerosol seasonal variability over the Mediterranean region and relative impact of maritime, continental and Saharan dust particles over the basin from MODIS data in the year 2001, Atmos. Chem. Phys., 4, 2367–2391, doi: 10.5194/acp-4-2367-2004, 2004.

Basart, S., Pérez, C., Cuevas, E., Baldasano, J. M., and Gobbi, G. P.: Aerosol characterization in Northern Africa, Northeastern Atlantic, Mediterranean Basin and Middle East from direct-sun AERONET observations, Atmos. Chem. Phys., 9, 8265–8282, doi: 10.5194/acp-9-8265-2009, 2009.

Bergametti, G., Gomes, L., Remoudaki, E., Desbois, M., Martin, D., and Buat-Ménard, P.: Present transport and deposition patterns of African dusts to the north-western Mediterranean, In Paleoclimatology and Paleometeorology: Modern and Past Patterns of Global Atmospheric Transport. Leinen, M., and Sarnthein, M., Eds., Kluwer, 227-251, 1989.

Bergametti, G., Remoudaki, E., Losno, R., Steiner, E., Chatenet, B. and Buat-Mnard, P.: Source, transport and deposition of atmospheric phosphorus over the northwestern Mediterranean, J. Atmos. Chem., 14, 501–513, doi: 10.1007/BF00115254, 1992.

Bergstrom, R.W., Pilewskie, P., Russell, P. B., Redemann, J., Bond, T. C., Quinn, P. K., and Sierau, B.: Spectral absorption properties of atmospheric aerosols, Atmos. Chem. Phys., 7, 5937–5943, doi: 10.5194/acp-7-5937-2007, 2007.

Boucher, O., and Tanré, D.: Estimation of the aerosol perturbation to the Earth's radiative budget over oceans using POLDER satellite aerosol retrievals, Geophys. Res. Lett., 27, 1103– 1106, doi: 10.1029/1999GL010963, 2000.

Con formato: Fuente de párrafo predeter., Color de fuente: Automático, Alemán (Alemania)

Con formato: Inglés (Estados Unidos)

Con formato: Resaltar

Con formato: Inglés (Estados Unidos)

Con formato: Inglés (Estados Unidos)

Con formato: Inglés (Estados Unidos)

Con formato: Inglés (Estados Unidos)

Con formato: Inglés (Estados Unidos)

~~Burton, S. P., Ferrare, R. A., Hostetler, C. A., Hair, J. W., Rogers, R. R., Obland, C. F., Butler, M. D., Cook, A. L., Harper, D. B., and Froyd, K. D.: Aerosol classification using airborne High Spectral Resolution Lidar measurements – methodology and examples Atmos. Meas. Technol., 5, 73–98, 2012.~~

Cachorro, V. E., Toledano, C., Prats, N., Sorribas, M., Mogo, S., Berjón, A., Torres, B., Rodrigo, R., de la Rosa, J., and De Frutos, A. M.: The strongest desert dust intrusion mixed with smoke over the Iberian Peninsula registered with Sun photometry, J. Geophys. Res., 113, D14S04, doi: 10.1029/2007JD009582, 2008.

CERES: CERES Terra Edition2B SSF TOA Fluxes - Accuracy and Validation: https://eosweb.larc.nasa.gov/sites/default/files/project/ceres/quality_summaries/ssf_toa_terra_ed2B.pdf, last access: 11 April 2016.

~~Chazette, P., Marnas, F. and Totems, J., The mobile Water vapor Aerosol Raman LIdar and its implication in the framework of the HyMeX and ChArMEx programs: application to a dust transport process, Atmos. Meas. Tech., 7, 1629–1647, 2014.~~

Denjean, C., Cassola, F., Mazzino, A., Triquet, S., Chevaillier, S., Grand, N., Bourrianne, T., Momboisse, G., Sellegri, K., Schwarzenbock, A., Freney, E., Mallet, M., and Formenti, P.: Size distribution and optical properties of mineral dust aerosols transported in the western Mediterranean, Atmos. Chem. Phys.~~ Discuss.~~, 1~~5~~6, ~~21607~~1081-~~21669~~1104, doi: 10.5194/acp-16-1081-2016~~acpd-15-21607-2015~~, 2016~~5~~.

Derimian, Y., Léon, J.-F., Dubovik, O., Chiapello, I., Tanré, D., Sinyuk, A., Auriol, F., Podvin, T., Brogniez, G., and Holben, B. N.: Radiative properties of aerosol mixture observed during the dry season 2006 over M'Bour, Senegal (African Monsoon Multidisciplinary Analysis campaign), J. Geophys. Res., 113, D00C09, doi: 10.1029/2008JD009904, 2008.

Di Biagio, C., Di Sarra, A., Meloni, D., Monteleone, F., Piacentino, S., and Sferlazzo, D.: Measurements of Mediterranean aerosol radiative forcing and influence of the single scattering albedo, J. Geophys. Res., 114, D06211, doi:10.1029/2008JD011037, 2009.

Di Sarra, A., Pace, G., Meloni, D., De Silvestri, L., Piacentino, S., and Monteleone, F.: Surface shortwave radiative forcing of different aerosol types in the Mediterranean, Geophys. Res. Lett., 35, L02714, doi: 10.1029/2007GL032395, 2008.

Dubovik, O. and King, M. D., A flexible inversion algorithm for retrieval of aerosol optical properties from Sun and sky radiance measurements, J. Geophys. Res., 105, 20673–20696, doi: 10.1029/2000JD900282, 2000a.

Con formato: Fuente de párrafo predeter., Color de fuente: Automático, Alemán (Alemania)

Dubovik, O., Smirnov, A., Holben, B.N., King, M.D., Kaufman, Y. J., Eck, T.F., and Slutsker, I.: Accuracy assessment of aerosol optical properties retrieval from AERONET sun and sky radiance measurements, J. Geophys. Res ,105, 9791-9806, doi: 10.1029/2000JD900040, 2000b.

Dubovik, O., Holben, B. N., Lapyonok, T., Sinyuk, A., Mishchenko, M. I., Yang, P., and Slutsker, I.: Non-spherical aerosol retrieval method employing light scattering by spheroids, Geophys. Res. Lett., 10, 1415, doi: 10.1029/2001GL014506, 2002a.

Dubovik, O., Holben, B. N., Eck, T. F., Smirnov, A., Kaufman, Y. J., King, M. D., Tanré, D., and Slutsker, I.: Variability of absorption and optical properties of key aerosol types observed in worldwide locations, J. Atmos. Sci., 59, 590–608, 2002b.

Dubovik, O., Sinyuk, A., Lapyonok, T., Holben, B. N., Mishchenko, M., Yang, P., Eck, T. F., Volten, H., Muñoz, O., Veihelmann, B., van der Zande, W. J., Leon, J.-F., Sorokin, M., and Slutsker, I.: Application of spheroid models to account for aerosol particle nonsphericity in remote sensing of desert dust, J. Geophys. Res., 111, D11208, doi:10.1029/2005JD006619, 2006.

Dubuisson, P., Buriez, J.C., and Fouquart, Y.: High ~~S~~spectral ~~R~~reresolution ~~S~~solar ~~R~~radiative ~~T~~transfer in ~~A~~absorbing and ~~S~~scattering media~~, a~~: Application to the satellite simulation, J. Quant. Spectros. Radiat. Transfer., 55~~(1)~~, 103-126, doi: 10.1016/0022-4073(95)00134-4, 1996.

Dubuisson, P., Dessailly, D., Vesperini, M., and Frouin, R.: Water Vapor Retrieval Over Ocean Using Near-Infrared Radiometry, J. Geophys. Res., 109, D19106, doi:10.1029/2004JD004516, 2004.

Dubuisson, P., Roger, J., Mallet, M., and Dubovik, O.: A Code to Compute the Direct Solar Radiative Forcing: Application to Anthropogenic Aerosols during the Escompte Experiment, Proc. International Radiation Symposium (IRS 2004) on Current Problems in Atmospheric Radiation, edited by: Fischer, H., Sohn, B.-J., and Deepak, A., Hampton, 127–130, 23–28 August 2004, Busan, Korea, 2006.

Dulac, F., An overview of the Chemistry-Aerosol Mediterranean Experiment (ChArMEx), European Geosciences Union General Assembly, Geophys~~ical~~ Res~~earch~~, Abstracts, ~~Vol.~~ 16, EGU2014-11441, Vienna (Austria), 27 April – 2 May 2014.

Eck, T. F., Holben, B. N., Reid, J. S., Dubovik, O. Kinne, S., Smirnov, A., O'Neill, N. T., and Slutsker, I.: ~~The w~~Wavelength dependence of the optical depth of biomass burning, urban

and desert dust aerosols, J. Geophys. Res., 104, 31333-31349, doi: 10.1029/1999JD900923, 1999.

Escudero, M., Querol, X., Ávila, A., and Cuevas, E.: Origin of the exceedances of the European daily PM limit value in regional background areas of Spain, Atmos. Environ., 41, 730–744, doi: 10.1016/j.atmosenv.2006.09.014, 2007.

Formenti, P., Boucher, O. Reiner, T., Sprung, D., Andreae, M. O., Wendisch, M., Wex, H., Kindred, D., Tzortziou, M., Vasaras, A., and Zerefos, C.: STAAARTE-MED 1998 summer airborne measurements over the Aegean Sea: 2. Aerosol scattering and absorption, and radiative calculations, J. Geophys. Res., 107(D21), 4551, doi:10.1029/2001JD001536, 2002.

~~Freudenthaler, V., Esselborn, M., Wiegner, M., Heese, B., Tesche, M., Ansmann, A., Müller, D., Althausen, D., Wirth, M., Fix, A., Ehret, G., Knippertz,, P., Toledano, C., Gasteiger, J., Garhammer, M., and Seefeldner, M., Depolarization ratio profiling at several wavelengths in pure Saharan dust during SAMUM 2006, Tellus, 61B, 165–179, 2008.~~

Gangoiti, G., Millán, M. M., Salvador, R., and Mantilla, E.: Long-range transport and re-circulation of pollutants in the western Mediterranean during the project Regional Cycles of Air Pollution in the West-Central Mediterranean Area, Atmos. Environ., 35, 6267-6276, doi: 10.1016/S1352-2310(01)00440-X, 2001.

García, O. E., Díaz, A. M., Expósito, F. J., Díaz, J. P., Dubovik, O., Dubuisson, P., Roger, J.-C., Eck, T. F., Sinyuk, A., Derimian, Y., Dutton, E. G., Schafer, J. S., Holben, B. N., and García, C. A., Validation of AERONET estimates of atmospheric solar fluxes and aerosol radiative forcing by ground-based broadband measurements, J. Geophys. Res., 113, D21207, doi:10.1029/2008JD010211, 2008.

García, O. E., Expósito, F. J., Díaz, J. P., and Díaz, A. M.: Radiative forcing under aerosol mixed conditions, J. Geophys. Res., 116, D01201, doi:10.1029/2009JD013625, 2011.

García, O.E., Díaz, J.P., Expósito, F.J., Díaz, A.M., Dubovik, O., and Derimian, Y., Aerosol Radiative Forcing: AERONET-Based Estimates, Climate Models, Dr. Leonard Druyan (Ed.), ISBN: 978-953-51-0135-2, InTech, Available from: http://www.intechopen.com/books/climate-models/aerosol-radiative-forcing-aeronet-based-estimates (last access: 16 December 2015), 2012a.

García, O. E., Díaz, J. P., Expósito, F. J., Díaz, A. M., Dubovik, O., Derimian, Y., Dubuisson, P., and Roger, J.-C.: Shortwave radiative forcing and efficiency of key aerosol types using

Con formato: Sin subrayado

AERONET data, Atmos. Chem. Phys., 12, 5129–5145, doi:10.5194/acp-12-5129-2012, 2012b.

Giorgi, F.: Climate change hot-spots, Geophys. Res. Lett., 33, L08707, doi:10.1029/2006GL025734, 2006.

Giorgi, F. and Lionello, P., Climate change projections for the Mediterranean region, Global Planet. Change, 63, 90–104, doi: 10.1016/j.gloplacha.2007.09.005, 2008.

Gkikas, A., Houssos, E.E., Hatzianastassiou, N., Papadimas, C.D., and Bartzokas, A.: Synoptic conditions favouring the occurrence of aerosol episodes over the broader Mediterranean basin, Q. J. R. Meteorol. Soc., 138, 932–949, doi:10.1002/qj.978, 2012.

Gkikas, A., Basart, S., Hatzianastassiou, N., Marinou, E., Amiridis, V., Kazadzis, S., Pey, J., Querol, X., Jorba, O., Gassó, S., and Baldasano, J. M.: Mediterranean desert dust outbreaks and their vertical structure based on remote sensing data, Atmos., Chem. Phys., 16, in press, 2016.

Gobbi, G. P., Kaufman, Y. J., Koren, I., and Eck, T. F.: Clasification of aerosol properties derived from AERONET direct sun data, Atmos. Chem. Phys. 7, 453–458, doi: 10.5194/acp-7-453-2007, 2007.

Granados-Muñoz, M. J., Navas-Guzmán, F., Bravo-Aranda, J. A., Guerrero-Rascado, J. L., Lyamani, H., Valenzuela, A., Titos, G., Fernández-Gálvez, J., and Alados-Arboledas, L.: Hygroscopic growth of atmospheric aerosol particles based on active remote sensing and radiosounding measurements: selected cases in southeastern Spain, Atmos. Meas. Tech., 8, 705-718, doi:10.5194/amt-8-705-2015, 2015.

Guieu, C., Bonnet, S., and Wagener, T.: Biomass burning as a source of dissolved iron to the open ocean?, Geophys. Res. Lett., 32, L19608, doi:10.1029/2005GL022962, 2005.

Holben, B. N., Eck, T. F., Slutsker, I., Tanré, D., Buis, J. P., Setzer, A., Vermote, E. F., Reagan, J. A., Kaufman, Y. J., Nakajima, T., Lavenu, F., Jankowiak, I., and Smirnov, A., AERONET – A federated instrument network and data archive for aerosol characterization, Remote Sens. Environ., 66, 1–16, doi:10.1016/S0034-4257(98)00031-5, 1998.

Holben, B.N., Eck, T. F., Slutsker, I., Smirnov, A., Sinyuk, A., Schafer, J., Giles, D., and Dubovik, O.: AERONET's Version 2.0 quality assurance criteria, in Remote Sensing of the Atmosphere and Clouds, edited by: Tsay, S.-C., Nakajima, T., Ramesh P. S., and Sridharan, R., Proc. of SPIE Vol. 6408, 64080Q, doi: 10.1117/12.706524, 2006.

Con formato: Inglés (Estados Unidos)
Con formato: Inglés (Estados Unidos)
Con formato: Inglés (Estados Unidos)
Con formato: Inglés (Estados Unidos)

Hurrell, J. W.: Decadal trends in the North Atlantic Oscillation: Regional temperatures and precipitation, Science, 269, 676-679, doi: 10.1126/science.269.5224.676, 1995.

Kallos, G., Cortón, V., Lagouvardos, K., and Papadopoulos, A.: On the long range transport of air pollutants from Europe to Africa, Geophys. Res. Lett., 25 (5), 619-622, 1998.

Kallos, G., Astitha, M., Katsafados, P., and Spyrou, C.: Long-range transport of anthropogenically and naturally produced particulatematter in the Mediterranean and North Atlantic: Current state of knowledge, J. Appl. Meteorol. Clim., 46, 1230–1251, doi: 10.1175/JAM2530.1, 2007.

Kaufman, Y. J.: Aerosol optical thickness and atmospheric path radiance, J. Geophys. Res., 98, 2677–2692, doi: 10.1029/92JD02427, 1993.

Lack, D. A. and Cappa, C. D.: Impact of brown and clear carbon on light absorption enhancement, single scatter albedo and absorption wavelength dependence of black carbon, Atmos. Chem. Phys., 10, 4207–4220, doi:10.5194/acp-10-4207-2010, 2010.

Lambert, D. and Argence, S.: Preliminary study of an intense rainfall episode in Corsica, 14 September 2006, Adv. Geosci., 16, 125-129, 2008.

Lambert, D., Mallet, M., Ducrocq, V., Dulac, F., Gheusi, F., and Kalthoff, N.: CORSiCA: a Mediterranean atmospheric and oceanographic observatory in Corsica within the framework of HyMeX and ChArMEx, Adv. Geosci., 26, 125-131, doi:10.5194/adgeo-26-125-2011, 2011.

Lelieveld, J., Berresheim, H., Borrmann, S., Crutzen, P.J., Dentener, F.J., Fischer, H., Feichter, J., Flatau, P.J., Heland, J., Holzinger, R., Korrmann, R., Lawrence, M.G., Levin, Z., Markowicz, K.M., Mihalopoulos, N., Minikin, A., Ramanathan, V., de Reus, M., Roelofs, G.J., Scheeren, H.A., Sciare, J., Schlager, H., Schultz, M., Siegmund, P., Steil, B., Stephanou, E.G., Stier, P., Traub, M.,Warneke, C., Williams, J., and Ziereis, H.: Global air pollution crossroads over the Mediterranean, Science, 298, 794–799, doi: 10.1126/science.1075457, 2002.

Léon, J. F., Augustin, P., Mallet, M., Bourrianne, T., Pont, V., Dulac, F., Fourmentin, M., Lambert, D., and Sauvage, B.: Aerosol vertical distribution, optical properties and transport over Corsica (western Mediterranean), Atmos. Chem. Phys. Discuss., 15, 9507-9540, doi:10.5194/acpd-15-9507-2015, 2015.

Loeb, N. G., Kato, S., Loukachine, K., Manalo-Smith, N., and Doelling, D. R.: Angular Distribution Models for Top-of-Atmosphere Radiative Flux Estimation from the Clouds and

the Earth's Radiant Energy System Instrument on the Terra Satellite. Part II: Validation, J. Atmos. Oceanic Technol., 24, 564-584, doi:10.1175/JTECH1983.1, 2007.

~~Lurton, T., Renard, J.-B., Vignelles, D., Jeannot, M., Akiki, R., Mineau, J.-L., and Tonnelier, T., Light scattering at small angles by atmospheric irregular particles: modelling and laboratory measurements, Atmos., Meas. Tech., 7, 931-939, 2014.~~

Lyamani, H., Olmo, F. J., Alcántara, A., and Alados-Arboledas, L.: Atmospheric aerosols during the 2003 heat wave in southeastern Spain II: Microphysical columnar properties and radiative forcing, Atmos. Environ., 40, 6465–6476, doi: 10.1016/j.atmosenv.2006.04.047, 2006.

Lyamani, H., Fernández-Gálvez, J., Pérez-Ramírez, D., Valenzuela, A., Antón, M., Alados, I., Titos, G., Olmo, F.J., Alados-Arboledas, L.: Aerosol properties over two urban sites in South Spain during an extended stagnation episode in winter season, Atmos. Environ., 62, 424-432, http://dx.doi.org/10.1016/j.atmosenv.2012.08.050 2012.

Con formato: Fuente de párrafo predeter., Color de fuente: Automático

Lyamani, H., Valenzuela, A., Perez-Ramirez, D., Toledano, C., Granados-Muñoz, M. J., Olmo, F. J., and Alados-Arboledas, L.: Aerosol properties over the western Mediterranean basin: temporal and spatial variability, Atmos. Chem. Phys., 15, 2473-2486, doi: 10.5194/acp-15-2473-2015, 2015.

Maheras, P., Xoplaki, E., Davies, T., Vide, J. V., Bariendos, M., and Alcoforado, M.: Warm and cold monthly anomalies across the Mediterranean basin and their relationship with circulation: 1860–1990, Int. J. Climatol., 19, 1697-1715, doi: 10.1002/(SICI)1097-0088(199912)19:15<1697::AID-JOC442>3.0.CO;2-S, 1999.

Mallet, M., Dubovik, O., Nabat, P., Dulac, F., Kahn, R., Sciare, J., Paronis, D. and Léon, J. F., Absorption properties of Mediterranean aerosols obtained from multi-year ground-based remote sensing observations, Atmos. Chem. Phys., 13, 9195–9210, doi:10.5194/acp-13-9195-2013, 2013.

Mallet, M., Dulac, F., Formenti, P., Nabat, P., Sciare, J., Roberts, G., Pelon, J., Ancellet, G., Tanré, D., Parol, F., di Sarra, A., Alados, L., Arndt, J., Auriol, F., Blarel, L., Bourrianne, T., Brogniez, G., Chazette, P., Chevaillier, S., Claeys, M., D'Anna, B., Denjean, C., Derimian, Y., Desboeufs, K., Di Iorio, T., Doussin, J.-F., Durand, P., Féron, A., Freney, E., Gaimoz, C., Goloub, P., Gómez-Amo, J. L., Granados-Muñoz, M. J., Grand, N., Hamonou, E., Jankowiak, I., Jeannot, M., Léon, J.-F., Maillé, M., Mailler, S., Meloni, D., Menut, L., Momboisse, G., Nicolas, J., Podvin, J., Pont, V., Rea, G., Renard, J.-B., Roblou, L.,

Schepanski, K., Schwarzenboeck, A., Sellegri, K., Sicard, M., Solmon, F., Somot, S., Torres, B., Totems, J., Triquet, S., Verdier, N., Verwaerde, C., Wenger, J., and Zapf, P.: Overview of the Chemistry-Aerosol Mediterranean Experiment/Aerosol Direct Radiative Forcing on the Mediterranean Climate (ChArMEx/ADRIMED) summer 2013 campaign, ~~,~~ Atmos. Chem. Phys. ~~Discuss.~~, 1~~5~~6, ~~19615~~455~~–19727~~504, doi: 10.5194/acp-16-455-2016~~10.5194/acpd-15-19615-2015~~, 201~~5~~6.

Mariotti, A., Pan, Y., Zeng, N., and Alessandri, A.: Long-term climate change in the Mediterranean region in the midst of decadal variability, Clim. Dynam., 44, 1437–1456, ~~20~~ doi: 10.1007/s00382-015-2487-3, 2015.

Markowicz, K. M., Flatau, P. J., Ramana, M. V., Crutzen, P. J., and Ramanathan, V., Absorbing ~~m~~Mediterranean aerosols lead to a large reduction in the solar radiation at the surface, Geophys. Res. Lett., 29, 1968, doi:10.1029/2002GL015767, 2002.

Meloni, D., di Sarra, A., Di Iorio, T., and Fiocco G.: Influence of the vertical profile of Saharan dust on the visible direct radiative forcing, J. Quant. Spectrosc. Radiat. Transfer, 93, 397–413, doi: 10.1016/j.jqsrt.2004.08.035, 2005.

Meloni, D., Junkermann, W., di Sarra, A., Cacciani, M., De Silvestri, L., Di Iorio, T., Estellés, V., Gómez-Amo~~,4~~, J. L., Pace, G., and Sferlazzo, D. M.: Altitude-resolved shortwave and longwave radiative effects of desert dust in the Mediterranean during the GAMARF campaign: Indications of a net daily cooling in the dust layer, J. Geophys. Res., 120, 3386–3407, doi:10.1002/2014JD022312, 2015.

Millán, M. M., Salvador R., Mantilla E., and Kallos, G.: Photooxidant dynamics in the Mediterranean basin in summer: results from European research projects, J. Geophys. Res., 102, 8811-8823, doi: 10.1029/96JD03610, 1997.

Mishra, A. K., Klingmueller, K., Fredj, E., Lelieveld, J., Rudich, Y., and Koren, I.: Radiative signature of absorbing aerosol over the eastern Mediterranean basin, Atmos. Chem. Phys., 14, 7213-7231, doi:10.5194/acp-14-7213-201, 2014.

Moosmüller, H., Chakrabarty, R. K., and Arnott,W. P., Aerosol light absorption and its measurement: A review, J. Quant. Spectrosc. Radiat. Transf., 110, 844–878, doi: 10.1016/j.jqsrt.2009.02.035, 2009.

Moulin C., Lambert, C. E., Dulac, F., and Dayan, U: Control of atmospheric export of dust from North Africa by the North Atlantic Oscillation, Nature, 387, 691–694, doi: 10.1038/42679, 1997.

Moulin C., Lambert, C. E., Dayan, U., Masson, V., Ramonet, M., Bousquet, P., Legrand, M., Balkanski, Y. J., Guelle, W., Marticorena, B., Bergametti, G., and Dulac, F., Satellite climatology of African dust transport in the Mediterranean atmosphere, J. Geophys. Res., 103, 13137–13144, doi: 10.1029/98JD00171, 1998.

~~Müller, T., Schladitzm A., Massling, A., Kaaden, N., Kandler, K., and Wiedensohler, A.: Spectral absorption coefficients and imaginary parts of refractive indices of Saharan dust during SAMUM-1, Tellus, 61B, 79–95, 2009.~~

Nabat, P., Solmon, F., Mallet, M., Kok, J. F., and Somot, S.: Dust emission size distribution impact on aerosol budget and radiative forcing over the Mediterranean region: a regional climate model approach, Atmos. Chem. Phys., 12, 10545–10567, doi:10.5194/acp-12-10545-2012, 2012.

Nabat, P., Somot, S., Mallet, M., Chiapello, I., Morcrette, J. J., Solmon, F., Szopa, S., Dulac, F., Collins, W., Ghan, S., Horowitz, L. W., Lamarque, J. F., Lee, Y. H., Naik, V., Nagashima, T., Shindell, D., and Skeie, R.: A 4-D climatology (1979–2009) of the monthly tropospheric aerosol optical depth distribution over the Mediterranean region from a comparative evaluation and blending of remote sensing and model products, Atmos. Meas. Tech., 6, 1287–1314, doi:10.5194/amt-6-1287-2013, 2013.

Nabat, P., Somot, S., Mallet, M., Sanchez-Lorenzo, A., and Wild, M.: Contribution of anthropogenic sulfate aerosols to the changing Euro-Mediterranean climate since 1980, Geophys. Res. Lett., 41, 5605-5611, doi:10.1002/2014GL060798, 2014.

Nabat, P., Somot, S., Mallet, M., Sevault, F., Chiacchio, M., and Wild, M.: Direct and semi-direct aerosol radiative effect on the Mediterranean climate variability using a coupled regional climate system model, Clim. Dyn., 44, 1127-1155, doi:10.1007/s00382-014-2205-6, 2015.

Nicolas, J., Sciare, J., Petit, J.-E., Bonnaire, N., Féron, A., Dulac, F., Hamonou, E., Gros, V., Mallet, M., Lambert, D., Sauvage, S., Léonardis, T., Tison, E., Colomb, A., Fresney., E., Pichon, J.-M., Bouvier, L., Bourrianne, T., and Roberts, G.: New insights on aerosol sources and properties of organics in the west Mediterranean basin, Geophys. Res. Abstracts, 15, EGU2013-12852, Vienna (Austria), 7-12 April 2013.

Con formato: Resaltar

~~Nakajima, T., Tonna, G., Rao, R., Boi, P., Kaufman, Y., and Holben, B.: Use of sky brightness measurements from ground for remote sensing of particulate dispersion, Appl. Opt., 35, 2672–2686, 1996.~~

Norris, J. R., and Wild, M.: Trends in aerosol radiative effects over Europe inferred from observed cloud cover, solar ''dimming'' and solar ''brightening,'', J. Geophys. Res., 112, D08214, doi:10.1029/2006JD007794, 2007.

~~Olmo, F. J., Quirantes, A., Lara, V., Lyamani, H., and Alados-Arboledas, L.: Aerosol optical properties assessed by an inversion method using the solar principal plane for non-spherical particles, J. Quant. Spectrosc. Radiat. Transfer, 109, 1504–1516, 2008.~~

Omar, A.H., Won, J.G., Winker, D.M., Yoon, S.C., Dubovik, O., and McCormick, M.P.: Development of global aerosol models using cluster analysis of Aerosol Robotic Network (AERONET) measurements. J. Geophys. Res., 110, D10S14, doi:10.1029/2004JD004874, 2005.

O'Neill, N. T., Dubovik, O., and Eck, T. F.: Modified Ångström coefficient for the characterization of submicrometer aerosols, App. Opt., 40, 2368-2375, doi: 10.1364/AO.40.002368, 2001.

~~O'Neill, N. T., Dubovik, O., and Eck, T. F.: A modified Angstrom coefficient for the characterization of sub-micron aerosols, App. Opt., 40 (15), 2368-2374, 2001.~~

O'Neill, N. T.,~~T.,~~ Eck, T. F., Smirnov, A., Holben, B. N., and Thulasiraman, S.: Spectral discrimination of coarse and fine mode optical depth, J. Geophys. Res., 108 (D17), 4559-4573, doi: 10.1029/2002JD002975, 2003.

Pace, G., Meloni, D., and di Sarra, A.: Forest fire aerosol over the Mediterranean basin during summer 2003, J. Geophys. Res., 110, D21202, doi: 10.1029/2005JD005986, 2005.

Pandolfi, M., Gonzalez-Castanedo, Y., Alastuey, A., de la Rosa, J. D., Mantilla, E., Sanchez de la Campa, A., Querol, X., Pey, J., Amato, F., and Moreno, T.: Source apportionment of PM_{10} and $PM_{2.5}$ at multiple sites in the strait of Gibraltar by PMF: impact of shipping emissions, Environ. Sci. Pollut. Res., 18, 260–269, doi: 10.1007/s11356-010-0373-4, 2011.

Papadimas, C. D., Hatzianastassiou, N., Mihalopoulos, N., Querol, X., and Vardavas, I.: Spatial and temporal variability in aerosol properties over the Mediterranean basin based on 6-year (2000–2006) MODIS data, J. Geophys. Res., 113, D11205, doi: 10.1029/2007JD009189, 2008.

Con formato: Resaltar

Con formato: Resaltar

~~Petzold, A., Rasp, K., Weinzierl, B., Esselborn, M., Hamburger, T., Dörnbrack, A., Kandler, K., Schütz, L., Knippertz, P., Fiebig, M., and Virkkula, A.: Saharan dust absorption and refractive index from aircraft-based observations during SAMUM 2006, Tellus, 61B, 118–130, 2009.~~

Pérez, C., Sicard, M., Jorba, O., Comerón, A., and Baldasano, J. M.: Summertime Re-Circulations of Air Pollutants Over the North-Eastern Iberian Coast Observed From Systematic EARLINET Lidar Measurements in Barcelona, Atmos. Environ., 38, 3983-4000, doi: 10.1016/j.atmosenv.2004.04.010, 2004.

Perrone, M. R., De Tomasi, F., and Gobbi, G. P.: Vertically resolved aerosol properties by multi-wavelength lidar measurements, Atmos. Chem. Phys., 14, 1185-1204, doi:10.5194/acp-14-1185-2014, 2014.

Petzold, A., Rasp, K., Weinzierl, B., Esselborn, M., Hamburger, T., Dörnbrack, A., Kandler, K., Schütz, L., Knippertz, P., Fiebig, M., and Virkkula, A.: Saharan dust absorption and refractive index from aircraft-based observations during SAMUM 2006, Tellus, 61B, 118–130, doi:10.1111/j.1600-0889.2008.00383.x, 2009.

Pey, F., Querol, X., and Alastuey, A., Variations of levels and composition of PM10 and PM2.5 at an insular site in the Western Mediterranean, Atmos. Res., 94, 285–299, 2009.

Pey, J., Querol, X., Alastuey, A., Forastiere, F., and Stafoggia, M.: African dust outbreaks over the Mediterranean Basin during 2001–2011: PM10 concentrations, phenomenology and trends, and its relation with synoptic and mesoscale meteorology, Atmos. Chem. Phys., 13, 1395–1410, doi:10.5194/acp-13-1395-2013, 2013.

Pincus, R., and Baker, M. B.:Precipitation, solar absorption, and albedo susceptibility in marine boundary layer clouds, Nature, 372, 250–252, doi:10.1038/372250a0, 1994.

Pruppacher, H. R., and Klett, J. D.: Microphysics of Clouds and Precipitation, Kluwer Academic Publishers, Dordrecht, 1997.

Redemann, J., Turco, R.P., Liou, K.N., Russell, P.B., Bergstrom, R.W., Schmid, B., Livingston, J.M., Hobbs, P.V., Hartley, W.S., Ismail, S., Ferrare, R.A., and Browell, E.V.: Retrieving the vertical structure of the effective aerosol complex index of refraction from a combination of aerosol in situ and remote sensing measurements during TARFOX, J. Geophys. Res., 105, 9949–9970, doi: 10.1029/1999JD901044, 2000.

Con formato: Inglés (Estados Unidos)

Con formato: Fuente: 12 pto, Inglés (Estados Unidos)

Con formato: Español (España)

Ricchiazzi, P., Yang, S., Gautier, C., and Sowle, D.: SBDART: A research and teaching software tool for plane-parallel radiative transfer in the Earth's atmosphere, Bull. Am. Meteorol. Soc., 79, 2101–2114, 1998.

~~Renard, J. B., Dulac, F., Berthet, G., Lurton, T., Vignelles, Jégou, F., D., Tonnelier, T., Thaury, C., Jeannot, M., Couté, M., Akiki, R., Mineau, J. L., Verdier, N., Mallet, M., Gensdarmes, F., Charpentier, P., Mesmin, P., Duverger, V., Dupont, J. C., Elias, T., Crenn, V., Sciare, J., Giacomoni, J., Gobbi, M., Hamonou, E., Olafsson, H., Dagsson-Waldhauserova, P., Camy-Peyret, C., Mazel, C., Décamps, T., Piringer, M., Surein, J., and Daugeron, D.: LOAC: a small aerosol optical counter/sizer for ground-based and balloon measurements of the size distribution and nature of atmospheric particles – Part 1: Principle of measurements and instrument evaluation, Atmos. Meas. Tech. Discuss., 8, 1203-1259, doi:10.5194/amtd-8-1203-2015 2015.~~

Rodríguez, S., Alastuey, A., Alonso-Perez, S., Querol, X., Cuevas, E., Abreu-Afonso, J., Viana, M., Pérez, N., Pandolfi, M., and de la Rosa, J.: Transport of desert dust mixed with North African industrial pollutants in the subtropical Saharan Air Layer, Atmos. Chem. Phys., 11, 6663–6685, doi: 10.5194/acp-11-6663-2011, 2011.

Russell, P. B., Bergstrom, R. W., Shinozuka, Y., Clarke, A. D., De-Carlo, P. F., Jimenez, J. L., Livingston, J. M., Redemann, J., Dubovik, O., and Strawa, A.: Absorption Angstrom Exponent in AERONET and related data as an indicator of aerosol composition, Atmos. Chem. Phys., 10, 1155–1169, doi:10.5194/acp-10-1155-2010, 2010.

Sanchez-Gomez, E., Somot, S., and Mariotti, A.: Future changes in the Mediterranean water budget projected by an ensemble of regional climate models, Geophys. Res. Lett., 36, L21401, doi:10.1029/2009GL040120, 2009.

Schuster, G. L., Dubovik, O., and Holben, B. N.: Angstrom exponent and bimodal aerosol size distributions, J. Geophys. Res., 111, D07207, doi:10.1029/2005JD006328, 2006.

Sciare, J., Dulac, F., Feron, A., Crenn, V., Sarda Esteve, R., Baisnee, D., Bonnaire, N., Hamonou, E., Mallet, M., Lambert, D., Nicolas, J. B., Bourrianne, T., Petit, J.E., Favez, O., Canonaco, F., Prevot, A., Mocnik, G., Drinovec, L., Marpillat, A., and Serrie, W., Carbonaceous aerosols in the Western Mediterranean during summertime and their contribution to the aerosol optical properties at ground level: First results of the ChArMEx-ADRIMED 2013 intensive campaign in Corsica, European Geosciences Union General Assembly, Geophys. Res. Abstracts, 16, EGU2014-2358, Vienna (Austria), 27 April-2 May 2014.

Sciare, J., Dulac, F., Feron, A., Crenn, V., Sarda Esteve, R., Baisnee, D., Bonnaire, N., Hamonou, E., Mallet, M., Lambert, D., Nicolas, J. B., Bourrianne, T., Petit, J.E., Favez, O., Canonaco, F., Prevot, A., Mocnik, G., Drinovec, L., Marpillat, A., and Serrie, W., Carbonaceous aerosols in the Western Mediterranean during summertime and their contribution to the aerosol optical properties at ground level: First results of the ChArMEx-ADRIMED 2013 intensive campaign in Corsica, European Geosciences Union General Assembly, Geophysical Research Abstracts Vol. 16, EGU2014-2358, Vienna (Austria), 27 April - 2 May 2014.

Sicard, M., Pérez, C., Rocadenbosch, F., Baldasano, J. M., and García-Vizcaino, D.: Mixed-layer depth determination in the Barcelona coastal area from regular lidar measurements: methods, results and limitations, Bound.-Lay. Meteorol., 119, 135-157, doi: 10.1007/s10546-005-9005-9, 2006.

Sicard, M., Totems, J., Barragan, R., Dulac, F., Mallet, M., Comerón, A., Alados-Arboledas, L., Augustin, P., Chazette, P., Léon, J.-F., Olmo, F. J., Renard, J.-B., Rocadenbosch, F.: Variability of Mediterranean aerosols properties at three regional background sites in the western Mediterranean Basin, in Proc. SPIE 9242, Comerón, A., Kassianov, E.I., Schäfer, K., Picard, R.H., Stein, K.,and Gonglewski, J.D., Eds., SPIE, Washington (EE.UU.), (2014), CCC code: 0277-786X/14/$18, doi:10.1117/12.2068694, 2014.

Sicard, M., Totems, J., Barragan, R., Dulac, F., Mallet, M., Comerón, A., Alados-Arboledas, L., Augustin, P., Chazette, P., Léon, J.-F., Olmo, F. J., Renard, J.-B., Rocadenbosch, F.: Variability of Mediterranean aerosols properties at three regional background sites in the western Mediterranean Basin, in Proc. SPIE 9242, A. Comerón, E. I. Kassianov, K. Schäfer, R. H. Picard, K. Stein, J. D. Gonglewski (eds), SPIE, Washington (EE.UU.), (2014), CCC code: 0277-786X/14/$18, doi: 10.1117/12.2068694, 2014.

Sinyuk, A., Dubovik, O., Holben, B.N., Eck, T. F., Breon, F.-M., Martonchik, J., Kahn, R., Diner, D. J., Vermote, E. F., Roger, J.-C., Lapyonok, T., and Slutsker, I.: Simultaneous retrieval of aerosol and surface properties from a combination of AERONET and satellite data, Remote Sens. of Environ., 107, 90-108, doi:10.1016/j.rse.2006.07.022, 2007.

Smirnov, A., Holben, B. N., Eck, T. F., Dubovik, O., and Slutsker, I., Clouds creening and quality control algorithms for the AERONET database, Remote Sens. Environ., 73, 337–349, doi: 10.1016/S0034-4257(00)00109-7, 2000.

Smirnov, A., Holben, B. N., Kaufman, Y. J., Dubovik, O., Eck, T. F., Slutsker, I., Pietras, C., and Halthore, R. N., Optical properties of atmospheric aerosol in maritime environments. J.

Atmos. Sci., 59, 501–523, doi: 10.1175/1520-0469(2002)059<0501:OPOAAI>2.0.CO;2, 2002.

Stamnes, K., Tsay, S., Wiscombe, W., and Jayaweera, K.: Numerically stable algorithm for discrete–ordinate-method radiative transfer in multiple scattering and emitting layered media, Appl. Optics, 27, 2502–2509, 1988.

Tegen, I., and Lacis, A. A.: Modeling of particle size distribution and its influence on the radiative properties of mineral dust aerosol, J. Geophys. Res., 101, 19237-19244, doi:10.1029/95JD03610, 1996.

Titos, G., Lyamani, H., Cazorla, A., Sorribas, M., Foyo-Moreno, I., Wiedensohler, A. and Alados-Arboledas, L.: Study of the relative humidity dependence of aerosol light-scattering in southern Spain, Tellus B, 66, 24536, http://dx.doi.org/10.3402/tellusb.v66.24536, 2014.

Toledano, C., Cachorro, V. E., Berjon, A., de Frutos, A. M., Sorribas, M., de la Morena, B. A., and Goloub, P.: Aerosol optical depth and Ångström exponent climatology at El Arenosillo AERONET site (Huelva, Spain), Q. J. R. Meteorol. Soc., 133, 795–807, doi: 10.1002/qj.54, 2007.

Twomey, S.: Pollution and the planetary albedo, Atmos. Environ., 8, 1251– 1256, doi:10.1016/0004-6981(74)90004-3, 1974.

Valenzuela, A., Olmo, F.J., Lyamani, H., Antón, M., Quirantes, A., and Alados-Arboledas, L.: Classification of aerosol radiative properties during African desert dust intrusions over southeastern Spain by sector origins and cluster analysis, J. Geophys. Res., 117, D06214, doi:10.1029/2011JD016885, 2012a.

Valenzuela, A., Olmo, F. J., Lyamani, H., Antón, M., Quirantes, A., and Alados-Arboledas, L.: Aerosol radiative forcing during African desert dust intrusions (2005–2010) over Southeastern Spain, Atmos. Chem. Phys., 12, 10331–10351, doi: 10.5194/acp-12-10331-2012, 2012b~~a~~.

~~Valenzuela, A., Olmo, F. J., Lyamani, H., Antón, M., Quirantes, A., and Alados-Arboledas, L.: Classification of aerosol radiative properties during African desert dust intrusions over southeastern Spain by sector origins and cluster analysis, J. Geophys. Res., 117, D06214, doi:10.1029/2011JD016885, 2012b.~~

Valenzuela, A., Olmo, F.J., Lyamani, H., Granados-Muñoz, M.J., Antón, M., Guerrero-Rascado, J.L., Quirantes, A., Toledano, C., Pérez-Ramírez, D., and Alados-Arboledas, L., Aerosol transport over the western Mediterranean basin: Evidence of the contribution of fine

Con formato: Inglés (Estados Unidos)

Con formato: Fuente de párrafo predeter., Color de fuente: Automático

Con formato: Inglés (Estados Unidos)

Con formato: Fuente de párrafo predeter., Color de fuente: Automático

Con formato: Resaltar

particles to desert dust plumes over Alborán Island, J. Geophys. Res. Atmos., 119, 14028-14044, doi: 10.1002/2014JD022044, 2015.

Site	Wavelengths	2011	2012	2013	2014	2011-2014
Ersa	340, 380, 440, 500, 675, 870, 1020, 1640 nm	JFMAMJJASOND	J MJJASOND	JFMA	JFMAMJJASO	JFMAMJJASOND 433333333322
Palma	340, 380, 440, 500, 675, 870, 1020 nm	ASOND	MJJASOND	JFMAMJJASOND		JFMAMJJASOND 111122233333
Alborán	340, 380, 440, 500, 675, 870, 1020 nm	JJASOND	J			

Table 1. Wavelengths of the AERONET sun-photometers at Ersa, Palma and Alborán and level 2.0 data availability during the period 2011-2014. In the last column the numbers below each month indicate the number of that month with data in the period 2011-2014.

		Summer	Autumn	Winter	Spring	Year
				(N) Mean ± sStd		
AOD_{440}	Ersa	(13093 17003) 0.189±0.10	(6327 7993) 0.13±0.09	(2620 3692) 0.098±0.05	(6656 7837) 0.16±0.110	(2869 36525) 0.16±0.10
	Palma	(8667) 0.23±0.12	(6062) 0.16±0.11	(1831) 0.07±0.04	(2319) 0.10±0.06	(18879) 0.18±0.12
	Alborán	(2233) 0.27±0.14	(2167) 0.17±0.11	(586) 0.08±0.03	(0) -	(4986) 0.20±0.13
$AE_{440-870}$	Ersa	(17003) 1.46±0.45 (13093) 1.44±0.47	(7993) 1.40±0.51 (6327) 1.46±0.51	(3692) 1.13±0.46 (2620) 1.14±0.49	(7837) 1.27±0.44 (6656) 1.28±0.45	(36525) 1.37±0.47 (28696) 1.38±0.48
	Palma	(8667) 1.14±0.47	(6062) 1.21±0.48	(1831) 1.11±0.43	(2319) 0.99±0.34	(18879) 1.14±0.46
	Alborán	(2233) 0.61±0.33	(2167) 1.02±0.36	(586) 0.85±0.36	(0) -	(4986) 0.81±0.40
δAE	Ersa	(2809) 0.05±0.22	(633) 0.04±0.25	(24) -0.01±0.17	(843) 0.04±0.23	(4309) 0.05±0.23
	Palma	(2917) 0.29±0.19	(876) 0.13±0.23	(4) 0.05±0.10	(68) 0.34±0.12	(3865) 0.25±0.21
$AAOD_{440}$	Ersa	(26) 0.018±0.011	(12) 0.023±0.017	(0) -	(11) 0.035±0.027	(49) 0.023±0.018
	Palma	(57) 0.043±0.019	(25) 0.034±0.021	(0) -	(0) -	(82) 0.040±0.020
	Alborán	(15) 0.016±0.010	(0) -	(0) -	(0) -	(15) 0.016±0.010
$AAE_{440-870}$	Ersa	(26) 1.64±0.52	(12) 1.28±0.44	(0) -	(11) 2.11±0.89	(49) 1.66±0.66
	Palma	(57) 1.98±0.49	(25) 1.64±0.55	(0) -	(0) -	(82) 1.88±0.53
r_V^f [µm]	Ersa	(993) 0.16±0.02	(538) 0.17±0.02	(158) 0.18±0.03	(518) 0.17±0.02	(2207) 0.17±0.02
	Palma	(809) 0.14±0.02	(548) 0.15±0.02	(177) 0.15±0.02	(184) 0.15±0.02	(1718) 0.15±0.02
C_V^f [$\mu m^3 \cdot \mu m^{-2}$]	Ersa	(993) 0.019±0.012	(538) 0.014±0.011	(158) 0.009±0.006	(518) 0.019±0.013	(2207) 0.017±0.012
	Palma	(809) 0.025±0.013	(548) 0.021±0.017	(177) 0.010±0.007	(184) 0.011±0.008	(1718) 0.021±0.014
r_V^c [µm]	Ersa	(993) 2.49±0.41	(538) 2.73±0.43	(158) 2.73±0.44	(518) 2.27±0.46	(2207) 2.52±0.46
	Palma	(809) 2.43±0.41	(548) 2.61±0.37	(177) 2.43±0.37	(184) 2.10±0.44	(1718) 2.46±0.42
C_V^c [$\mu m^3 \cdot \mu m^{-2}$]	Ersa	(993) 0.032±0.036	(538) 0.021±0.040	(158) 0.018±0.021	(518) 0.027±0.053	(2207) 0.027±0.041
	Palma	(809) 0.063±0.063	(548) 0.038±0.052	(177) 0.013±0.011	(184) 0.025±0.021	(1718) 0.046±0.056
$AAOD_{440}$	Ersa	(26) 0.018±0.011	(12) 0.023±0.017	(0) -	(11) 0.035±0.027	(49) 0.023±0.018
	Palma	(57) 0.043±0.019	(25) 0.034±0.021	(0) -	(0) -	(82) 0.040±0.020
$AAE_{440-870}$	Ersa	(26) 1.64±0.52	(12) 1.28±0.44	(0) -	(11) 2.11±0.89	(49) 1.66±0.66
	Palma	(57) 1.98±0.49	(25) 1.64±0.55	(0) -	(0) -	(82) 1.88±0.53
RRI_{440}	Ersa	(26) 1.45±0.03	(12) 1.46±0.06	(0) -	(11) 1.44±0.04	(49) 1.45±0.04
	Palma	(57) 1.43±0.05	(25) 1.42±0.06	(0) -	(0) -	(82) 1.43±0.06

Tabla con formato

IRI_{440} ($\times 10^{-3}$)	Ersa	(26) 2.6±1.3	(12) 3.6±1.8	(0) -	(11) 3.6±1.3	(49) 3.1±1.3
	Palma	(57) 4.7±1.6	(25) 4.8±2.3	(0) -	(0) -	(82) 4.7±1.8
	~~Alborán~~	~~(15) 1.05±0.26~~	~~(0)~~	~~(0)~~	~~(0)~~	~~(15) 1.05±0.26~~
~~Sphericity [%]~~	~~Ersa~~	~~(321) 57±45~~	~~(92) 87±31~~	~~(8) 74±46~~	~~(142) 75±38~~	~~(563) 67±43~~
	~~Palma~~	~~(408) 41±41~~	~~(145) 69±40~~	~~(0)~~	~~(13) 60±43~~	~~(566) 49±42~~
	~~Alborán~~	~~(85) 25±32~~	~~(66) 38±37~~	~~(0)~~	~~(0)~~	~~(151) 31±35~~

Table ~~1~~2. Summary of the seasonal variations of the following aerosol ~~optical~~ properties: ~~(~~AOD_{440}, $AE_{440\text{-}870}$, δAE (=$AE_{440\text{-}675}$ – $AE_{675\text{-}870}$), ~~$AAOD_{440}$, $AAE_{440\text{-}870}$ and sphericity)~~ the particle volume size distribution, $AAOD_{440}$, $AAE_{440\text{-}870}$ and the real (RRI) and imaginary (IRI) part of the refractive index ~~at Ersa~~at Ersa and ~~,~~Palma derived from AERONET level 2.0 inversion products available in the period 2011 – 2015 ~~and Alborán~~. r_V and C_V are the volume median radius and the volume concentration, respectively. *f*/*c* indicate fine and coarse modes, respectively.The values of δAE are given for $AOD_{675} > 0.15$ as suggested by Gobbi et al. (2007). ~~In the last column (E) and (I) indicate if the parameter is an extensive or intensive parameter, respectively.~~ The values of $AAOD_{440}$, $AAE_{440\text{-}870}$, RRI_{440} and IRI_{440} are given for $50 < SZA < 80º$ and $AOD_{440} > 0.40$.

Con formato: Fuente: Sin Negrita
Con formato: Fuente: Sin Negrita
Código de campo cambiado
Código de campo cambiado
Con formato: Subíndice
Con formato: Subíndice
Con formato: Subíndice

		Summer	Autumn	Winter	Spring	Year
		N (percentage)				
Mineral dust ($\delta AE < 0.3$, $AE < 0.75$)	Ersa	15 (58 %)	4 (33 %)	-	7 (64 %)	26 (53 %)
	Palma	48 (84 %)	10 (40 %)	-	-	58 (71 %)
Pollution ($AE > 1$)	Ersa	11 (42 %)	8 (67 %)	-	4 (36 %)	23 (47 %)
	Palma	9 (16 %)	15 (60 %)	-	-	24 (29 %)
		AOD_{440} ± Std				
Mineral dust ($\delta AE < 0.3$, $AE < 0.75$)	Ersa	0.50±0.04	0.66±0.31	-	0.61±0.07	0.55±0.17
	Palma	0.51±0.14	0.51±0.09	-	-	0.51±0.13
Pollution ($AE > 1$)	Ersa	0.47±0.07	0.47±0.02	-	0.43±0.03	0.46±0.05
	Palma	0.46±0.05	0.48±0.04	-	-	0.47±0.04

Table 2. Seasonal number (and percentage of data in parenthesis) and AOD_{440} (± standard deviation) of the (δAE, AE) points fulfilling ($\delta AE < 0.3$, $AE < 0.75$) and corresponding to mineral dust outbreaks, and fulfilling ($AE > 1$) and corresponding to pollution events. The data are those of Figure 6 (AERONET level 2.0 inversion products available in the period 2011 – 2015, which means that the following criteria apply on these data: $50 < SZA < 80^{\circ}$ and $AOD_{440} > 0.4$).

Con formato: Inglés (Estados Unidos)
Tabla con formato
Con formato: Izquierda: 1,5 cm, Derecha: 1,5 cm, Arriba: 2 cm, Abajo: 2 cm, Ancho: 21 cm, Alto: 29,7 cm
Tabla con formato
Con formato: Centrado
Con formato: Subíndice
Tabla con formato
Con formato: Subíndice
Código de campo cambiado
Con formato: Fuente: 12 pto, Sin Negrita
Con formato: Fuente: 12 pto
Con formato: Fuente: Sin Negrita
Con formato: Fuente: Sin Negrita

Con formato: Justificado, Espacio Antes: 6 pto, Interlineado: 1,5 líneas

		Summer	Autumn	Winter	Spring	Year
				(N) Mean±std		
r_V^f	Ersa	(993) 0.16±0.02	(538) 0.17±0.02	(158) 0.18±0.03	(518) 0.17±0.02	(2207) 0.17±0.02
[μm]	Palma	(809) 0.14±0.02	(548) 0.15±0.02	(177) 0.15±0.02	(184) 0.15±0.02	(1718) 0.15±0.02
	Alborán	(164) 0.17±0.02	(175) 0.18±0.02	(34) 0.19±0.02	(0) -	(373) 0.18±0.02
C_V^f	Ersa	(993) 0.019±0.012	(538) 0.014±0.011	(158) 0.009±0.006	(518) 0.019±0.013	(2207) 0.017±0.012
[$\mu m^3 \cdot \mu m^{-2}$]	Palma	(809) 0.025±0.013	(548) 0.021±0.017	(177) 0.010±0.007	(184) 0.011±0.008	(1718) 0.021±0.014
	Alborán	(164) 0.023±0.011	(175) 0.021±0.012	(34) 0.012±0.005	(0) -	(373) 0.021±0.011
r_V^c	Ersa	(993) 2.49±0.41	(538) 2.73±0.43	(158) 2.73±0.44	(518) 2.27±0.46	(2207) 2.52±0.46
[μm]	Palma	(809) 2.43±0.41	(548) 2.61±0.37	(177) 2.43±0.37	(184) 2.10±0.44	(1718) 2.46±0.42
	Alborán	(164) 2.33±0.45	(175) 2.53±0.47	(34) 2.70±0.38	(0) -	(373) 2.46±0.47
C_V^c	Ersa	(993) 0.032±0.036	(538) 0.021±0.040	(158) 0.018±0.021	(518) 0.027±0.053	(2207) 0.027±0.041
[$\mu m^3 \cdot \mu m^{-2}$]	Palma	(809) 0.063±0.063	(548) 0.038±0.052	(177) 0.013±0.011	(184) 0.025±0.021	(1718) 0.046±0.056
	Alborán	(164) 0.083±0.063	(175) 0.050±0.041	(34) 0.019±0.012	(0) -	(373) 0.062±0.055
RRI_{440}	Ersa	(26) 1.45±0.03	(12) 1.46±0.06	(0) -	(11) 1.44±0.04	(49) 1.45±0.04
	Palma	(57) 1.43±0.05	(25) 1.42±0.06	(0) -	(0) -	(82) 1.43±0.06
	Alborán	(15) 1.44±0.06	(0) -	(0) -	(0) -	(15) 1.44±0.06
IRI_{440} ($\times 10^3$)	Ersa	(26) 2.6±1.3	(12) 3.6±1.8	(0) -	(11) 3.6±1.3	(49) 3.1±1.3
	Palma	(57) 4.7±1.6	(25) 4.8±2.3	(0) -	(0) -	(82) 4.7±1.8
	Alborán	(15) 1.5±0.8	(0) -	(0) -	(0) -	(15) 1.5±0.8

Table 3. Summary of the seasonal variations of the aerosol microphysical properties (size distribution and refractive index) at Ersa, Palma and Alborán. r_V and C_V are the volume median radius and the volume concentration, respectively. *f/c* indicate fine and coarse modes, respectively. In the last column (E) and (I) indicate if the parameter is an extensive or intensive parameter, respectively.

Tabla con formato

		Summer	Autumn	Winter	Spring	Year
				(N) Mean±std		
SSA_{440}	Ersa	(26) 0.96±0.02	(12) 0.96±0.02	(0) -	(11) 0.94±0.02	(49) 0.96±0.03
	Palma	(57) 0.92±0.03	(25) 0.93±0.04	(0) -	(0) -	(82) 0.92±0.03
	~~Alborán~~	~~(15) 0.97±0.02~~	~~(0) -~~	~~(0) -~~	~~(0) -~~	~~(15) 0.97±0.02~~
g_{440}	Ersa	(993) 0.69±0.02	(538) 0.70±0.03	(158) 0.72±0.05	(518) 0.70±0.03	(2207) 0.69±0.03
	Palma	(809) 0.69±0.03	(548) 0.71±0.03	(177) 0.68±0.04	(184) 0.69±0.03	(1718) 0.70±0.03
	~~Alborán~~	~~(164) 0.74±0.02~~	~~(175) 0.75±0.02~~	~~(34) 0.75±0.02~~	~~(0) -~~	~~(373) 0.75±0.02~~
ARF_{BOA}	Ersa	(413) -17.5±9.5	(205) -13.6±10.0	(23) -17.6±8.3	(195) -18.0±9.2	(836) -16.7±9.7
$[W \cdot m^{-2}]$	Palma	(282) -22.8±13.4	(193) -16.5±12.1	(14) -6.7±3.3	(65) -9.6±6.0	(554) -18.7±13.2
	~~Alborán~~	~~(63) -27.8±13.8~~	~~(75) -18.3±10.4~~	~~(8) -14.8±11.8~~	~~(0) -~~	~~(146) -22.2±13.0~~
ARF_{TOA}	Ersa	(413) -12.8±7.0	(205) -9.7±6.6	(23) -7.4±4.9	(195) -10.9±5.7	(836) -11.4±6.7
$[W \cdot m^{-2}]$	Palma	(282) -13.0±6.8	(193) -10.7±6.5	(14) 5.5±2.8	(65) -6.9±3.6	(554) -11.3±6.7
	~~Alborán~~	~~(63) -18.8±10.4~~	~~(75) -13.4±7.7~~	~~(8) -6.0±1.8~~	~~(0) -~~	~~(146) -15.3±9.5~~
$ARFE_{BOA}$	Ersa	(413) -139.1±23.6	(205) -137.8±18.8	(23) -182.9±31.4	(195) -157.9±39.7	(836) -144.4±29.3
$[W \cdot m^{-2} \cdot AOD_{550}^{-1}]$	Palma	(282) -136.4±40.9	(193) -129.6±27.4	(14) -130.7±13.9	(65) -122.0±24.6	(554) -132.2±34.8
	~~Alborán~~	~~(63) -142.1±30.4~~	~~(75) -132.5±49.0~~	~~(8) -191.4±85.5~~	~~(0) -~~	~~(146) -139.9±46.4~~
$ARFE_{TOA}$	Ersa	(413) -101.2±10.2	(205) -100.7±12.1	(23) -74.7±11.6	(195) -96.3±15.1	(836) -99.2±12.8
$[W \cdot m^{-2} \cdot AOD_{550}^{-1}]$	Palma	(282) -79.7±18.9	(193) -88.5±15.4	(14) -107.0±13.3	(65) -93.8±12.9	(554) -85.1±18.1
	~~Alborán~~	~~(63) -91.9±7.3~~	~~(75) -95.5±13.8~~	~~(8) -94.0±30.0~~	~~(0) -~~	~~(146) -93.8±12.9~~

Table 3~~4~~. ~~Summary of the seasonal variations of the aerosol radiative properties (SSA_{440} and g_{440}) and the solar radiative forcing and forcing efficiency at Ersa, Palma and Alborán.~~Summary of the seasonal variations of the following aerosol properties: SSA_{440}, g_{440}, the solar aerosol radiative forcing (ARF) and the solar aerosol radiative forcing efficiency (ARFE) at Ersa and Palma derived from AERONET level 2.0 inversion products available in the period 2011 – 2015. BOA and TOA stand for bottom of the atmosphere and top of the atmosphere, respectively. The values of SSA_{440} are given for $50 < SZA < 80º$ and $AOD_{440} > 0.40$~~. In the last column (E) and (I) indicate if the parameter is an extensive or intensive parameter, respectively.~~. The values of ARF and ARFE are given for $50 < SZA < 60º$.

Tabla con formato

Con formato: Fuente: Cursiva

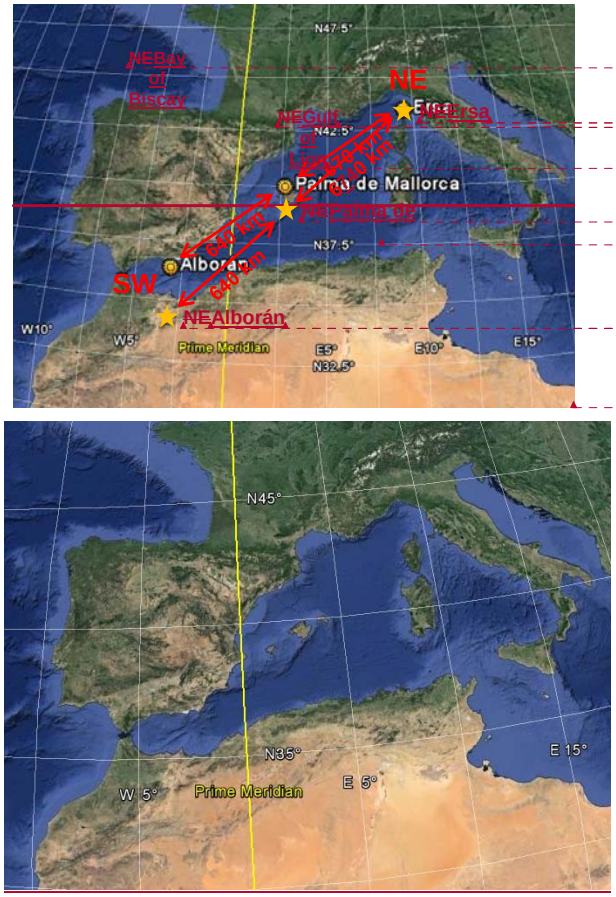

Figure 1. Geographical situation of Ersa, Palma and Alborán AERONET stations in the western Mediterranean Basin~~WMB~~. Credits: map adapted from Google Earth.

5

Con formato: Inglés (Estados Unidos)

Con formato: Fuente: 9 pto, Color de fuente: Fondo 1

Con formato: Espacio Antes: 0 pto, Interlineado: sencillo

Con formato: Fuente: 10 pto, Color de fuente: Fondo 1

Con formato: Izquierda, Espacio Antes: 0 pto, Interlineado: sencillo

Con formato: Fuente: 10 pto, Color de fuente: Fondo 1

Con formato: Fuente: 9 pto, Color de fuente: Fondo 1

Con formato: Fuente: 9 pto, Color de fuente: Fondo 1

Con formato: Espacio Antes: 0 pto, Interlineado: sencillo

Con formato: Fuente: 9 pto, Color de fuente: Fondo 1

Con formato: Fuente: 10 pto, Color de fuente: Fondo 1

Con formato: Izquierda, Espacio Antes: 0 pto, Interlineado: sencillo

Con formato: Fuente: 10 pto, Color de fuente: Fondo 1

Con formato: Fuente: 10 pto, Color de fuente: Fondo 1

Con formato: Fuente: 10 pto

Con formato: Fuente: 10 pto, Color de fuente: Fondo 1

Con formato: Izquierda, Espacio Antes: 0 pto, Interlineado: sencillo

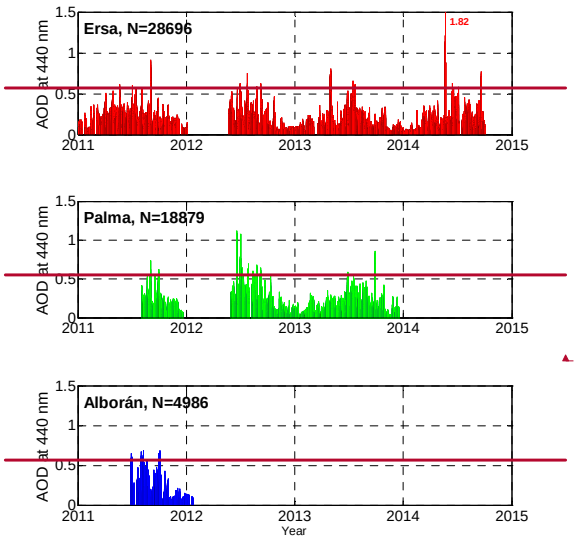

Figure 2. Instantaneous AOD at 440 nm at the three sites during the period 2011 – 2014. In this figure and in the rest of the paper N represents the number of points used in the plot shown.

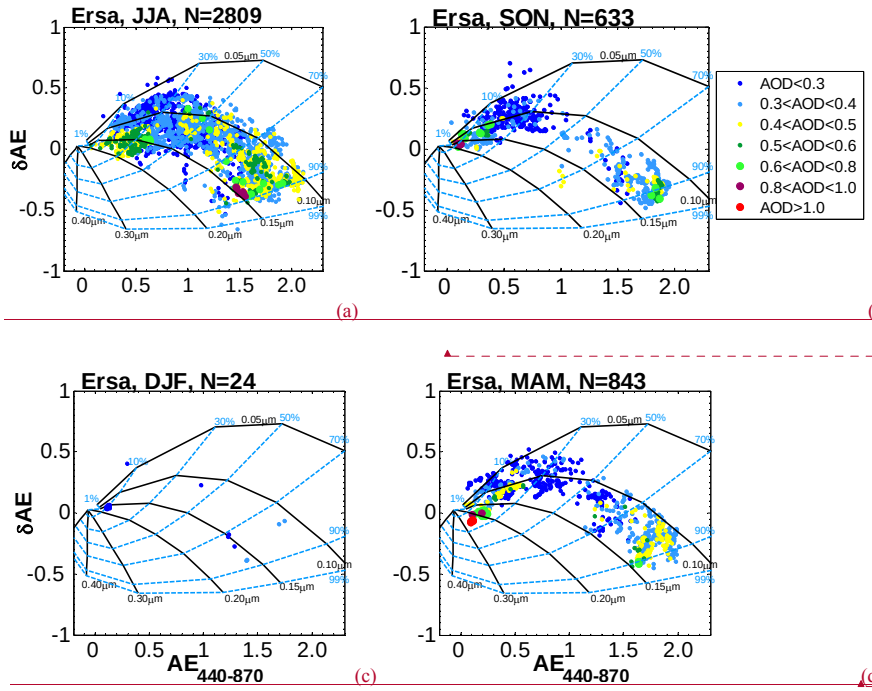

Con formato: Fuente: (Predeterminada) Arial, 16 pto,

Con formato: SPIE body text, Centrado, Interlineado: sencillo

Con formato: Inglés (Estados Unidos)

Con formato: Inglés (Estados Unidos)

Figure 2. Ångström exponent difference ($\delta AE = AE_{440\text{-}675} - AE_{675\text{-}870}$) as a function of the Ångström exponent calculated between 440 and 870 nm ($AE_{440\text{-}870}$) at Ersa during (a) summer, (b) autumn, (c) winter and (d) spring, for the whole 2011-2015 AERONET level 2.0 AOD dataset. Only points with $AOD_{675} > 0.15$ are represented. However the AOD plotted is AOD_{440} (and not AOD_{675}) in order to be directly comparable with the AERONET inversion criteria based on AOD_{440}. The legend applies for all plots. A bimodal, lognormal size distribution and a refractive index of 1.4-0.001*i* were considered to construct the grid. The black solid lines are each for a fixed fine mode radius and the dashed blue lines for a fixed fraction of the fine mode contribution to the AOD at 675 nm. In this figure and in the rest of the paper N represents the number of points or observations shown in the plot or used to calculate the means shown in the plot.

Con formato: Subíndice
Con formato: Subíndice
Con formato: Subíndice
Con formato: Subíndice
Con formato: Fuente: Cursiva

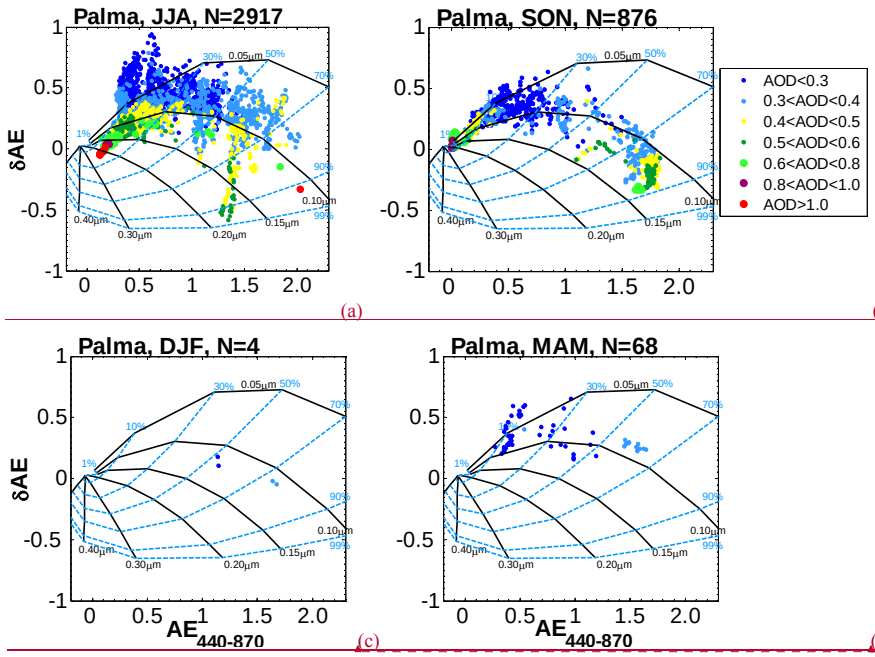

Figure 3. Ångström exponent difference ($\delta AE = AE_{440\text{-}675} - AE_{675\text{-}870}$) as a function of the Ångström exponent calculated between 440 and 870 nm ($AE_{440\text{-}870}$) at Palma during (a) summer, (b) autumn, (c) winter and (d) spring, for the whole 2011-2015 AERONET level 2.0 AOD dataset. Only points with $AOD_{675} > 0.15$ are represented. However the AOD plotted is AOD_{440} (and not AOD_{675}) in order to be directly comparable with the AERONET inversion criteria based on AOD_{440}. The legend applies for all plots. A bimodal, lognormal size distribution and a refractive index of 1.4-0.001*i* were considered to construct the grid. The black solid lines are each for a fixed fine mode radius and the dashed blue lines for a fixed fraction of the fine mode contribution to the AOD at 675 nm.

Con formato: Descripción, Interlineado: 1,5 líneas
Con formato: Inglés (Estados Unidos)
Con formato: Fuente: Sin Negrita, Inglés (Estados Unidos)
Con formato: Fuente: Sin Negrita, Inglés (Estados Unidos)
Con formato: Inglés (Estados Unidos)
Con formato: Fuente: 10 pto, Sin Negrita, Inglés (Estados Unidos)
Con formato: Fuente: 10 pto, Sin Negrita, Inglés (Estados Unidos)
Con formato: Fuente: 10 pto, Inglés (Estados Unidos)
Con formato: Fuente: 10 pto, Sin Negrita, Inglés (Estados Unidos)
Con formato: Fuente: 10 pto, Inglés (Estados Unidos)
Con formato: Fuente: 10 pto, Sin Negrita, Inglés (Estados Unidos)
Con formato: Normal, Izquierda
Con formato: Fuente: 10 pto, Sin Negrita, Inglés (Estados Unidos)
Con formato: Fuente: 10 pto, Inglés (Estados Unidos)
Con formato: Fuente: 10 pto, Sin Negrita, Inglés (Estados Unidos)
Con formato: Fuente: 10 pto, Inglés (Estados Unidos)
Con formato: Fuente: 10 pto, Sin Negrita, Inglés (Estados Unidos)
Con formato: Fuente: 10 pto, Inglés (Estados Unidos)
Con formato: Fuente: 10 pto, Sin Negrita, Inglés (Estados Unidos)
Con formato: Inglés (Estados Unidos)

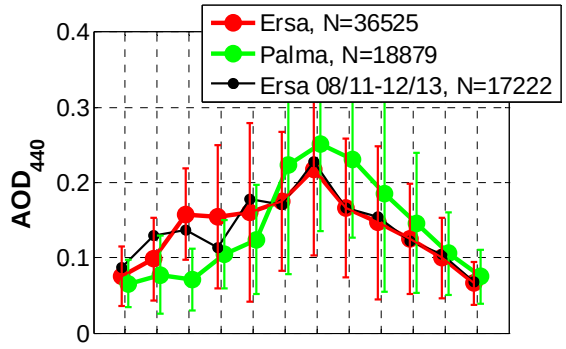
Ersa, N=36525
Palma, N=18879
Ersa 08/11-12/13, N=17222
AOD440
0.4
0.3
0.2
0.1
0

(a)

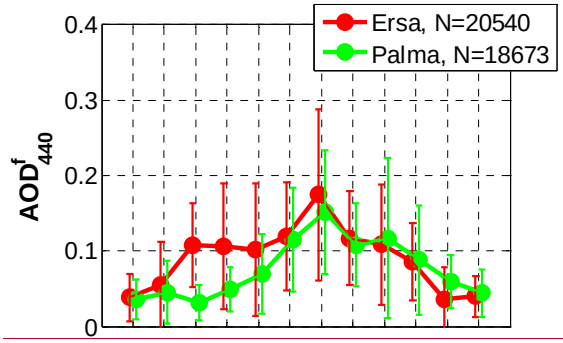
Ersa, N=20540
Palma, N=18673
AODf440
0.4
0.3
0.2
0.1
0

(b)

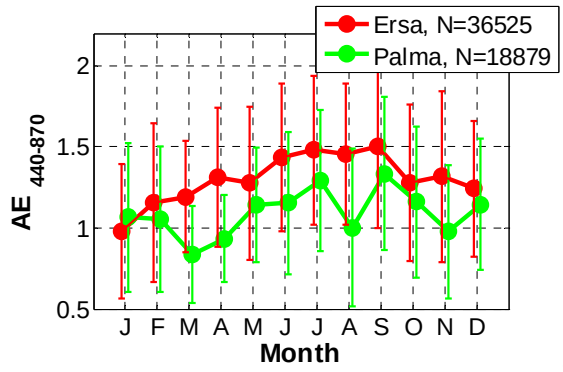
Ersa, N=36525
Palma, N=18879
AE 440-870
2
1.5
1
0.5
J F M A M J J A S O N D
Month

(c)

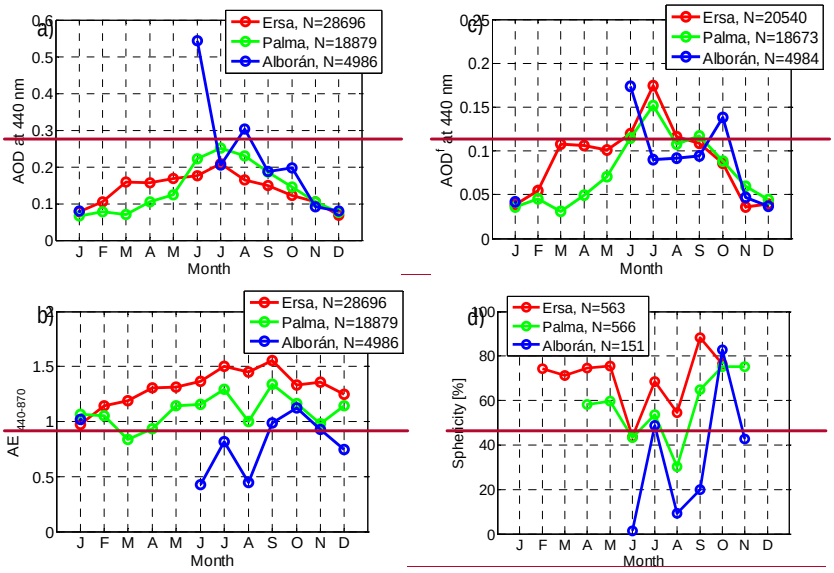

Figure ~~43~~. Monthly average variations calculated with instantaneous measurements ~~over the whole dataset~~ of a) AOD_{440}; b) AOD^{f}_{440}; and c) $AE_{440-870}$; ~~c) AOD^{f}_{440} and d) the sphericity.~~ derived from AERONET level 2.0 inversion products available in the period 2011 – 2015. The error bars represent the standard deviation. On the AOD_{440} plot we have also plotted the monthly values at Ersa calculated over the limited period for which data are also available at Palma, i.e. August 2011 – December 2013.

Con formato: Justificado

Con formato: Fuente: Negrita

Con formato: Normal, Izquierda, Interlineado: sencillo

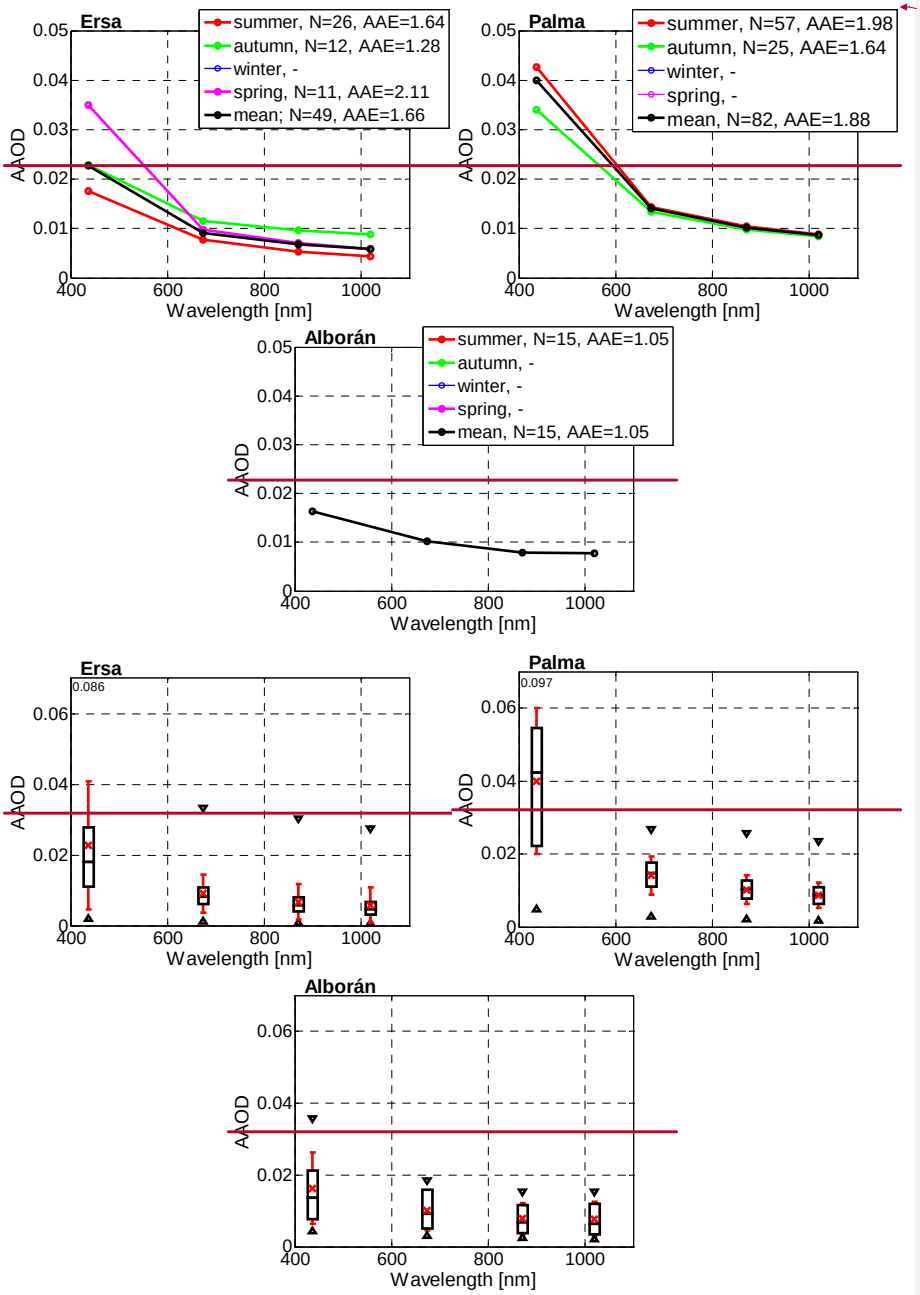

Figure 4. (top) Seasonal variation of the spectral AAOD at the three sites. (bottom) Box-and-whisker plots (median, first and third quartile and minimum and maximum values) representing the spectral AAOD on an

Con formato: Izquierda: 2,5 cm, Derecha: 2,5 cm, Arriba: 2 cm, Abajo: 2 cm, Ancho: 21 cm, Alto: 29,7 cm

annual basis at the three sites. The red whiskers represent the standard deviation around the mean value (red cross sign). Upward and downward triangles indicate minimum and maximum values, respectively.

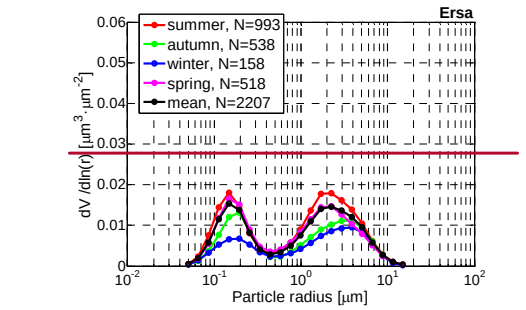

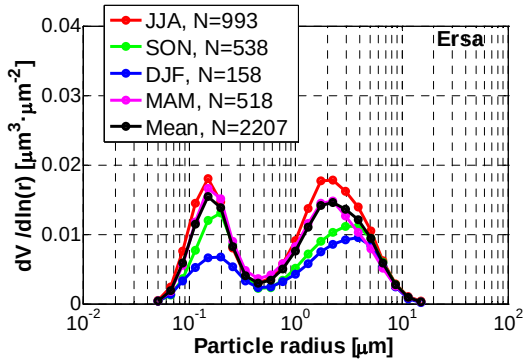

(a)

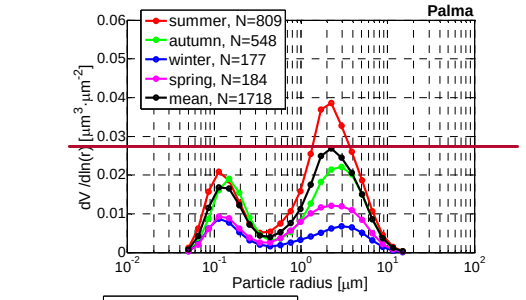

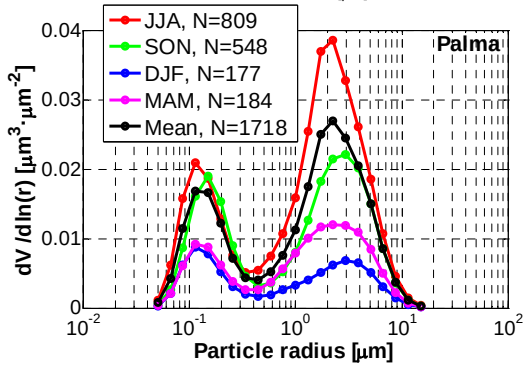

(b)

Con formato: Descripción

Con formato: Inglés (Estados Unidos)

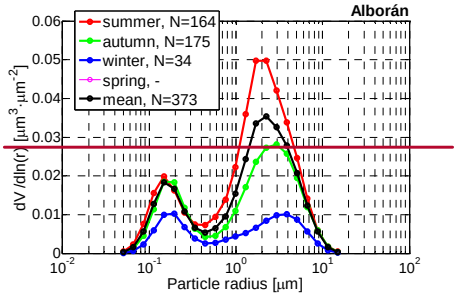

Figure 55. Seasonal variation of the particle volume size distribution ~~at the three sites~~at (a) Ersa and (b) Palma derived from AERONET level 2.0 inversion products available in the period 2011 – 2015.

Con formato: Fuente: Sin Negrita

Con formato: Fuente: Sin Negrita

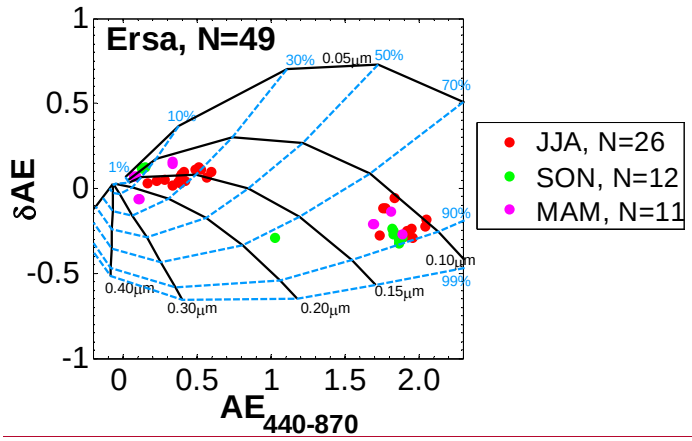

(a)

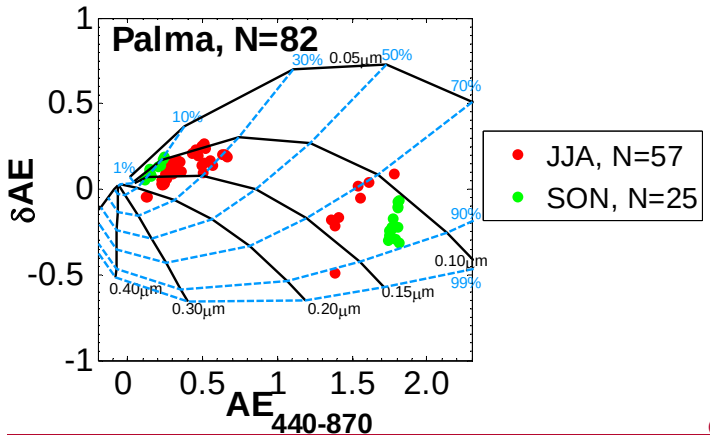

(b)

Figure 6. Ångström exponent difference ($\delta AE = AE_{440\text{-}675} - AE_{675\text{-}870}$) as a function of the Ångström exponent calculated between 440 and 870 nm ($AE_{440\text{-}870}$) at (a) Ersa and (b) Palma, derived from AERONET level 2.0 inversion products available in the period 2011 – 2015, which means that the following criteria apply on these data: $50 < SZA < 80º$ and $AOD_{440} > 0.4$. A bimodal, lognormal size distribution and a refractive index of 1.4-0.001*i* were considered to construct the grid. The black solid lines are each for a fixed fine mode radius and the dashed blue lines for a fixed fraction of the fine mode contribution to the AOD at 675 nm.

Con formato: Centrado

Con formato: Fuente: Sin Negrita

Con formato: Fuente: Sin Negrita

Con formato: Fuente: Sin Negrita

Con formato: Subíndice

Con formato: Fuente: Sin Negrita

Con formato: Fuente: Sin Negrita

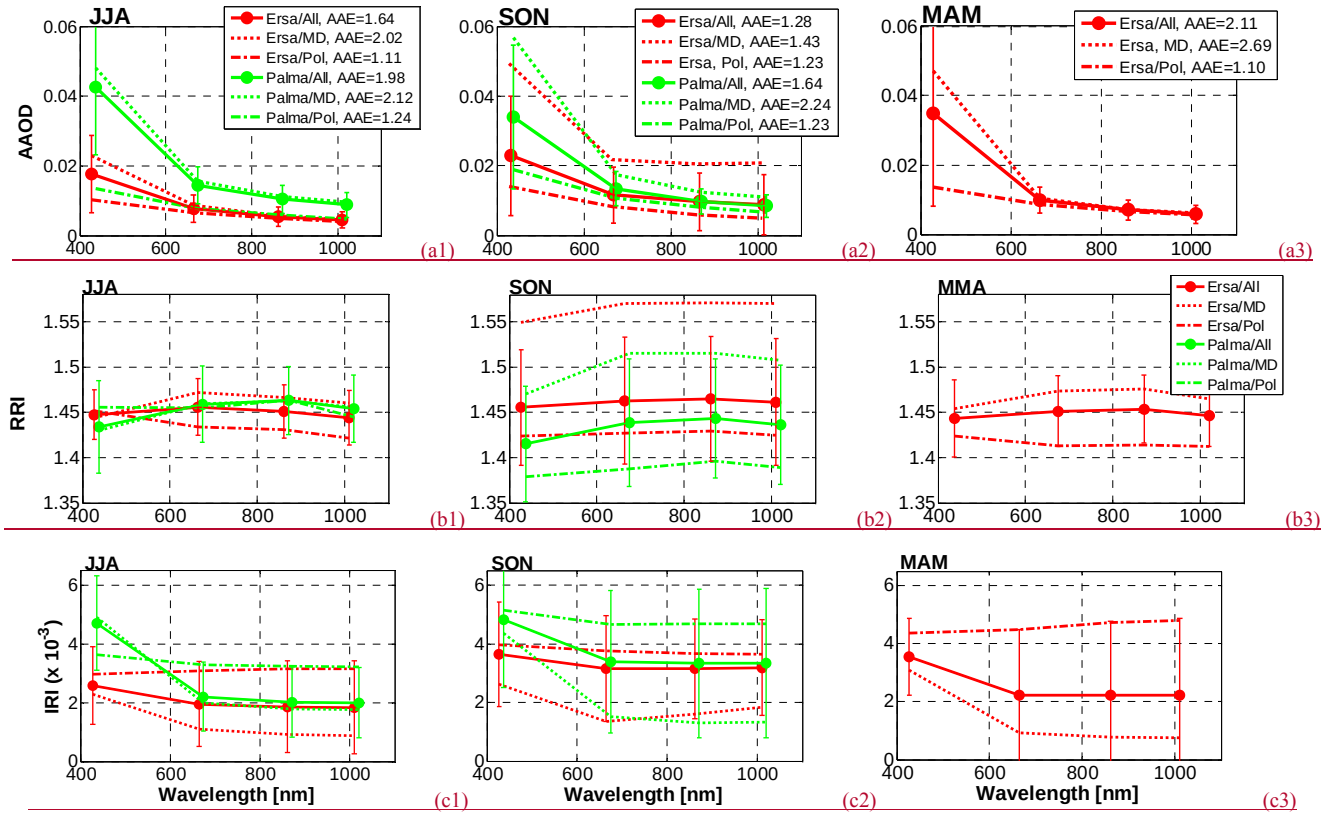

Con formato: Izquierda: 2 cm, Derecha: 2 cm, Ancho: 29,7 cm, Alto: 21 cm, Distancia del pie de página desde el borde: 1,5 cm

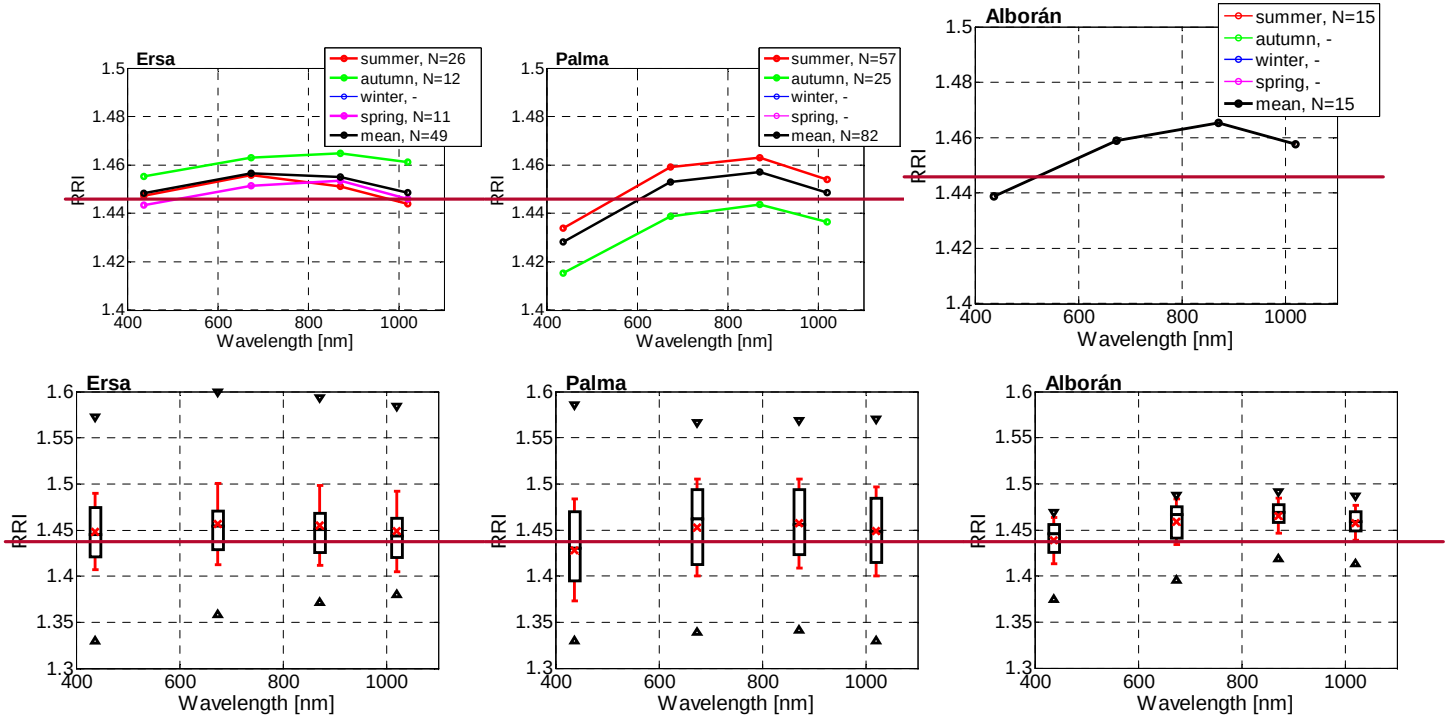

Figure 7~~6~~. Seasonal variation of the spectra of (a) the aerosol absorption optical depth (AAOD), (b) the real part of the refractive index (RRI) and (c) the imaginary part of the refractive index (IRI) during (1) summer, (2) autumn and (3) spring, derived from AERONET level 2.0 inversion products available in the period 2011-2015. The legend in plot (b3) applies for all plots (b) and (c). All three parameters are retrieved with the following restrictions: $50 < SZA < 80^{o}$ and $AOD_{440} > 0.4$. The error bars represent the standard deviation. The seasonal mean is represented for the whole dataset (All), and separately for mineral dust (MD) and pollution (Pol) cases determined with the classification obtained from Figure 6 (see first paragraph of Section 5.3).

Código de campo cambiado

Con formato: Fuente: Sin Negrita

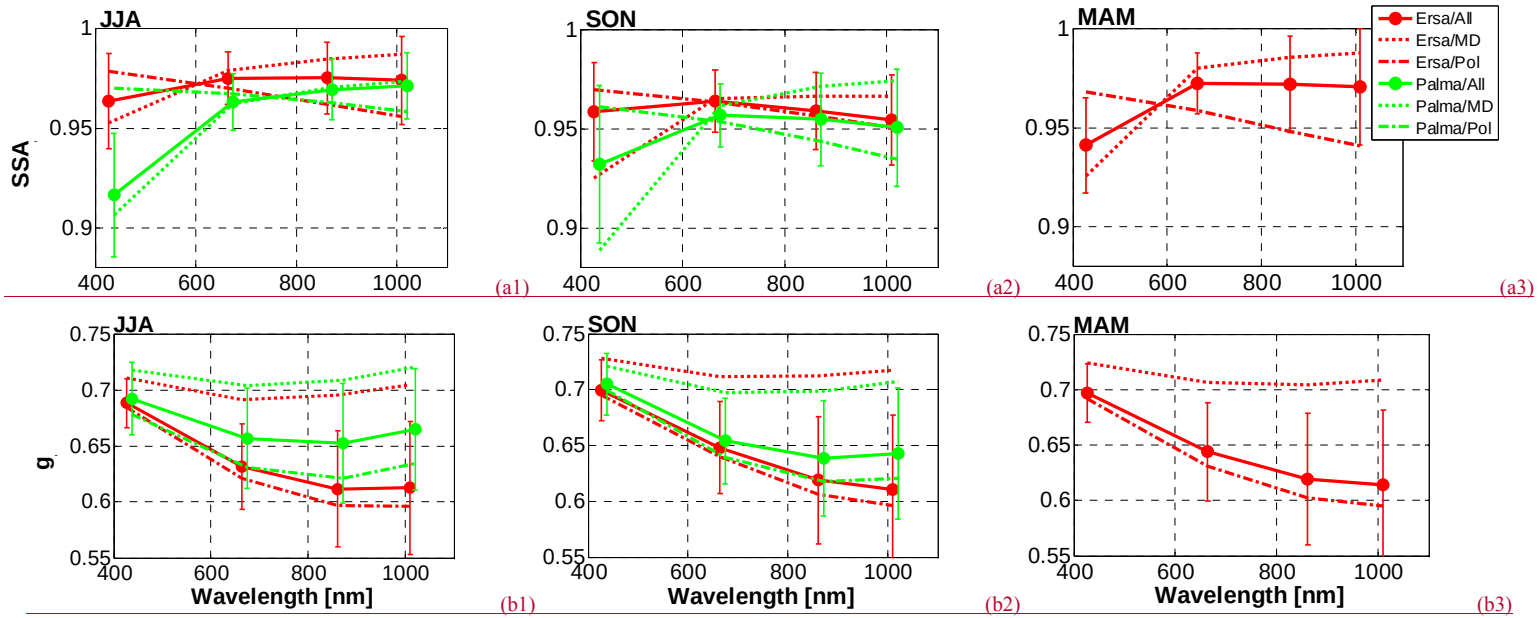

Figure 8. Seasonal variation of the spectra of (a) the single scattering albedo (SSA) and (b) the asymmetry factor (g) at 440 nm during (1) summer, (2) autumn and (3) spring, derived from AERONET level 2.0 inversion products available in the period 2011-2015. The legend in plot (a3) applies for all plots (a) and (b). SSA is retrieved with the following restrictions: $50 < SZA < 80^{o}$ and $AOD_{440} > 0.4$. The error bars represent the standard deviation. The seasonal mean is represented for the whole dataset (All), and separately for mineral dust (MD) and pollution (Pol) cases determined with the classification obtained from Figure 6 (see first paragraph of Section 5.3).

~~ame as Figure 4 for the spectral real part of the refractive index (RRI) at the three sites.~~

Con formato: Fuente: Sin Negrita
Con formato: Fuente: Sin Negrita
Código de campo cambiado
Con formato: Fuente: Sin Negrita
Con formato: Fuente: Sin Negrita
Con formato: Fuente: Sin Negrita
Con formato: Fuente: Sin Negrita
Con formato: Fuente: Sin Negrita
Con formato: Fuente: Sin Negrita
Con formato: Fuente: Sin Negrita
Con formato: Fuente: Sin Negrita
Código de campo cambiado
Con formato: Fuente: Sin Negrita
Con formato: Fuente: Sin Negrita
Con formato: Fuente: Sin Negrita
Con formato: Fuente: Sin Negrita

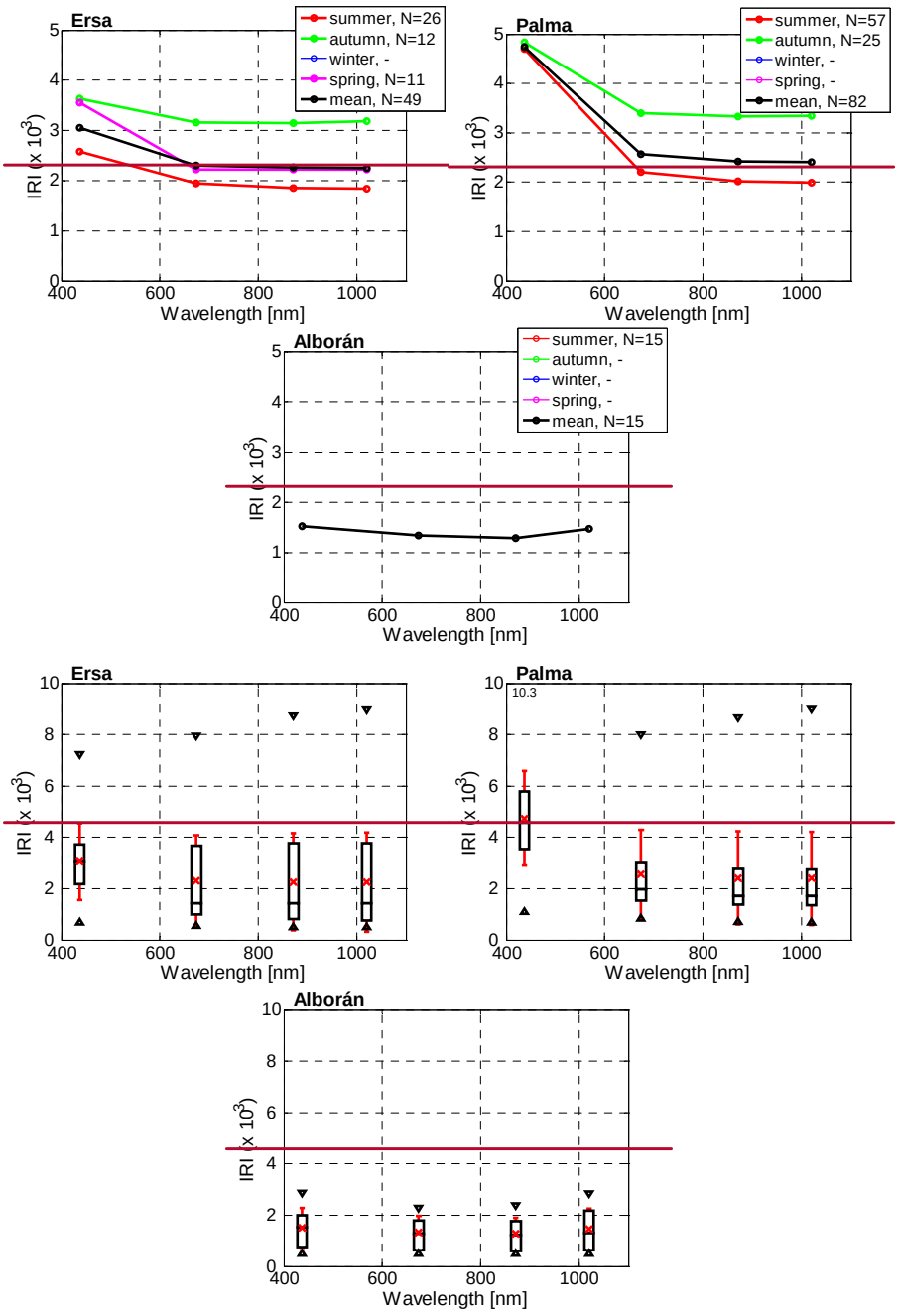

Figure 7. Same as Figure 4 for the spectral imaginary part of the refractive index (IRI) at the three sites.

Con formato: SPIE body text, Centrado, Interlineado: sencillo

Con formato: Justificado

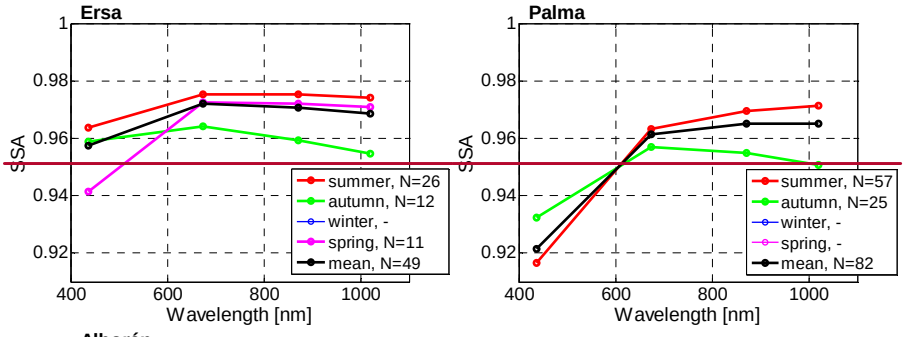
Ersa
SSA
Wavelength [nm]
summer, N=26
autumn, N=12
winter, -
spring, N=11
mean, N=49

Palma
SSA
Wavelength [nm]
summer, N=57
autumn, N=25
winter, -
spring, -
mean, N=82

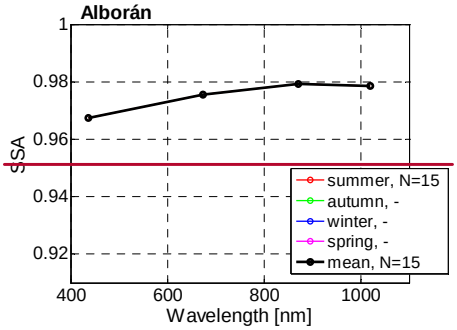
Alborán
SSA
Wavelength [nm]
summer, N=15
autumn, -
winter, -
spring, -
mean, N=15

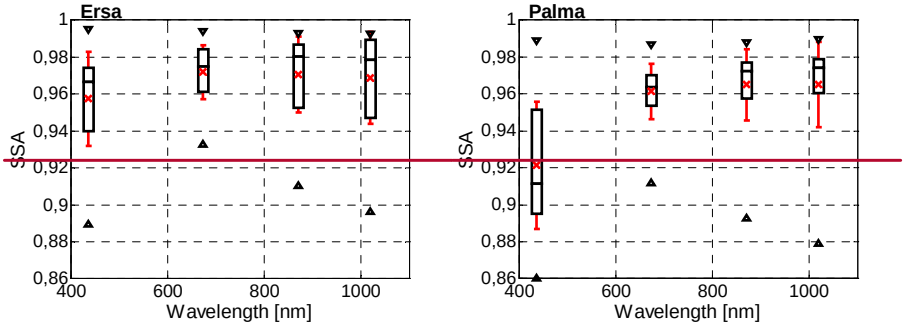
Ersa
SSA
Wavelength [nm]

Palma
SSA
Wavelength [nm]

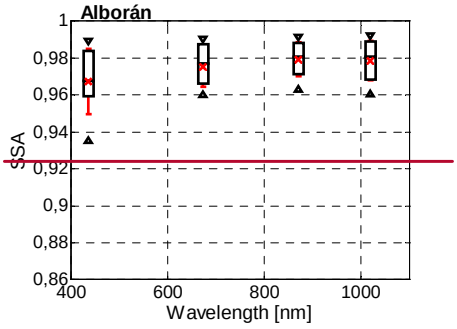
Alborán
SSA
Wavelength [nm]

~~Figure 8. Same as Figure 4 for the spectral SSA at the three sites.~~

Con formato: SPIE body text, Interlineado: 1,5 líneas

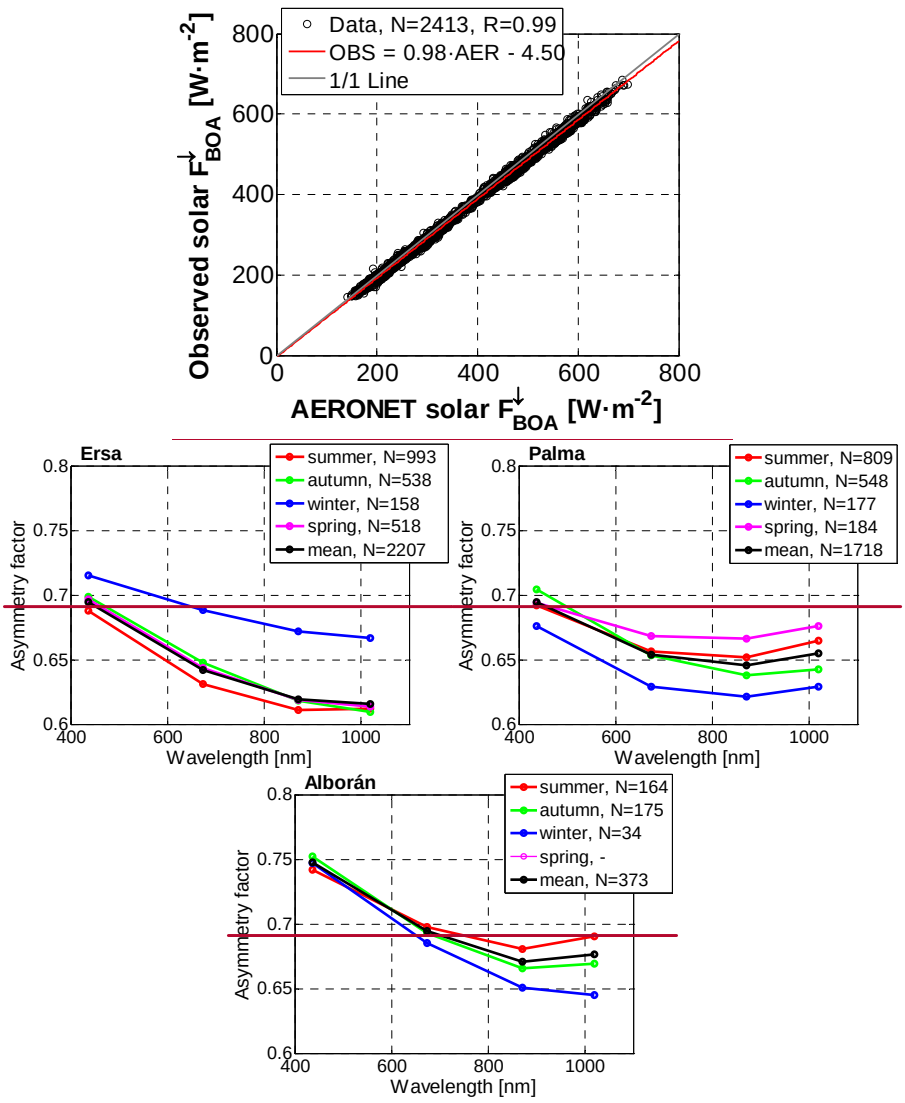
Data, N=2413, R=0.99
OBS = 0.98·AER - 4.50
1/1 Line
Observed solar F↓BOA [W·m-2]
AERONET solar F↓BOA [W·m-2]
Ersa
summer, N=993
autumn, N=538
winter, N=158
spring, N=518
mean, N=2207
Palma
summer, N=809
autumn, N=548
winter, N=177
spring, N=184
mean, N=1718
Alborán
summer, N=164
autumn, N=175
winter, N=34
spring, -
mean, N=373
Asymmetry factor
Wavelength [nm]

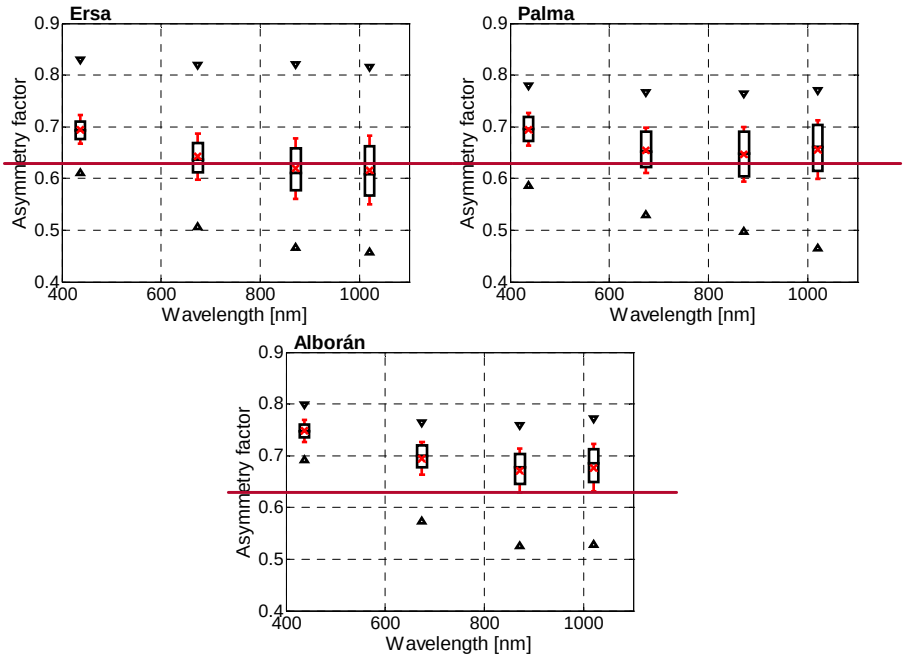

Figure 9. Same as Figure 4 for the spectral asymmetry factor at the three sites.

Con formato: SPIE body text, Centrado

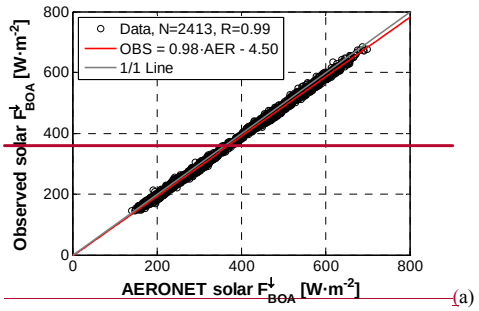

(a)

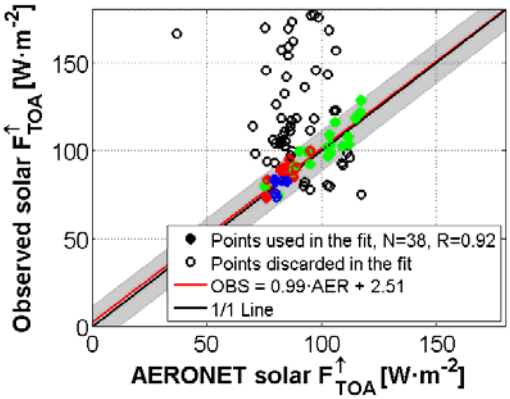

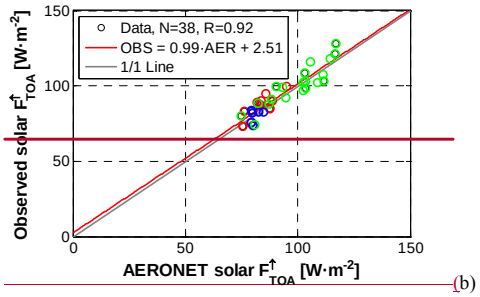

(b)

Figure 9~~10~~. (a) Observed SolRad-Net level 1.5 versus modeled AERONET level 2.0 instantaneous solar downward fluxes at the surface in Barcelona over the period May 2009 – October 2014~~.~~; (b) Observed CERES versus modeled AERONET level 1.5 instantaneous solar upward fluxes at the TOA ~~in Ersa~~at Ersa (2008 – 2014, red solid bullets~~circles~~), Palma (2011 – 2014, green ~~circles~~solid bullets) and Alborán (2011 – 2012, blue ~~circles~~solid bullets). The maximum time difference allowed between observed and AERONET fluxes is ± 1 and ± 15 min. at the BOA and TOA, respectively. In (b) the shaded area indicates the CERES uncertainty, namely ± 13.5 W·m^{-2}

around the 1/1 line; and the open bullets represent the pairs of points (CERES, AERONET), shown for completeness but discarded in the fit, that have a difference larger than CERES uncertainty.

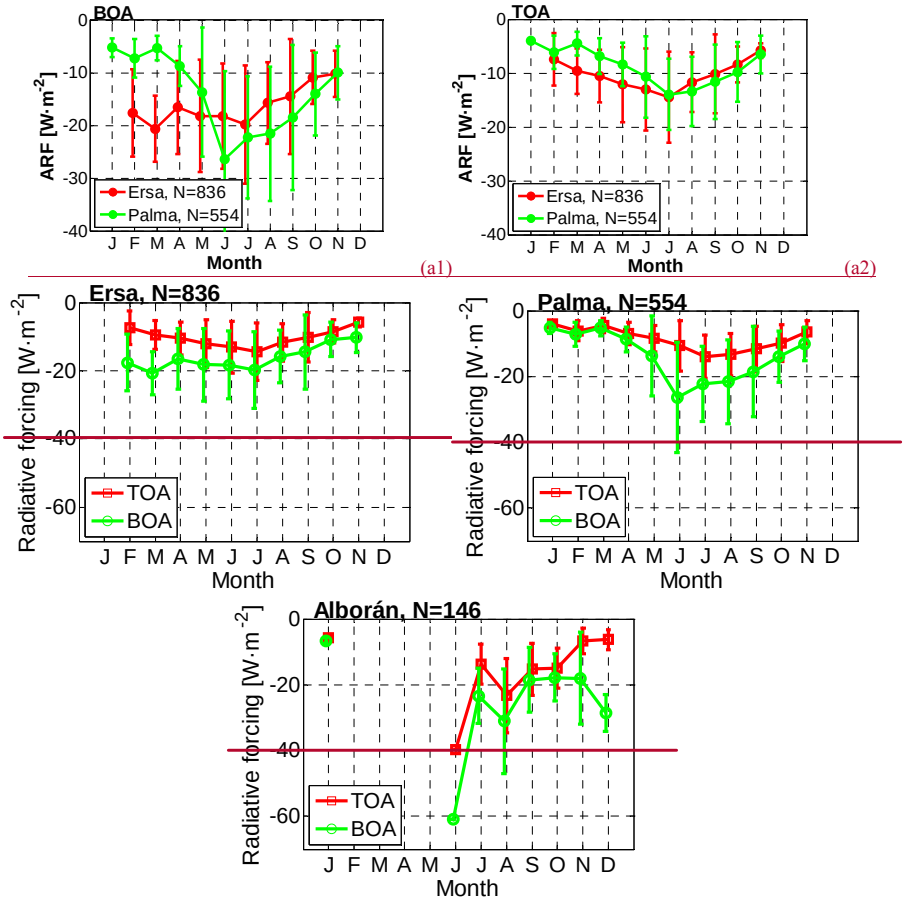
BOA
TOA
ARF [W·m-2]
Ersa, N=836
Palma, N=554
J F M A M J J A S O N D
Month
(a1)
(a2)
Ersa, N=836
Palma, N=554
Alborán, N=146
Radiative forcing [W·m-2]
TOA
BOA

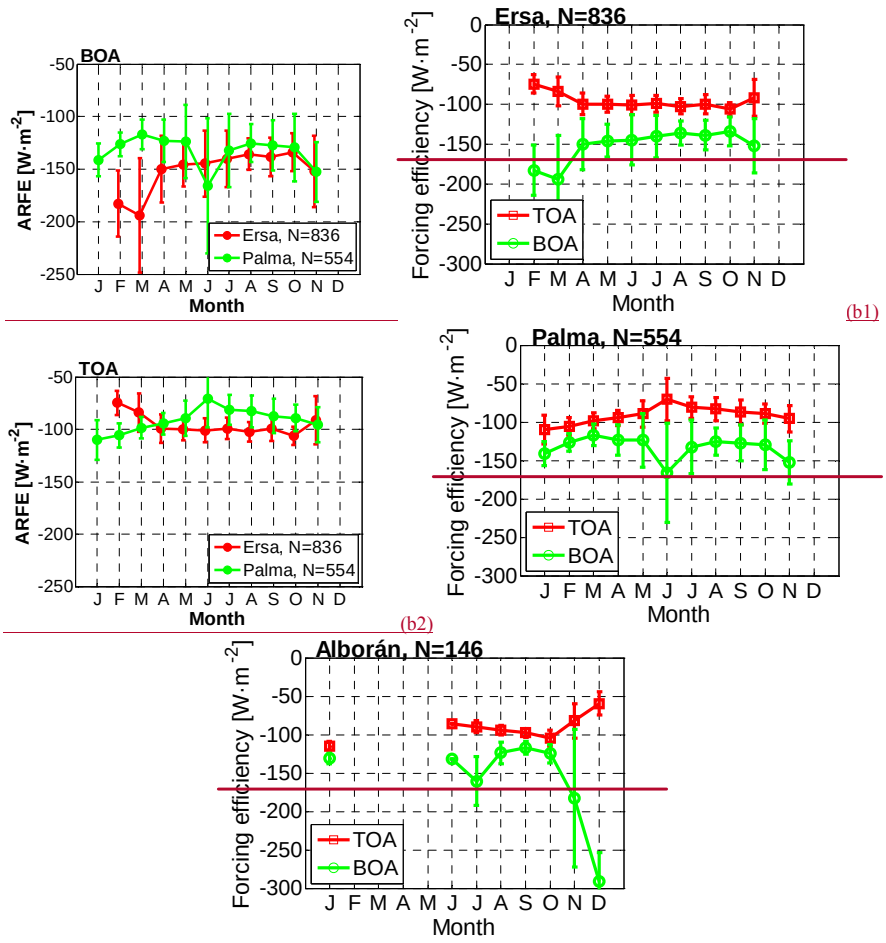

Figure 10~~11~~. ~~Seasonal~~ Monthly variation of (~~top~~a) the solar aerosol radiative forcing (ARF) and of (b~~ottom~~) the solar aerosol radiative forcing efficiency (ARFE) at the (1) BOA and (2) TOA, derived from AERONET level 2.0 inversion products available in the period 2011-2015. Both the ARF and the ARFE were estimated for 50 ≤ SZA ≤ 60º. The error bars represent the standard deviation.

Con formato: Normal

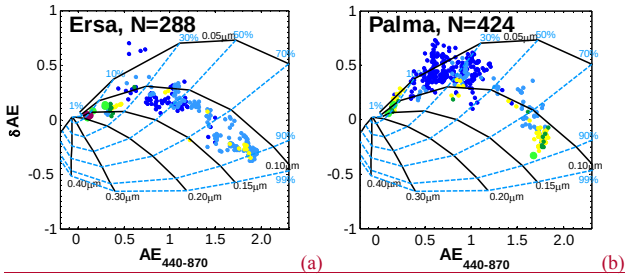

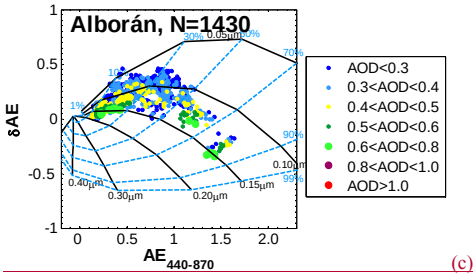

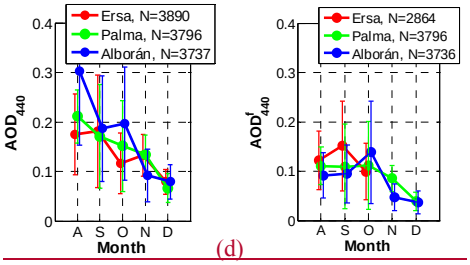

Con formato: Izquierda: 2,5 cm, Derecha: 2,5 cm, Arriba: 2 cm, Abajo: 2 cm, Ancho: 21 cm, Alto: 29,7 cm

Con formato: Normal, Centrado

Con formato: Fuente: (Predeterminada) Arial, 9 pto, Negrita

Con formato: Fuente: (Predeterminada) Arial, 9 pto, Negrita, Español (España - alfabetización tradicional)

Con formato: Fuente: (Predeterminada) Arial, 9 pto, Negrita

Con formato: Fuente: (Predeterminada) Arial, 9 pto, Negrita, Español (España - alfabetización tradicional)

Con formato: Fuente: 9 pto

Con formato: Fuente: (Predeterminada) Arial, 9 pto, Negrita

Con formato: Fuente: (Predeterminada) Arial, 9 pto, Negrita, Español (España - alfabetización tradicional)

Con formato: Fuente: 9 pto

Con formato: Fuente: (Predeterminada) Arial, 9 pto, Negrita

Con formato: Fuente: (Predeterminada) Arial, 10 pto, Negrita, Español (España - alfabetización tradicional)

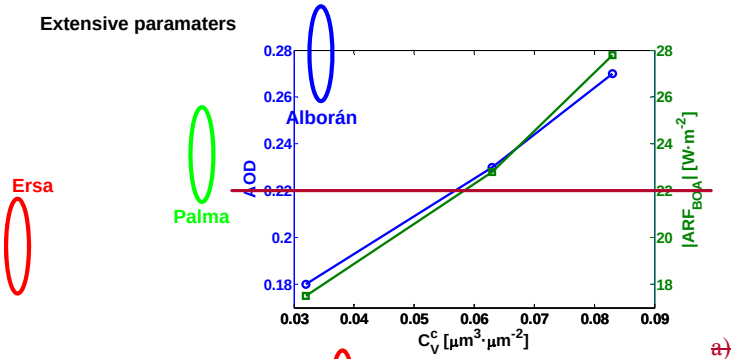

a)

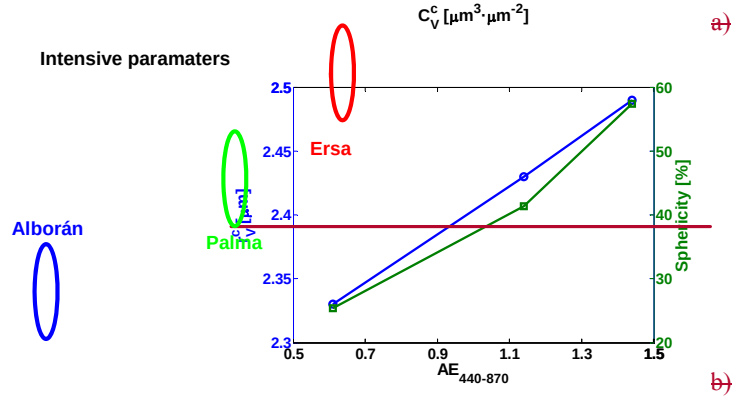

b)

Figure 12. Summer NE–SW gradient for a) extensive parameters (AOD_{440}, C_V^c and ARF_{BOA}) and for b) intensive parameters ($AE_{440-870}$, r_V^c and the sphericity).

Con formato: Normal

Con formato: Normal, Centrado

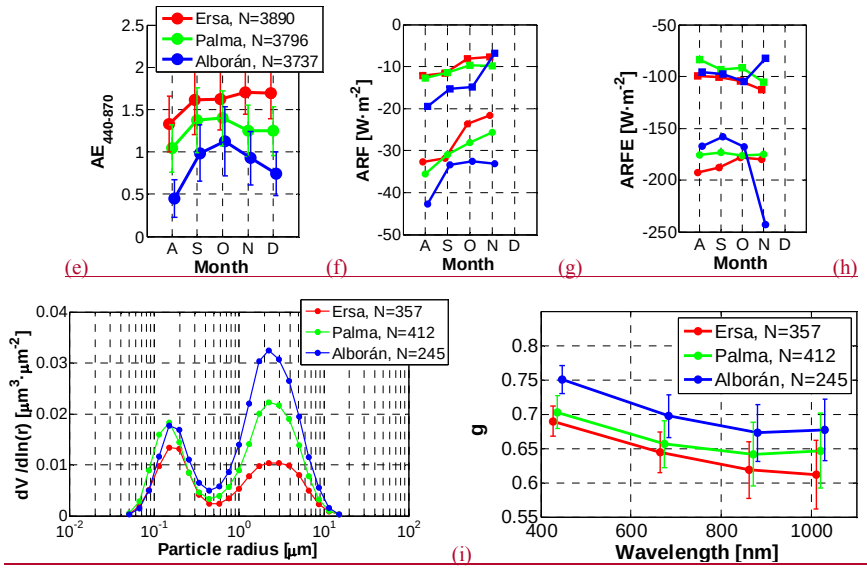

Figure 11. (δAE, AE) plot at (a) Ersa, (b) Palma and (c) Alborán over the whole period; monthly variations of (d) AOD_{440}, (e) AOD^{f}_{440}, (f) $AE_{440\text{-}870}$, (g) ARF and (h) ARFE; (i) size distribution and (j) spectra of *g* averaged over the whole period. The data are from AERONET level 2.0 inversion products during the period August to December 2011. The numbers of points in the plots (g) and (h) (not indicated in the plots for the sake of clarity) are 123, 133 and 101 for Ersa, Palma and Alborán, respectively. The color code is the same in all figures (d)-(j): red, green and blue for Ersa, Palma and Alborán, respectively. In (g)-(h) the error bars have been omitted for the sake of clarity.

Con formato: Inglés (Estados Unidos)
Con formato: Inglés (Estados Unidos)
Con formato: Subíndice
Con formato: Subíndice
Con formato: Interlineado: 1,5 líneas
Código de campo cambiado
Con formato: Fuente: Cursiva
Con formato: Alemán (Alemania)